Ontario

Ministry
of
Transportation

Transportation
Technology and
Energy Branch

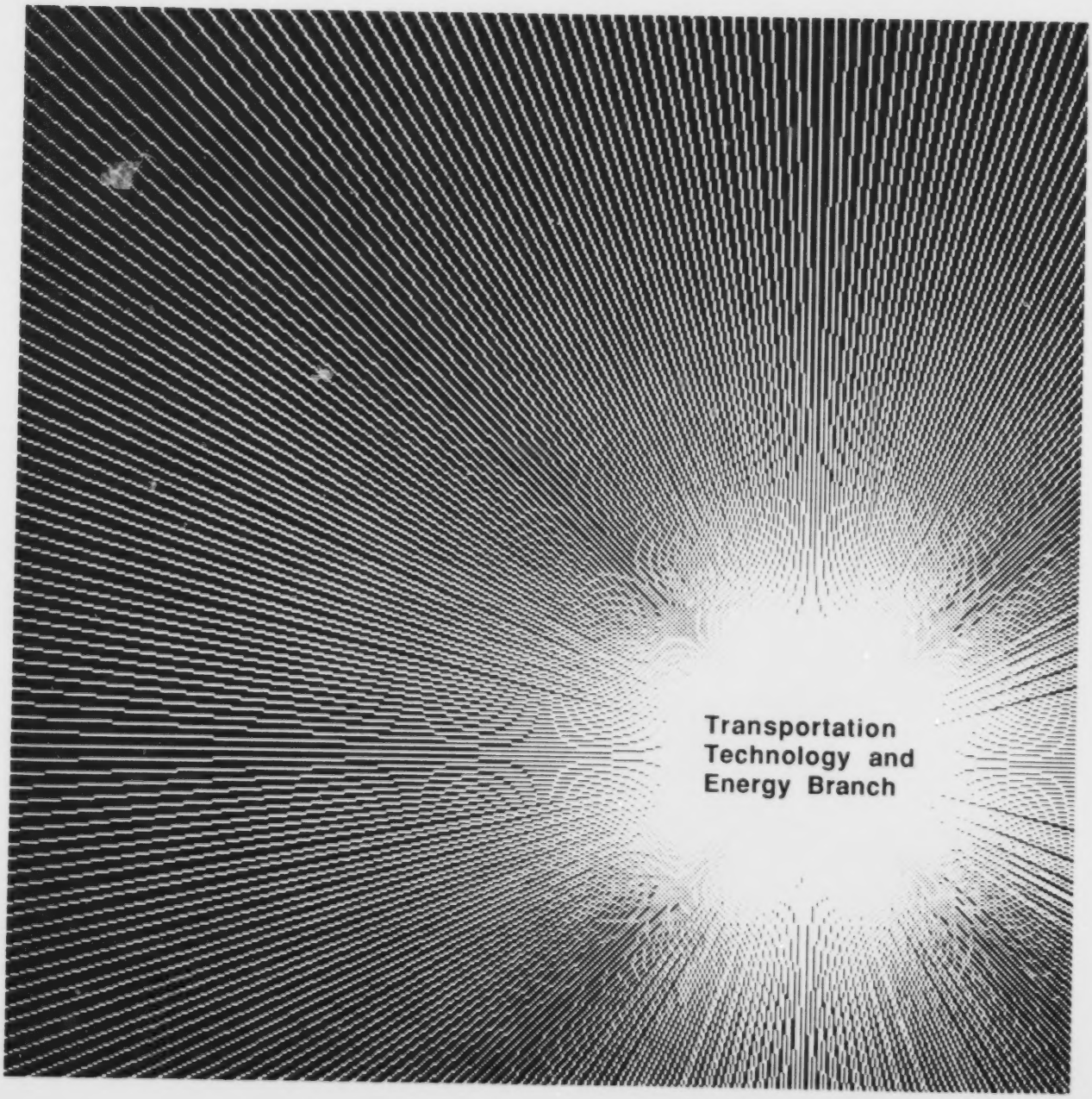

89-06301/

Fundamental Flammability Data for Methanol-based Spark-ignition Engine Fuels

AF-89-02

AF-89-02

Fundamental Flammability Data for Methanol-based Spark-ignition Engine Fuels

Prepared for:
D. Elliott
Project Manager
Vehicle Technology Office

Prepared by:
M.F. Bardon
G.W. Nicks
D. Gauthier
V.K. Rao
O.P. Nijhawan
R. Valvads
J. Holland
Department of Mechanical Engineering
Royal Military College of Canada
Kingston, Ontario
K7K 5L0

Published by:
Transportation Technology and Energy Branch
Ontario Ministry of Transportation
William Wrye, Minister

Ontario Ministry of Energy
Lyn McLeod, Minister

Published without prejudice as to the application of the findings. Crown copyright reserved; however, this document may be reproduced for non-commercial purposes with attribution to the ministry.

For additional copies, write:
Transportation Technology and Energy Branch
Technical Publications
Ministry of Transportation
Room 321, Central Building
1201 Wilson Avenue
Downsview, Ontario
Canada M3M 1J8
(416) 235-3465

September 1989

Technical Report Documentation Page

MTO Report Number AF-89-02	ISBN Number:	Other Document Number:	Date: Sept 1989
Title: Fundamental Flammability Data for Methanol-based Spark-ignition Engine Fuels			
Authors (name, title and/or organization): M.F. Bardon, G.W. Nicks, D. Gauthier, V.K. Rao, O.P. Nijhawan, R. Vaivads, J. Holland			
Published by: Transportation Technology and Energy Branch, MTO		**Client Group:**	
Participating Agencies: Royal Military College Ontario Ministry of Transportation Ministry of Energy			

Abstract:

The purpose of this program was to develop fundamental data related to the combustion behaviour of methanol fuel blends in spark-ignited engines. The following are the principal results: The distribution of methanol and hydrocarbon components in the vapour phase was determined experimentally for states consisting of different proportions of liquid and vapour; a mathematical model was developed which predicts the vapour pressure and phase composition of methanol blends; the model was validated by direct comparison with experimental data; the model was used to show that decreased temperature affects M85 more than gasoline in reducing vapour pressure; and the lean flammability limits have been predicted for M85 blends at the various stages of evaporation, and verified experimentally.

Key Words: methanol, blends, vapour pressure, combustion, droplets, flammability

Comments:

Distribution: by request

Copyright Status: Crown copyright

DISCLAIMER

This report is published as a public service. The Ministry of Transportation (MTO) does not, however, warrant the accuracy of its contents and cannot guarantee or assume liability for the effectiveness of the devices and processes described in the report or that their use does not infringe on privately owned rights.

TABLE OF CONTENTS

	PAGE
DISCLAIMER	ii
EXECUTIVE SUMMARY	vi
NOMENCLATURE	vii
1/ INTRODUCTION	1
2/ FLAMMABILITY OF THE VAPOUR PHASE OF METHANOL/HYDROCARBON MIXTURES	2
2.1/ Determination of the Composition of the Vapour Phase.	2
2.2/ Equations for Vapour Pressure and Related Quantities.	5
2.2.1/ Theoretical Background	5
2.2.2/ Model for M85 Vapour Pressure.	7
2.2.3/ Direct Measurement of M85 Vapour Pressure.	10
2.2.4/ Comparison of Theoretical and Experimental Vapour Pressure of M85.	11
2.2.5/ Discussion	12
2.2.6/ Conclusions.	13
2.3/ Analytical Prediction of Vapour Phase Flammability.	14
2.4/ Experimental Determination of Flammability Limits	15
2.5/ Recommendations and Conclusions	15
3/ IGNITION AND FLAME PROPAGATION IN VAPOUR/DROPLET MIXTURES	16
3.1/ Literature Review	16
3.2/ Recommended Models for Ignition and Flame Propagation	17
3.2.1/ Ignition	17
3.2.2/ Flame Propagation.	18
3.3/ Results and Conclusions Derived from the Analytical Models	18
3.3.1/ Ignition	18
3.4/ Experimental Study of Heterogeneous Combustion.	20
3.4.1/ Background	20
3.4.2/ Rapid Compression Machine Experiments.	21
3.4.3/ Results and Discussion	22
3.5/ Recommendations and Conclusions	22
4/ CONCLUSIONS	23
5/ REFERENCES	24
APPENDICES	
A/ Details of the Chromatographic Apparatus and Test Procedure	60
B/ Internal Report #860201 "Ignition and Combustion of Mixtures of Air, Fuel Droplets, and Fuel Vapour"	72

LIST OF TABLES

PAGE

1/ Composition of Methanol Fuel Blends. 25

2/ Constants for Use with M10 and M85 Vapour Fractions. 26

3/ Constants for Use with the Volatility Equations. 27

4/ Dimensions of Rapid Compression Machine. 28

LIST OF FIGURES

PAGE

1/ Gas Globe with Septum. 29
2/ Vapour Fraction for M10 Fuels. 30
3/ Vapour Fraction for M85 Fuels. 31
4/ Vapour Fraction for M85 Fuels with Butane. 32
5/ Vapour Fraction for M85 Fuels with DME 33
6/ Methanol Vapour Fraction for M85 Fuels 34
7/ Methanol Vapour Fraction for M85 Fuels with Butane -- Linear Plot. 35
8/ Methanol Vapour Fraction for M85 Fuels with Butane -- Curved PLot 36
9/ Vapour Pressure Experimental Apparatus 37
10/ Vapour Pressure vs Density: M85 at 0°C 38
11/ Vapour Pressure vs Density: M85 at 25°C. 39
12/ Vapour Pressure vs Density: M85 at 40°C. 40
13/ Vapour Pressure vs Vapour Fraction: M85 at 0°C 41
14/ Vapour Pressure vs Vapour Fraction: M85 at 25°C. 42
15/ Vapour Pressure vs Vapour Fraction: M85 at 40°C. 43
16/ Methanol Vapour Concentration: M85 at 25°C 44
17/ Proportion of Gasoline Evaporated from M85 (15% Gasoline) at 0°C. 45
18/ Calculated Peak Vapour Pressure of M85 (15% Gasoline) 46
19/ Vapour Pressure Advantage of Indolene Compared to M85 47
20/ Lean Burn Limits for Hydrocarbons 48
21/ Lean Burn Limits for M85/Butane 49
22/ Flame Tube Cylindrical Fuel Bomb. 50
23/ Minimum Ignition Energy vs VF 51
24/ Schematic of Rapid Compression Machine. 52
25/ Complete Installation 53
26/ Optical Disc. 54
27/ Quartz Head 54
28/ Optical Disc and Quartz Head Assembly 55
29/ Compression Pressure and Piston Position Record 55
30/ Fuel Spray Pattern. 56
31a/ Combustion with Excess Fuel 57
b/ Combustion with Less Fuel. 58
c/ Combustion with Lean Air-Fuel Mixture. 59

EXECUTIVE SUMMARY

The Transportation Technology and Energy Branch (TT&E) of the Ministry of Transportation (MTO) is investigating the use of methanol and other alternatives to conventional transportation fuels. In support of this, work has been carried out in the Mechanical Engineering Department of the Royal Military College of Canada, Kingston Ontario, directed and funded by MTO and funded by the Ministry of Energy.

The aim of the project is to develop fundamental data related to the distribution and composition of fuel components in a spark ignition engine, and to develop analytical techniques for use in other programs such as studies to improve the cold weather starting and running of automotive engines fuelled with various methanol-hydrocarbon blends. The following are the principal results:

1/ The distribution of methanol and hydrocarbon components in the vapour phase has been determined experimentally for states consisting of different proportions of liquid and vapour.

2/ A new model is proposed for predicting the vapour pressure of methanol blends. It uses a previously developed multi-component volatility model for the gasoline component, pseudo-binary mixing and a modified form of Raoult's Law, corrected for non-ideality. The model predicts M85 vapour pressure and vapour phase composition very well over the temperature range studied experimentally (i.e., 0 to 40°C).

3/ It has been shown that decreased temperature affects M85 more than gasoline in reducing vapour pressure.

4/ The lean flammability limits have been predicted for M85 blends at various stages of evaporation, and verified experimentally.

5/ Recommended equations are given for ignition in droplet-vapour-air mixtures under engine conditions.

6/ The theoretical analysis suggests that combustion failure under rich heterogeneous conditions is caused by the quenching of propagation, rather than by ignition failure. Rich droplet-laden mixtures can actually be ignited more easily under most circumstances than gaseous stoichiometric ones.

NOMENCLATURE

Latin Letters

a	constant
B	transfer number for droplet combustion
Cp	specific heat at constant pressure
C_1, C_2, C_3	droplet size distribution parameters
C_{11}	fuel concentration at the lean limit
d	spark kernel diameter
D	droplet diameter
D_{32}	Sauter mean diameter
E	activation energy
E_{min}	minimum ignition energy
f	fuel/air ratio by mass
k	thermal conductivity
ℓ	inter-droplet spacing
$\dot{m}$	rate of mass transfer
n	number of moles
Nu	Nusselt number
Pr	Prandtl number
$\dot{q}$	rate of heat generation or loss
R	universal gas constant
Re	Reynolds number
Sl	laminar burning velocity
St	turbulent burning velocity
t	characteristic time
T	temperature
ΔT	temperature rise
Tu	percentage turbulence intensity ($100u'/U$)
U	mainstream air velocity
u'	root mean square (RMS) of fluctuating velocity components
V	air velocity in the ignition zone
VF	vapour fraction = mass fraction of fuel in the form of vapour
w	constant
Z	droplet size distribution parameter

Greek Letters

α	thermal diffusivity
β	constant
ν	kinematic viscosity
ϕ	fuel/air equivalence ratio = f/f_{st}
ρ	density
Ω	mass fraction of fuel in the form of vapour

Subscripts

a	air
c	by conduction
ch	chemical term
D	based on sphere of diameter D
d	by diffusion
ev	evaporation term
f	fuel liquid
g	gas, or generation term, or gasoline value
l	liquid phase
m	methanol value
o	overall
ph	physical term
q	quenching
s	value at droplet surface
st	stoichiometric
t	value for total mixture
u'	based on turbulence intensity u' as characteristic velocity

1/ INTRODUCTION

In most respects, methanol or methanol-gasoline blends are excellent alternatives to ordinary gasoline as fuels for spark-ignition engines. However, the differences in volatility characteristics such as vapour pressure, evaporation rate, and latent heat result in driveability problems in the Canadian climate. In particular, cold starting and performance during warm-up deteriorate markedly with these substitute fuels. Before methanol-gasoline blends can make a significant contribution to Ontario's fuel needs, these problems must be overcome. Fuel additives or engine modifications must not only ensure that the new fuels will be technically feasible but that they will be accepted by the motorist.

There is, at present, a lack of certain basic fuel property data as they relate to combustion characteristics important to the performance of methanol-based fuels in engines. For example, to evaluate potential improvements in combustion chamber hardware modifications, the flame speed and flammability limits are essential. Similarly, these data are required by the mathematical models necessary for design optimization. The corresponding properties are well known for pure methanol and for most commercial hydrocarbons when fully vaporized. The difficulty lies in two aspects:

1/ the uncertainty in the composition of the vapour phase of methanol-hydrocarbon blends when there is some liquid fuel present, and
2/ the ignition and combustion behaviour of such multiphase mixtures under actual engine conditions.

These considerations are not relevant to warmed-up engines because there is no liquid fuel present in the cylinder during combustion. However, under cold-starting and cold weather warm-up conditions, such heterogeneous mixtures have a very important influence on engine performance.

The purposes of this program were

1/ to develop the required basic data concerning the composition and combustion characteristics of the vapour portion of two-phase methanol-hydrocarbon blends, and
2/ to elucidate the controlling physical and chemical processes important during ignition and combustion of multiphase mixtures of methanol-hydrocarbon fuel combinations.

2/ FLAMMABILITY OF THE VAPOUR PHASE OF METHANOL/HYDROCARBON MIXTURES

During cold starting only certain more volatile components of a fuel are in the form of vapour at the moment that the spark plug fires to ignite the mixture. In any form of mathematical modelling of this process, it is necessary to know the conditions required in the mixture so that it will be flammable at the moment of ignition. In the case of gasoline, this is relatively simple because the flammability limits of the various components in gasoline do not vary extensively. As a result, regardless of which components are in the vapour phase, the lean flammability limit is essentially constant. With alcohol-hydrocarbon mixtures, on the other hand, whether 90% gasoline and 10% methanol or fuels which are substantially methanol with hydrocarbon components, the vapour phase at the moment of ignition will be composed of both alcohol and hydrocarbons. Since the flammability characteristics of these two components are significantly different, there is a wide uncertainty in the lean combustible limit for the mixture existing in the vapour phase. The purposes of this subprogram were

- to determine the relative proportions of alcohol and hydrocarbon in the vapour as a function of the extent of vaporization for various particular mixtures of interest;
- to adapt an existing mathematical technique previously developed for gasoline to alcohol-hydrocarbon mixtures so that the experimental results could be correlated and cast into manageable functional relationships;
- to calculate the lean flammability limit of the various combinations that exist in the vapour phase, making use of existing theoretical techniques;
- to verify experimentally the calculated flammability limits so that other fuel combinations could be predicted confidently without experimental verifications each time.

2.1/ Determination of the Composition of the Vapour Phase

The objective was to predict the relative concentrations of alcohol and hydrocarbons in the vapour phase of a given mixture over the range of distributions from approximately 100% liquid to 100% vapour. The parameter used to define the extent of vaporization is the vapour fraction, VF, as employed in previous fuel volatility studies [3,4].

$$VF = (\text{mass of vapour})/(\text{total mass of fuel present})$$

The tests were conducted at room temperature by injecting weighed samples of each of the test fuels into a specially constructed sealable 6.5 L

spherical globe (Figure 1). This vessel was fitted with a standard laboratory 13 mm septum, which permitted insertion of hydrocarbon fuel mixtures and removal of liquid and gaseous samples without disrupting phase equilibrium within the globe.

Each sample was sprayed into the globe as a fine mist, which allowed more rapid evaporation and the attainment of equilibrium with minimum delay. Once equilibrium was reached, both liquid and vapour samples could be extracted for chromatographic analysis. The intent was to determine the percentage of each hydrocarbon present in every vapour phase so that an accurate determination of the lean flammability limit of each particular phase equilibrium attained by the different fuel mixtures could be achieved. Appendix A provides the details of the chromatograph and its apparatus and contains tables for all results, which are presented in Figures 2 to 8.

Some initial tests were performed on M10 (hydrocarbon fuel supplemented with 10% methanol). The emphasis was then placed on M85 (85% methanol by volume hydrocarbon fuels). The M85 fuels under study had the following nominal concentrations:

1/ M85/15, a baseline fuel containing 15% gasoline
2/ M85/13/2 with 13% gasoline and 2% butane
3/ M85/11/4 with 11% gasoline and 4% butane
4/ M85/9/6 with 9% gasoline and 6% butane
5/ M85/13/2 DME with 13% gasoline and 2% dimethyl ether (DME)
6/ M85/11/4 DME with 11% gasoline and 4% dimethyl ether
7/ M85/9/6 DME with 9% gasoline and 6% dimethyl ether

The actual concentrations are given in Table 1.

It was found possible to express satisfactorily all the vapour fractions observed from M10 and the diverse M85 fuels in the general form as an equation:

$$VF = AX^{(B)} \qquad (1)$$

where

A and B are constants, different for M10 than for M85
X = (the mass of sample fuel in grams) for a 6.5 L vessel

These relationships were initially derived for the baseline fuel and then the results from the other compounds for the same methanol fraction were superimposed on them. In the first instance, M10 lab mixture fuel was

used as a baseline to derive a mathematical relationship (Figure 2) and was prepared by mixing 10% methanol to indolene. Later samples provided by MTO and designated as M10-OMTO were superimposed on the initial curve with satisfactory results. Similarly, the baseline M85/15 fuel was used to derive curves for VF versus grams of fuel per litre (Figure 3). This curve was later used for over-plotting of the three butane additive M85s (Figure 4) and the three DME additive M85s (Figure 5), all with satisfactory results.

For the purpose of analytical work, it is necessary to express these results in terms of the percent of methanol present in the vapour phase with respect to some other external factor. Various equations were fitted to the data. The equations having the greatest applicability to our studies are of the same form:

$$Y = C\ VF^{(D)} \tag{2}$$

where C and D are, again, independent constants
Y = the percentage by mass of methanol in the vapour phase
VF = the vapour fraction of fuel present in the vessel

This expression is shown for the baseline M85/15 fuel in Figure 6, along with the individual data points generated. The results for the three M85 butane fuels were then superimposed on this expression in Figure 7. For low vapour fractions, it was evident that there was some dispersion from the M85/15 baseline curve. Mathematically, this can be expressed as a second line of a different intercept and exponent, still of the form

$$Y = C\ VF^{(D)} \tag{3}$$

with an intersection at 0.11 vapour fraction. Alternatively, it is possible to mathematically express this dispersion in an equation of the form

$$Y = E\ (\%VF)^{(F\ -\ G\ Ln(\%VF))} \tag{4}$$

where %VF = 100VF, and E, F, and G are all constants. The results of this analysis are shown in Figure 8. Values for the specific constants are presented in Table 2.

Unfortunately, it was not possible to provide similar results for the M85 DME fuels as of this writing, as the chromatographic equipment used for this project was insensitive to the small differences between DME and methanol.

2.2/ Equations for Vapour Pressure and Related Quantities

2.2.1/ Theoretical Background

Gasoline and other commercial fuels are mixtures of dozens of major pure components and often hundreds of minor ones. This renders the quantification of evaporative behaviour very complex. For a single component material such as neat methanol, vapour pressure, vapour phase molecular weight, and enthalpy of vaporization are all either constant or simple functions of temperature only. For real fuels, on the other hand, these all depend not only on temperature but also on the extent of vaporization. Our intuitive grasp of the physics concerned is evident in expressions such as "light ends," referring to those lower molecular weight components that evaporate readily and produce high vapour pressures when most of the fuel is still in the form of liquid. Similarly, the term "heavy ends" describes the higher boiling components remaining after most of the fuel has evaporated. Under these latter conditions, the saturation pressure is much lower than that of the original fuel. In fact, the vapour pressure of conventional gasoline decreases by an order of magnitude during the course of evaporation at constant temperature. This contrasts dramatically with a pure substance that has an exactly constant vapour pressure at any given temperature, provided there is at least some liquid present at equilibrium.

M85, produced by blending methanol, gasoline, and, sometimes, priming agents, has all the inherent complexity of other multi-component fuels. However, unlike ordinary hydrocarbon blends, which are nearly ideal mixtures obeying Raoult's Law, methanol blends are highly non-ideal, behaving as low-boiling azeotropes. This causes the characteristic flattening of their distillation curves and means that the Reid vapour pressure (RVP) is higher than would ordinarily be expected based on simple mixing rules. Formidable as this behaviour is, there are many cases of practical interest where proper qualitative understanding and quantitative analysis requires a manageable technique to predict the vapour pressure and related properties of methanol blends. Examples include the cold-start modelling being undertaken in a companion project, evaporative emissions, refuelling losses, and the "weathering" of fuels, which causes this behaviour to change with time in storage.

In the past, no manageable relations have been available for such situations. As a result, tractable mathematical analysis has either not been possible at all or else only crude solutions have been available, usually approximating the real fuel behaviour by using the properties of some pure substance. These latter are actually misleading for the example situations given, and so are worse than useless. More complete

descriptions of real fuels have been proposed, based on matching the desired distillation curve by a mixture of many pure substances and assuming Raoult's Law. Very recently, this approach has been used for some gasoline analysis related to evaporative emissions [1,2]. However, these models are very complex and difficult to replicate, so they do not offer a manageable tool for use in something such as a cold-start analysis. Furthermore, they require detailed chromatographic analysis of the gasoline so that the 30 or more components used to collectively simulate the gasoline concerned can be specified. In the case of fuels containing methanol in whatever concentration, they cannot be used at all because the mixture no longer closely obeys Raoult's Law.

A new technique has recently been developed for hydrocarbon fuels at the Royal Military College (RMC) [3,4]. It provides simple functional expressions for vapour pressure, enthalpy of evaporation, and mean vapour phase molecular weight for real fuels in the gasoline range, based only on overall specific gravity and the ASTM distillation curve. Because it provides explicit equations for these properties, it can readily be used in many other larger analyses, such as the cold-start modelling, which originally prompted its development. Before describing the way in which this technique was used in the present program, a brief outline of the approach will be given. Further details are available elsewhere [3,4].

The simplest functional relationship for vapour pressure is the Clausius-Clapeyron equation:

$$P_{sat} = C_1 \exp(-C_2/T) \tag{5}$$

where

P_{sat} = equilibrium saturation pressure
T = absolute temperature
C_1, C_2 = constants for a given pure substance

The basis of the method is the assumption that real multi-component behaviour can be described by treating C_1 and C_2 as functions of the extent of vaporization, defined by the vapour fraction, VF, which is the mass fraction of fuel in the form of vapour, as previously defined. The basic vapour pressure equation is therefore written as

$$P_{sat} = f_1 \exp(-f_2/T) \tag{6}$$

where f_1 and f_2 are temperature independent functions of VF alone, for any particular fuel.

The technique uses the ASTM distillation data [5] and specific gravity to determine the functions f_1 and f_2, as well as relations for mean vapour phase molecular weight, M, and enthalpy of vaporization, ΔH. Table 3, which is taken from [3], gives cubic polynominal equations for f_1, f_2, M, and ΔH for three representative fuels covering the usual range of motor gasoline. In this table, the constants shown are for the following equations:

$$f_1 = f_{10} + f_{11}VF + f_{12}VF^2 + f_{13}VF^3 \quad (Pa)$$

$$f_2 = f_{20} + f_{21}VF + f_{22}VF^2 + f_{23}VF^3 \quad (K)$$

$$M = M_0 + M_1VF + M_2VF^2 + M_3VF^3$$

$$\Delta H = \Delta H_0 + \Delta H_1VF + \Delta H_2VF^2 + \Delta H_3VF^3 \quad (J \cdot mol^{-1})$$

The technique makes a number of assumptions to derive the constants for a given fuel. Several of these are invalid for methanol blends, and there is not, at present, any satisfactory general way of predicting them for such a fuel. In this program, a means has been developed to use the existing way of generating gasoline data as part of a new overall analysis for M85 fuels.

2.2.2/ Model for M85 Vapour Pressure

The original fuel sample was composed of 85% methanol and 15% winter gasoline by volume. The M85 is treated as a non-ideal binary mixture of methanol and gasoline. The gasoline fraction was simulated using the properties of winter gasoline given in Table 3. Now Raoult's Law for ideal mixtures is

$$P_i = P_{isat}X_{iliq} \qquad (7)$$

where

P_i = partial pressure of component i in the vapour phase in equilibrium with the liquid

P_{isat} = saturation pressure of component i at the mixture temperature

X_{iliq} = mole fraction of component i in the liquid phase at equilibrium

For the M85 blend considered, Raoult's Law predicts a blend Reid vapour pressure (RVP) only about 60% as great as that which is actually found to occur. The effect of the methanol is, in fact, to suppress the gasoline vapour fraction much less than would be expected for an ideal mixture, under some conditions at least. Considered another way, the vapour pressure of gasoline over the blended liquid is greater than predicted by Equation 7.

It is reasonable to expect this effect to vary directly with the quantity of methanol in the liquid phase. In this work it is proposed to describe the "binary" methanol-gasoline mixture with a modified form of Raoult's Law, which takes into account the disproportionate vapour pressure of the gasoline component. It is assumed that the methanol vapour pressure is unaffected by the hydrocarbon, whereas that of the gasoline is given by

$$P_g = P_{gsat} X_g (1 + KX_m) \qquad (8)$$

where

P_g = partial pressure of gasoline
P_{gsat} = saturation pressure of the gasoline based on its own actual vapour fraction VF_g in the mixture
X_g = mole fraction of gasoline in the liquid at equilibrium
X_m = mole fraction of methanol in the liquid at equilibrium
K = a constant which accounts for non-ideality. In an ideal mixture $K = 0$

Note that the molecular weight of the liquid and vapour gasoline components are different. That of the vapour phase is given by the model equation as a function of VF_g (see Table 3). It may readily be shown that the molecular weight of the gasoline remaining in the liquid phase is given by

$$M_{gl} = (M_{gl} - VF_g M_{gv})/(1 - VF_g) \qquad (9)$$

where

M_{gl} = molecular weight of gasoline in the liquid phase

M_{gv} = molecular weight of gasoline in the vapour phase

VF_g = gasoline vapour fraction

M_{gl} = mean molecular weight of the entire gasoline sample = molecular weight of the vapour when all liquid has evaporated (i.e., at VF = 1 using the gasoline model equation data of Table 3)

Note that since gasoline evaporates preferentially in the early stages of vaporization (i.e., at low values of overall VF), in general, VF_g is greater than both methanol vapour fraction, VF_m, as well as the overall value for the entire mixture, VF_t. The density differences between the gasoline and methanol phases are sufficiently small that volume and mass fraction are nearly the same. With the assumption that this is exactly true,

$$VF_t = 0.15\ VF_g + 0.85\ VF_m \tag{10}$$

where

VF_t = total mixture vapour fraction
VF_m = methanol vapour fraction
VF_g = gasoline vapour fraction

In the usual calculation, it is easiest to begin by specifying gasoline vapour fraction, VF_g, as this allows gasoline vapour pressure to be determined directly, as well as its liquid and vapour phase molecular weights. The methanol vapour fraction is then found from the principle that all vapour occupies the same volume. Using the ideal gas law this implies

$$\frac{m_{gv}}{m_{mv}} = \frac{M_{gv}P_g}{M_mP_m} \tag{11}$$

where

m_{gv} = mass of gasoline vapour at equilibrium

m_{mv} = mass of methanol vapour at equilibrium

M_{gv} = molecular weight of gasoline vapour at equilibrium (function of VF_g)

M_m = molecular weight of methanol = 32

P_g = partial pressure of gasoline at equilibrium

P_m = partial pressure of methanol at equilibrium

In terms of original masses of methanol and gasoline in the blend,

$$\frac{VF_g}{VF_m} = \frac{m_{mo} M_{gr} P_g}{m_{go} M_m P_m} \qquad (12)$$

where

m_{mo} = overall mass of methanol in blend
m_{go} = overall mass of gasoline in blend

For M85 this becomes

$$VF = \frac{5.65\ VF_g P_m}{P_g M_{gv}} \qquad (13)$$

These equations are sufficient to permit total mixture saturation pressure to be determined along with overall vapour fraction, component distribution in the two phases, etc., all for some given value of gasoline vapour fraction, VF_g. If overall vapour fraction, VF_t, or some other variable is specified for the problem at hand, as is usually the case in practice, then iteration is required. However, this is straightforward, since it merely consists of finding the value of VF_g needed to result in the chosen value of the control variable.

Based on the experimental data, a value of 3.5 was selected for the non-ideality factor, K. The coefficients for high-volatility gasoline were used to model the gasoline component of the M85 in the absence of detailed distillation data for the actual winter gasoline used in its production.

2.2.3/ Direct Measurement of M85 Vapour Pressure

Apparatus and techniques developed in another research program at RMC were used to measure the vapour pressure of one M85 blend, which contained 15% winter gasoline.

Figure 9 shows a schematic of the apparatus. A weighed sample of fuel was placed into the small detachable vial (A), which was then attached to the remainder of the glassware. When assembled, the total interior volume was just over 3 L. To minimize the loss of volatile components

during weighing and handling, fuel samples were first chilled in an ice bath. Transfers were performed as rapidly as possible, and the fuel handling procedures generally conformed to the practice recommended for volatile fuel handling in conjunction with RVP tests [6].

Dissolved air can significantly affect fuel vapour pressure readings under some circumstances [7]. To eliminate any dissolved air and also to permit greater accuracy in the measured vapour pressure, the following procedure was employed:

The apparatus was immersed in a liquid nitrogen bath to condense any fuel vapour. A Welch Model 1400 vacuum pump was then used to evacuate the air, attaining a pressure of 0.02 to 0.03 torr. The apparatus was next permitted to return to room temperature so that any dissolved air trapped during freezing could escape. The chilling and pumping was then repeated to remove this additional air.

During the initial tests, equilibrium pressure in the apparatus was measured at the test temperature between pumping cycles. It was found that the second and subsequent cycles of freezing and evacuation produced no significant change in measured pressure; this was taken as evidence that all dissolved air had been removed. Two pumping cycles were, therefore, used in all subsequent tests. The repeatability of the vapour pressure was also considered to be corroboration that no significant fuel losses were incurred during the air removal procedure.

No attempt was made to remove any water vapour present in the air initially inside the apparatus. Instead, a correction factor was applied based on the water vapour pressure measured during tests conducted with no fuel present.

Using Bell and Howell and MKS Baratron pressure transducers, vapour pressure was measured with the fuel liquid and vapour in equilibrium at the test temperature. By using different masses of fuel, it was possible to establish conditions within the vessel so as to ensure a range of vapour fraction, and, hence, vapour pressures, at each temperature.

2.2.4/ Comparison of Theoretical and Experimental Vapour Pressure of M85

Tests were conducted at 0, 25, and 40°C. Figures 10 to 12 show the measured data. The abscissa is overall apparent density, i.e., total

fuel mass divided by total internal volume occupied by fuel vapour and liquid. Predicted vapour pressure computed using the model just described is shown as solid lines in the figures. The results are quite satisfactory.

The same data have been re-plotted in Figures 13 to 15 against the overall vapour fraction, VF_t, to bring out more fundamental information. Since vapour fraction could not be measured in the apparatus, values for the data had to be calculated using the model itself. This places some uncertainty in the horizontal positioning of data points, with the largest errors at higher values of VF. This generally accentuates any differences between predicted and measured values. In spite of this, the predicted curves are seen to follow the data quite well.

Data on the composition of vapour phases of the straight gasoline M85 at room temperature are given in Appendix A. These have been plotted in Figure 16, along with the predicted composition determined by the model. The results are excellent.

2.2.5/ Discussion

The previous section showed that the model agrees with measured M85 behaviour very well, at least in the temperature range studied. If the actual distillation data of the gasoline phase had been available, the agreement would be expected to be even better. However, other M85 blends (containing butane or dimethyl ether [DME], for example) would not necessarily have the same properties. Likewise, co-solvents can change the vapour pressure of methanol blends. For these reasons, it is perilous to extrapolate the data too far or to use the model indiscriminately for other methanol blends.

Notwithstanding this cautionary note, the pseudo-binary model using the RMC multi-component technique and a modified Raoult's Law, incorporating a non-ideality factor, shows excellent promise. It should certainly be directly applicable to gasoline-primed methanol formulations and, with appropriate non-ideality factors, can likely be used for other alcohol-hydrocarbon mixtures as well.

For general use in the absence of more detailed data, it is recommended that the constants used here (i.e., those of the high-volatility gasoline) be used and the non-ideality factor, K, be selected so as to match the actual RVP of the blend under consideration. Vapour pressure and related properties under different conditions can then be calculated assuming, as seems to be the case based on the data here, that K is approximately constant.

The model will now be used to derive some general observations about M85 behaviour.

Figure 17 shows the fraction of gasoline evaporated at equilibrium for M85 at 0°C. This shows the effect of the light ends of the gasoline. The dashed line is for comparison only and represents the behaviour which would occur if the gasoline made up the same fraction of the vapour as of the entire mixture. When 10% of the fuel is in the form of vapour, 30% of the gasoline is already vaporized. Since gasoline makes up only 15% of the original blend, the vapour phase at this point is, thus, three times richer in gasoline than its concentration in the original fuel would suggest. Part of this is caused by its inherent volatility and would occur in an ideal mixture as well; however, a large part is also due to non-ideal behaviour.

It is of great interest to compare the behaviour of M85 with conventional fuel. One interesting facet of the behaviour of alcohol blends can be seen in Figures 18 and 19. The first shows peak vapour pressure (i.e., at VF = 0) as a function of temperature. Of course, it rises exponentially with temperature, as usual, and is not fundamentally different from conventional gasoline in this regard. However, the blend studied here has virtually the same peak vapour pressure as indolene at 40°C. The second figure shows that the slight advantage of indolene at 40°C becomes dramatically greater as temperature falls. Thus, the driving potential for evaporation decreases more rapidly with temperature for M85 than for gasoline. At -40°C, the indolene vapour pressure is some 60% greater, but it was only 4% higher at +40°C. This difference would be expected to influence the cold weather behaviour of engines using M85 or other methanol blends.

2.2.6/ Conclusions

1/ A new model is proposed for predicting the vapour pressure of methanol blends. It uses a previously developed multi-component volatility model for the gasoline component, pseudo-binary mixing, and a modified form of Raoult's Law corrected for non-ideality.

2/ The model predicts M85 vapour pressure and vapour phase composition very well over the temperature range studied experimentally, namely, 0 to 40°C.

3/ The model can be extended to other methanol/gasoline blends, requiring only the measured RVP to determine the single non-ideality constant.

4/ It has been shown that decreased temperature affects M85 more than gasoline in reducing vapour pressure.

2.3/ Analytical Prediction of Vapour Phase Flammability

The property of most concern here is the lean flammability limit of the vapour phase created by the phase balances of the constituents of a multi-component fuel. There exists a number of predictive techniques designed to estimate the lean flammability limit of a mixture of gases based on the known limits of the individual components. The one chosen for use here is the "Weak Limits of Premixed Gases" developed by Odgers et al [8].

The Odgers correlating equation depends only on knowledge of the fuel composition, its calorific value, and the stoichiometric products at 298 K. The correlation is applicable to simple and complex mixtures, with or without inert addition, and applies over a range from 298 to 1000 K. The accuracy of this correlation is as good as or better than others currently in use.

The Odger's correlating equation is of the form

$$\Phi_L = 0.725/X^{1.3} \qquad (14)$$

where

$X = 1000\ Q\ \Theta/(C_p Y)$
Y is the fuel composition factor
Q is the net molar calorific value
Θ is the temperature correction factor
C_p is the specific heat at 298 K of the stoichiometric products per mole of fuel. Typical values are presented in Appendix A

Figure 20 shows the predicted lean limit line as developed by Odgers for his correlating factor, and Figure 21 illustrates this curve for the range of interest for methanol and for the M85 fuels. As detailed in Section 2.4, experiments were conducted with a cylindrical fuel bomb and a downward propagating flame. The ignition and non-ignition results are shown in Figure 21 and indicate excellent correlation with the previously determined Odgers predictions.

2.4/ Experimental Determination of Flammability Limits

To obtain experimental corroboration of the lean limits predicted for the mixtures, an apparatus used in some related work was modified for use as a flame tube.

Figure 22 shows the apparatus used. A known mass of the particular mixture to be studied was placed into the cylindrical fuel bomb, which was then sealed so as to allow the fuel to vaporize fully and diffuse uniformly throughout the interior. The test was then run by firing the spark to ignite the mixture (the cap at the top end allowing pressure release so that there would be no pressure increase in the bomb during combustion). Combustion was considered to have been successful only if the flame propagated the entire length of the tube. This is consistent with standard practice in such tests, which, in any case, are somewhat apparatus dependent and used to provide mainly comparative data.

The lean limits measured in tests such as this must be applied to particular real-life circumstances cautiously because of the importance of factors present in practical devices, which may have a strong influence on flammability. The direction of propagation has some effect, and turbulence can dramatically alter the behaviour. Nevertheless, test results such as these are the essential building blocks upon which more detailed models of real processes are founded.

2.5/ Recommendations and Conclusions

1/ The composition of the vapour phase of seven methanol M85 blends has been determined as a function of vapour fraction.

2/ A new model is proposed for predicting the vapour pressure of methanol blends. It uses a previously developed multi-component volatility model for the gasoline component, pseudo-binary mixing, and a modified form of Raoult's Law corrected for non-ideality. The model predicts M85 vapour pressure and vapour phase composition well over the temperature range studied experimentally, namely, 0 to 40°C. The model can be extended to other methanol-gasoline blends, requiring only the measured RVP to determine the single non-ideality constant.

3/ The Odgers equation has been used in conjunction with the composition data to calculate the vapour phase flammability limits as evaporation proceeds. These have been corroborated by a simple experimental evaluation. Further experimental evaluation is unwarranted because the prediction of the vapour phase composition and the extent of evaporation under real conditions are subject to much greater uncertainty than the inherent variation in flammability limits for those fuels.

3/ IGNITION AND FLAME PROPAGATION IN VAPOUR/DROPLET MIXTURES

The size of the droplets delivered to the cylinder by the fuel supply system affects the cold-starting and warm-up performance of an engine in two quite distinct ways:

1/ The initial droplet size influences the rates of heat transfer and evaporation during the movement through the induction system and during the compression stroke. These considerations determine the state of the mixture at the moment of ignition.

2/ The droplets influence ignition and flame propagation itself. The processes leading up to the moment of ignition are considered in other studies. The present work is restricted to the ignition and combustion behaviour for a specified heterogeneous mixture.

The effects of droplet size on both ignition and flame propagation (which may not necessarily be identical) are important in determining optimum conditions for best engine performance. Even if an artificial starting aid, such as ether injection, is used to start the engine, there is a considerable period of time before sufficient heat can be provided to the induction system to provide an essentially pre-vaporized mixture before combustion. Combustion during starting and warm-up, therefore, always involves flame propagation with various proportions of liquid and vapour present. The determination of the physical form and location of the liquid is not treated here. This study considers the general case in which there may be various combinations of droplets, air, and vapour present simultaneously.

3.1/ Literature Review

Appendix B contains a report describing, in detail, the results of a literature review on ignition and flame propagation in droplet-vapour-air mixtures. Although there has been a vast amount of work done in this general field, there still remain many unanswered questions. This is because of the very difficult nature of the experiments and the complexity of the physical and chemical processes that collectively govern flame behaviour.

Since the details of past work are discussed in considerable detail in Appendix B, no repetition will be given here. Rather, the following sections make specific recommendations on the best equations presently available for analytical prediction of the processes concerned. Some deductions based on a critical analysis of the cases of potential interest in modelling spark-ignition (SI) engine performance are given. Also,

the recommended equations are used to calculate some typical results and qualitative conclusions are drawn.

3.2/ Recommended Models for Ignition and Flame Propagation

3.2.1/ Ignition

Equation 65 of Appendix B is recommended for the determination of the ignition characteristics of droplet-vapour-air mixtures or any combination of these. It is a new equation developed in this program:

$$d_q = \{\frac{(1 - \Omega)\phi}{\rho_f D^2}\rho_\alpha [A\ Ln(1 + B) - (1 - A)\frac{L}{HV} Ln(1 + B_{ev})] + \frac{S_{L_o}^2}{100\alpha} \Omega\phi \left(\frac{P_t}{P_o}\right)^2 \left(\frac{1 + K}{1 + K\Omega\phi}\right)\}^{-1/2} \quad (15)$$

where

d_q = quenching distance

Ln = natural logarithm

$L = hfg + C_{pl}(T_S - T_o)$

HV = heating value of the fuel

B_{ev} = transfer number of evaporation

$A = 1$ if $\Omega\phi < 0.5$
$A = 2(1 - \Omega\phi)$ if $0.5 < \Omega\phi < 1.0$
$A = 0$ if $\Omega\phi > 1.0$

$K = f_{st} M_a / M_f$

Ω = vapour fraction (= VF), used here for consistency with the existing literature

The corresponding equation for minimum ignition energy is

$$E_{min} = \frac{\Pi d_q^3}{6} \rho_a C_{pa} \Delta T_{st} \quad (16)$$

3.2.2/ Flame Propagation

A new model was begun, in this part of the study, and is still under development. Until it is completed, the recommended equation for flame propagation is that of Ballal and Lefebvre (see Equation 38 of Appendix B, Section B.3.3.2).

3.3/ Results and Conclusions Derived from the Analytical Models

3.3.1/ Ignition

Equations 15 and 16, or others found in the literature, are primarily useful in delineating trends rather than actually providing a design value to be used for developing the ignition system. In any real device, the energy supplied is always many times the minimum value.

In principle, the equations could serve to show at what point the supplied energy (of a plug, which is, after all, primarily designed for a completely pre-vaporized mixture) is no longer adequate to ignite the mixture because of the presence of liquid droplets. However, the actual energy released in the spark gap is not, in fact, known -- energies generated are usually those supplied (via the capacitor, for example). The fraction of supplied electrical energy available for ignition is lower and depends in a complex way upon both the electrical and the physical conditions (p, T, drop size, electrical conductivity) in the gap between the electrodes.

In the past, ignition models have been used to obtain a better qualitative understanding of the important factors involved. This will also be the case here, and the new ignition model, incorporating the improvements that allow it to be used for the rich cases of interest for spark-ignition engines, will be used to draw some general conclusions of considerable interest.

Figure 23 will be used to illustrate the discussion. It shows the minimum ignition energy needed for several overall equivalence ratios, ϕ, as the vapour fraction, Q, varies, that is, as the mixture goes from one in which all fuel is liquid ($Q = 0$) to entirely vaporized ($Q = 1$). The example chosen uses iso-octane because the flammability data of the vapour and other physical properties are well defined. The conclusions are identical for other droplet sizes, fuels, etc.

All curves decrease as the quantity of vapour present increases, since the droplets require higher energies for ignition than vapour. It is seen in the figure that the difference is a factor of about 30. Thus, for some overall quantity of fuel present, ignition becomes easier if

more of the fuel can be vaporized before the arrival of the spark. However, the major conclusion of this part of the study, well illustrated in this example, is that minimum ignition energy decreases as the overall fuel quantity present goes up. We see for instance that, for the sample conditions, a rich mixture having $\Phi = 5$ requires about the same energy as a fully vaporized lean mixture having $\Phi = 0.5$.

This conclusion seems paradoxical when it is considered that combustion is usually optimum (i.e., highest temperature, fastest flame speeds, etc.) around $\Phi = 1$. All performance characteristics decline on both rich and lean sides of stoichiometric, and for fully vaporized mixtures, a flame will not propagate at all beyond a comparatively modest value of Φ (about 3 or less usually). An Arrhenius-type reaction rate equation contains the product of fuel and oxidant concentrations, which is responsible for the usual behaviour. If either fuel or oxygen are present in excess, there is less of the other present, and the reaction rate decreases. The excess quantity of either acts essentially as a heat sink which tends to suppress the temperature, thereby quenching reaction. The explanation lies in the nature of spark ignition, reflected in the mathematical model, that energy is supplied from outside the mixture. In the usual cases, including the subsequent propagation of the flame once ignited here, the energy to sustain reaction comes from the mixture. Excess of either reactant absorbs some of the heat liberated by combustion, lowers temperature, and quenches the flame. During spark ignition, on the other hand, the mixture is heated to very high temperature at no energy cost to itself. Then, reaction begins and propagation starts outward when the heat at this high temperature exceeds losses. In fact, if ϕ is sufficiently high, the droplets evaporating do ultimately absorb enough energy to have a quenching effect; however, this occurs at equivalence ratios in excess of 100 in the present example and so is of no practical interest.

The extreme right point ($\Omega = 1$) on the two upper curves would normally be beyond the lean flammability limit for vapour-air mixtures. Yet, here they are seen to be ignitable and will produce some initial propagation into the mixture. Again, this is because of the outside energy supplied. If heated to adiabatic flame temperature, even a very lean mixture produces a net rate of energy gain. It is the inability to attain the high temperature (and the fast reaction rates occurring there) that results in a flame propagation failure.

The conclusion is then that, as far as ignition is concerned, very rich mixtures, with or without droplets, will ignite better than a stoichiometric fully vaporized mixture. The only limit to this conclusion is at either astronomically rich mixtures or when the droplets are so large

that they wet the electrodes and cause a failure in spark passage. Rich misfire in an engine under cold-starting conditions must therefore be the result of a propagation failure. From the point of view of ignition alone, richer is better as long as electrode gap blockage can be avoided.

3.4/ Experimental Study of Heterogeneous Combustion

3.4.1/ Background

The propagation of a flame through a mixture of air, fuel vapour, and droplets is exceedingly complex. There have been numerous experimental and theoretical studies in this general area, and those are described in detail in Appendix B.

The aim of this entire project was to provide information needed for other programs in which specific candidate methanol fuels are evaluated in real engines under cold ambient conditions. In such work with actual engines, there are many aspects that are still poorly understood. One of these is the state of the mixture in the cylinder at the moment the spark plug fires. Although large quantities of liquid fuel are fed into the engine during cold cranking, much of this liquid passes the rings and enters the crankcase. Thus, the instantaneous fuel/air ratio at ignition is not known, but is clearly leaner than the delivered one. Furthermore, the condition of the fuel actually present during combustion is also uncertain. This is because the droplets present appear to be mainly formed as the film of liquid cascades through the intake valve during induction. The spray of droplets produced by the carburetor or injector is likely not the major influence on droplet size or size distribution in the cylinder because impact against the walls of the manifold destroys most of this spray before it enters the cylinder.

This part of the present study aimed to provide some qualitative guidance in establishing the overall behaviour of a flame propagating through a droplet-vapour mixture such as may exist under cold-starting conditions. The behaviour of a flame passing through a rich vapour phase that also contains droplets is expected to be qualitatively different than one passing through a mixture having a lean vapour phase and relay flame transmission from one droplet to the next. A thorough study of these complex situat ns would require a lengthy and costly program. In this small study, therefore, the intention was only to attempt to observe the nature of combustion in heterogeneous mixtures under engine-like conditions of pressure, temperature, and turbulence. This could potentially provide very valuable guidance to analytical modelling by revealing the gross behaviour typical of the conditions of interest. Without such

information, neither mathematical analysis nor design strategies can be directed at the appropriate areas.

The rapid compression machine available at RMC provides the facility needed to study engine combustion behaviour under conditions allowing visual access, better instrumentation, and control of a wide range of operating conditions.

The use of actual Escort engine hardware, as originally planned, would have provided the best simulation of the conditions under study in the companion cold-starting project. However, it became apparent as soon as detailed design began that the size and shape of the components would not permit the sort of optical access which was most needed. It was therefore decided, instead, to modify the compression machine to provide the best possible optical access so as to provide as much information on the flame/droplet interaction as possible. Accordingly, a quartz cylinder head and side windows were designed to use the larger core already available in the machine.

3.4.2/ Rapid Compression Machine Experiments

The rapid compression machine (RCM) was adapted to allow some preliminary observations to be made on the combustion of droplet-vapour-air mixtures under simulated engine conditions. Figure 24 is a schematic of the operation of the device. Figure 25 is a photograph of the complete installation. Figure 26 shows the details of the optical disc used to illuminate the combustion chamber. It consists of six quartz plate windows 3.8 x 5.1 x 0.6 cm (1.5 x 2 x 0.25 in) thick, through which the concentrated light is passed into the combustion chamber. Figure 27 is a quartz head. A 11.4 cm diameter x 2.5 cm (4.5 x 1 in) thick quartz disc is cemented in place, which gives a full view of the combustion chamber.

Figure 28 shows the optical disc and quartz head assembled to the machine. Provision for a mounting pressure transducer, temperature probe, glass plug, and fuel injection nozzle is made on the side of the optical disc.

The operation of the rapid compression machine (RCM) is simple. A single segmented rod extends the length of the machine and connects the pneumatic driver piston at the left end to the working piston at the right end. A hydraulic damping/snubbing cylinder is located between the driving and working cylinder so as to allow the velocity profile and compression ratio to be tailored to whatever circumstances are required in the test. Table 3 shows the main dimensions of the RCM.

3.4.3/ Results and Discussion

For these tests the RCM was fitted with a quartz head and optical disc to allow complete optical access and lighting of the combustion chamber. A small injector was built to supply fuel to the combustion chamber. A measured quantity of fuel was premixed with high-pressure air and sprayed into the combustion chamber close to TDC. The glow plug was used to ignite the mixture. A dual-beam oscilloscope with a camera was used to obtain a continuous record of the relative timing of compression, pressure rise, and piston position. Figure 29 shows a record of compression pressure (lower curve) and piston position (upper curve). Figures 30 and 31 show fuel spray and combustion of the air/fuel mixture. Driving air pressure used was 4826 kPa (700 psi). Each horizontal division represents 10 ms, and each vertical division is 1379 kPa (200 psi).

During these trials, ignition was observed several times through the quartz disc; however, there was not enough light for photographs. Several combustion pressure peaks were observed; however, expected compression pressures and temperatures were not attained.

3.5/ Recommendations and Conclusions

1/ Recommended equations for ignition and flame propagation are given. These are based on existing techniques plus new analyses conducted in this program.

2/ It has been shown that flame propagation failure rather than ignition failure is the main mechanism responsible for unsuccessful combustion for the rich droplet-vapour-air mixture.

3/ During RCM testing with a quartz head, ignition was observed through the quartz disc. Several combustion pressure peaks were observed. Further study is warranted after these leaks are repaired.

4/ CONCLUSIONS

The following are the main conclusions from this program:

1/ The composition of the vapour phase of seven methanol M85 blends has been determined experimentally as a function of vapour fraction.

2/ A new model is proposed for predicting the vapour pressure of methanol blends. It uses a previously developed multi-component volatility model for the gasoline component, pseudo-binary mixing, and a modified form of Raoult's Law corrected for non-ideality. The model predicts M85 vapour pressure and vapour phase composition very well over the temperature range studied experimentally, namely, 0 to 40°C. The model can be extended to other methanol-gasoline blends, requiring only the measured RVP to determine the single non-ideality constant.

3/ The Odgers equation has been used in conjunction with the composition data to calculate the vapour phase flammability limits as evaporation proceeds. These have been corroborated by a simple experimental evaluation. Further experimental evaluation is unwarranted because the prediction of the vapour phase composition and of the extent of evaporation under real conditions is subject to much greater uncertainty than the inherent variation in flammability limits for those fuels.

4/ Recommended equations for ignition and flame propagation are given. These are based on existing techniques plus new analyses conducted in this program.

5/ It has been shown that flame propagation failure rather than ignition failure is the main mechanism responsible for unsuccessful combustion for the rich droplet-vapour-air conditions expected in engines during cold starting and warm-up.

6/ During RCM testing with a quartz head, ignition was observed through the quartz disc. Several combustion pressure peaks were observed. These tests held promise and will continue after problem rectification.

5/ REFERENCES

[1] Shiller, J.W., "Mathematical Prediction of the Effects of Gasoline Composition on Reid Vapour Pressure, Refueling Emissions and Their Reactivity," SAE paper #860532 presented at the Society of Automotive Engineers' 1986 International Congress and Exposition, Detroit, February 24-28, 1986.

[2] Furey, R.L., and B.E. Nagel, "Composition of Vapor Emitted from a Vehicle Gasoline Tank during Refueling," SAE paper #860086, presented at the Society of Automotive Engineers' 1986 International Congress and Exposition, Detroit, February 24-28, 1986.

[3] Bardon, M.F., and V.K. Rao, "Calculation of Gasoline Volatility," J. Inst. Energy: 57, p. 343-348, Sept. 1984.

[4] Rao, V.K., and M.F. Bardon, "Estimating the Molecular Weight of Petroleum Fractions," Ind. Eng. Chem., Process Des. Dev., Vol. 27, No. 2, April 1985.

[5] "Distillation of gasoline, naphtha, kerosene an similar petroleum products," Test D86, American Society for Testing and Materials, Philadelphia, 1978.

[6] "Vapour pressure of petroleum products (Reid method)," Test D323, American Society for Testing and Materials, Philadelphia, 1979.

[7] Odgers, J., and D. Kretchmer, "On the Vapour Pressure of Hydrocarbons," Report No. J.O. 143, Universite Laval, January 1985.

[8] Odgers, J., D. Kretchmer, and J. Halpin, "Weak Limits of Premixed Gases," at the ASME Gas Turbine Conference 1984, Paper No. 84-GT-144.

Table 1/ Composition of Methanol Fuel Blends

Blend No.	Methanol		Super Non-leaded		n-Butane		Dimethyl Ether		Total	
	% by mass	kg	% by mass	kg	% by mass	kg	% by mass	kg	% by mass	kg
1	85.9	44.0	14.1	7.2	-	-	-	-	100.0	51.2
2	85.7	43.8	12.3	6.3	2.0	1.0	-	-	100.0	51.1
3	85.7	43.6	10.4	5.3	3.9	2.0	-	-	100.0	50.9
4	85.6	43.5	8.7	4.4	5.7	2.9	-	-	100.0	50.8
5	85.7	43.9	12.3	6.3	-	-	2.0	1.0	100.0	51.2
6	85.6	43.8	10.5	5.4	-	-	3.9	2.0	100.0	51.2
7	85.7	43.8	8.6	4.4	-	-	5.7	2.9	100.0	51.1

Table 2/ Constants for Use with M10 and M85 Vapour Fractions

Value	M10	M85	M85/BUT	
A	1.0	1.0	1.0	
B	-0.5	-0.92	-0.92	
			VF<0.11	VF >.11
C	----	42	1.53	42
D	----	0.17	1.55	0.17
E	----	----	6	
F	----	----	1.26	
G	----	----	0.145	

Table 3/ Constants for Use with the Volatility Equations

Value	Low-Volatility Gasoline	Indolene	High-Volatility Gasoline
f_{10}	1.2069×10^9	1.3648×10^9	1.6639×10^9
f_{11}	1.4798×10^9	-1.6359×10^9	-1.8462×10^9
f_{12}	-4.6577×10^9	2.6455×10^9	-3.6719×10^8
f_{13}	2.6188×10^9	-1.7111×10^9	1.4094×10^9
f_{20}	3299.6	3120.7	2992.4
f_{21}	1543.5	1933.0	1040.2
f_{22}	-1656.3	-2209.8	-364.04
f_{23}	938.68	1136.8	69.751
M_0	72.490	67.352	59.522
M_1	68.157	75.661	39.983
M_2	-71.724	-81.387	-8.1226
M_3	43.571	43.789	0.54229
ΔH_0	27669	26242	24217
ΔH_1	22682	28610	26140
ΔH_2	-32232	-43030	-30498
ΔH_3	27407	29853	19263

Note: Both M and ΔH are mean values for the vapour phase which exists at that VF.

Table 4/ Dimensions of Rapid Compression Machine

COMBUSTION CYLINDER	
Bore	9.848 cm (3.877 in)
Stroke	11.43 cm (4.50 in)
Displacement	868.5 cm^3 (53.0 in^3)
Compression ratio	17:1
HYDRAULIC BRAKING CYLINDER	
OD	17.78 cm (7.0 in)
ID	15.24 cm (6.0 in)
Stroke	11.43 cm (4.5 in) adjustable
DRIVING AIR CYLINDER	
OD	17.78 cm (7.0 in)
ID	15.24 cm (6.0 in)
Stroke	11.43 cm (4.5 in) adjustable
Max. pressure	6895 kPa (1000 psi)
Area	182.32 cm^2 (28.26 in^2)
Volume per stroke	2084.4 cm^3(127.2 in^3)

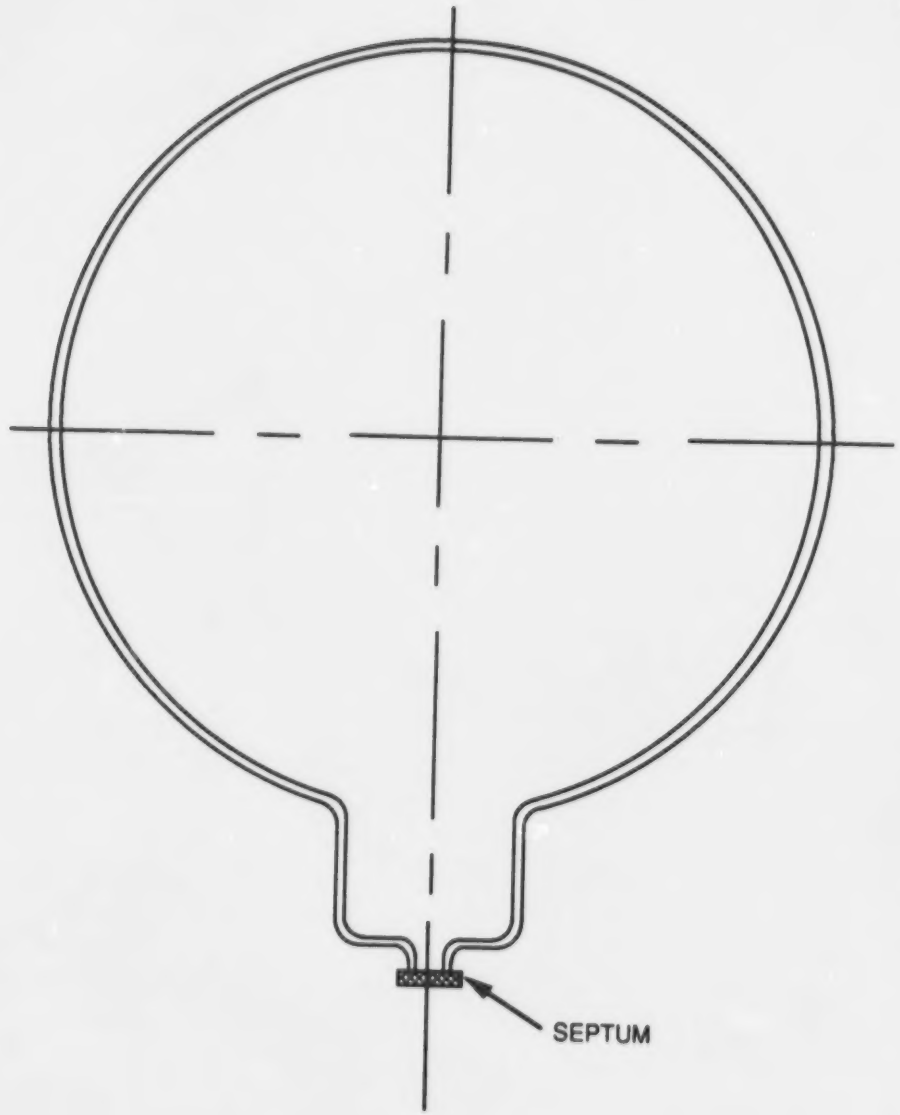

Figure 1/ Gas Globe with Septum

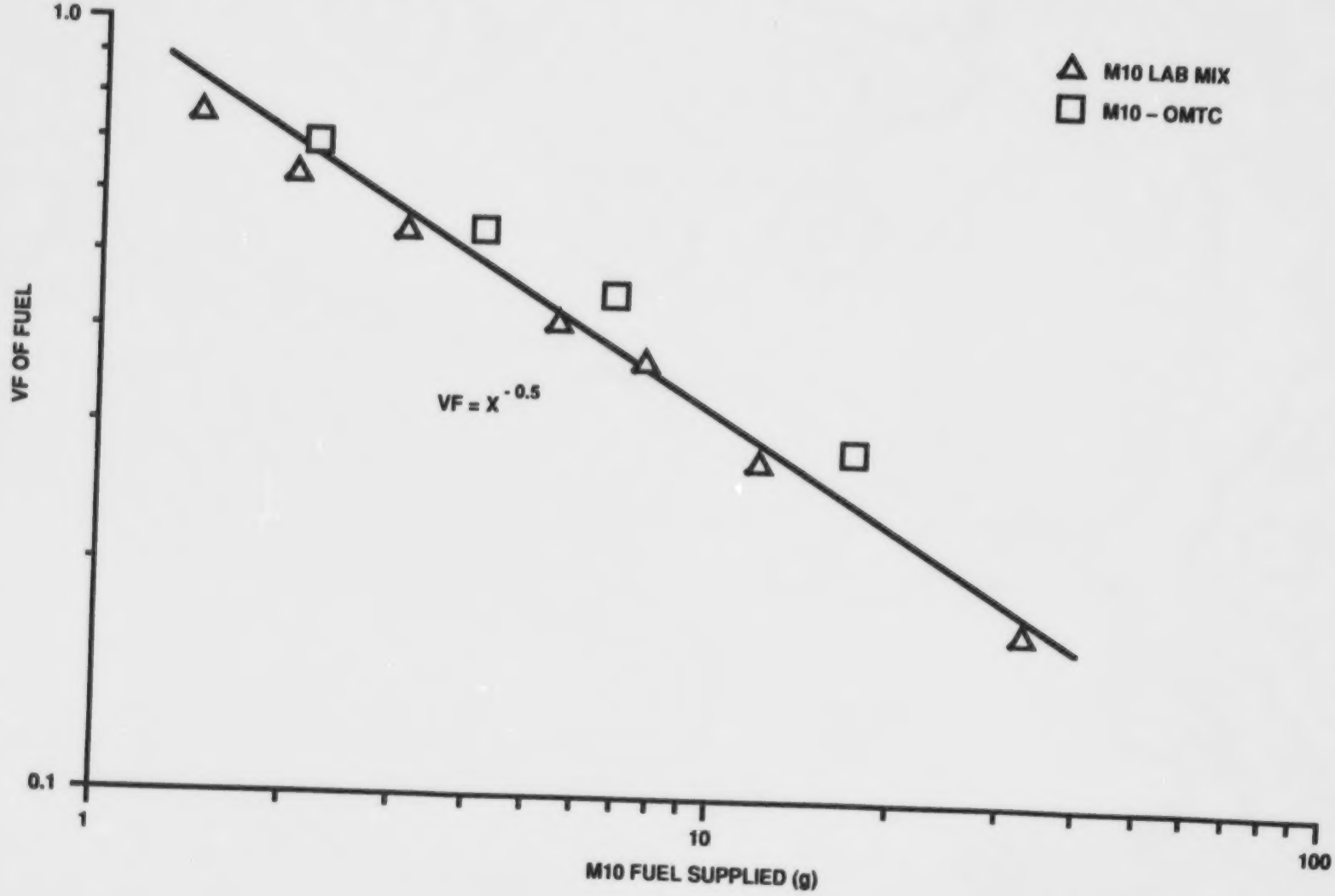

Figure 2/ Vapour Fraction for M10 Fuels

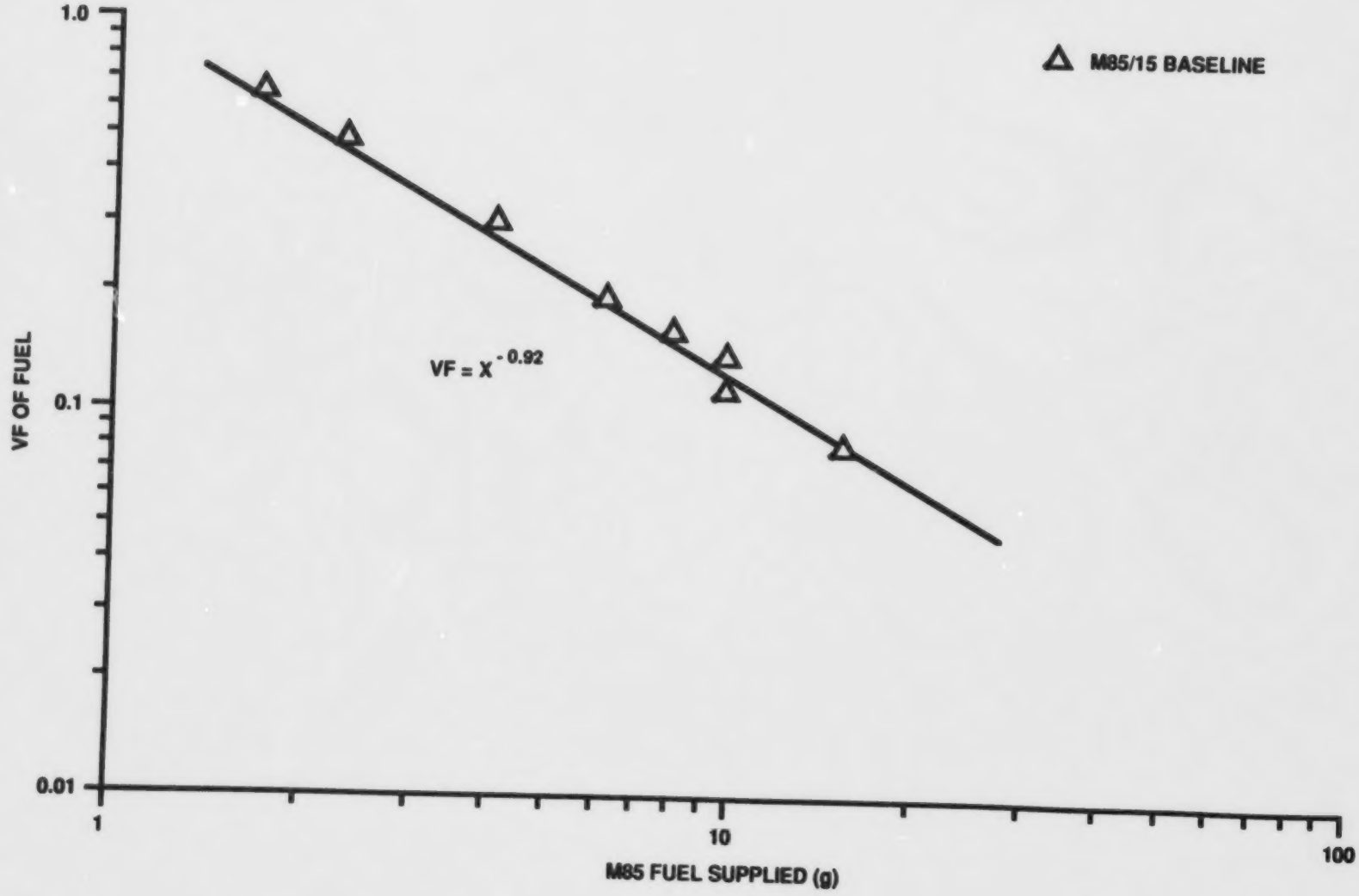

Figure 3/ Vapour Fraction for M85 Fuels

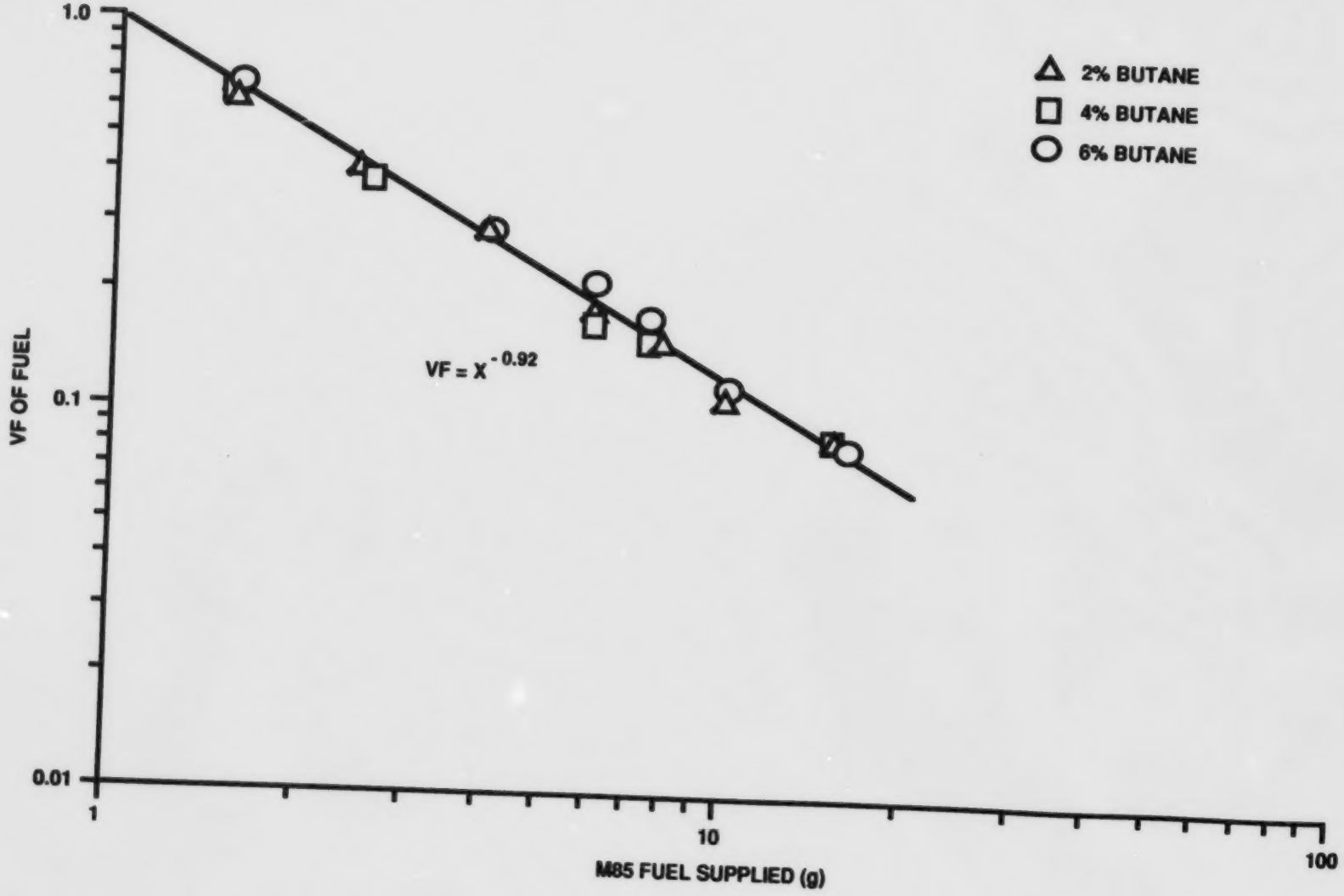

Figure 4/ Vapour Fraction for M85 Fuels With Butane

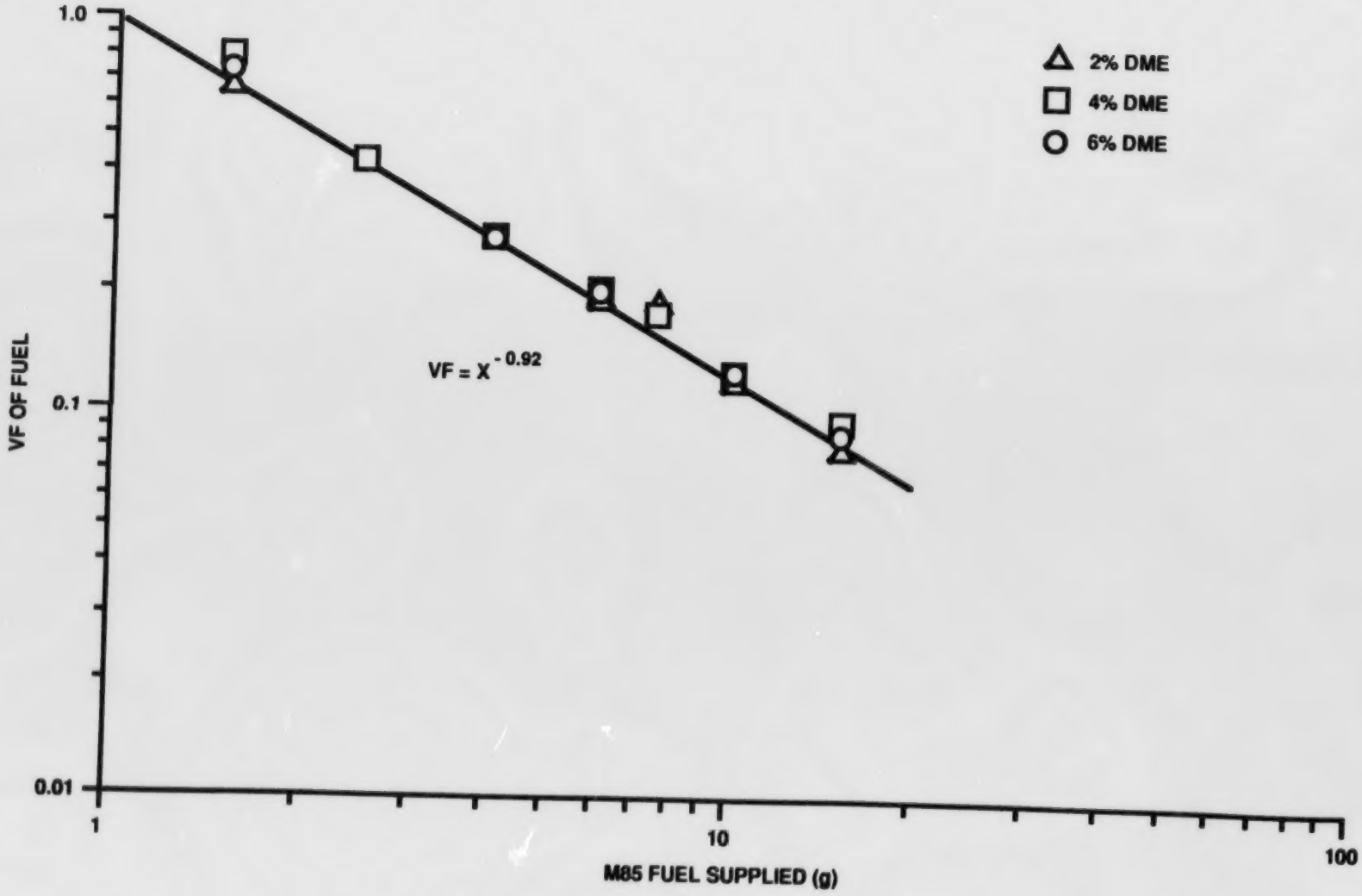

Figure 5/ Vapour Fraction for M85 Fuels with DME

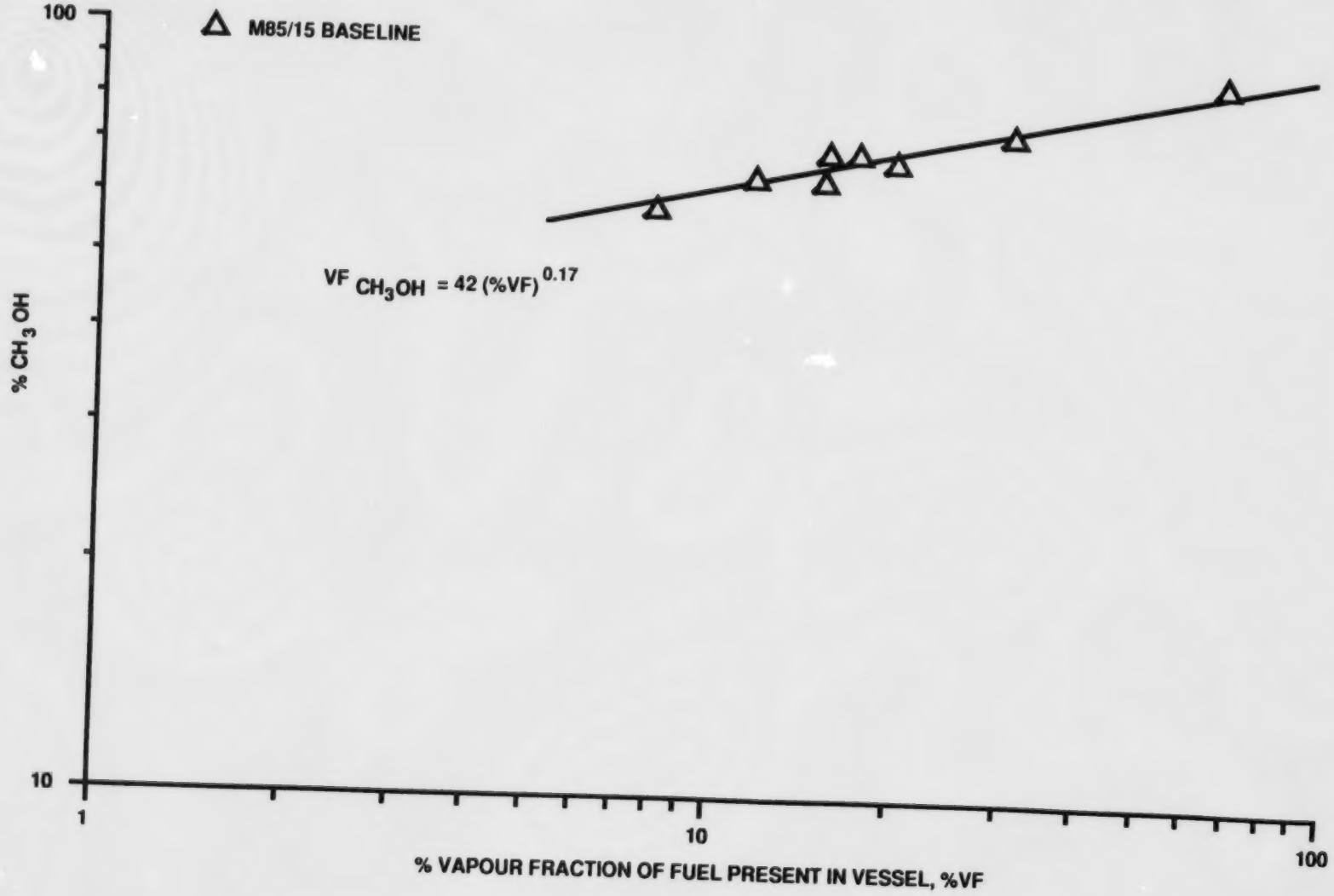

Figure 6/ Methanol Vapour Fraction for M85 Fuels

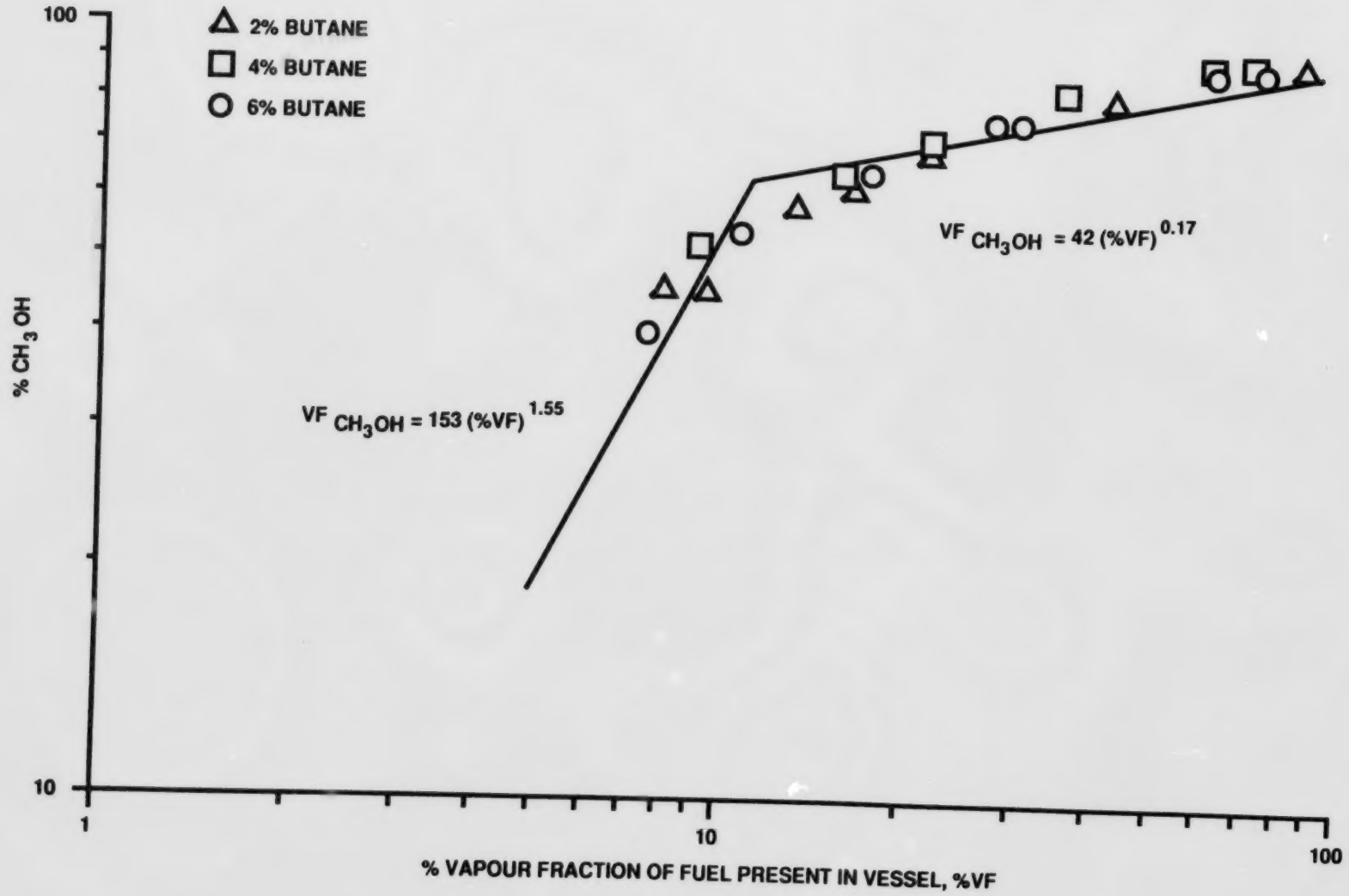

Figure 7/ Methanol Vapour Fraction for M85 Fuels with Butane – Linear Plot

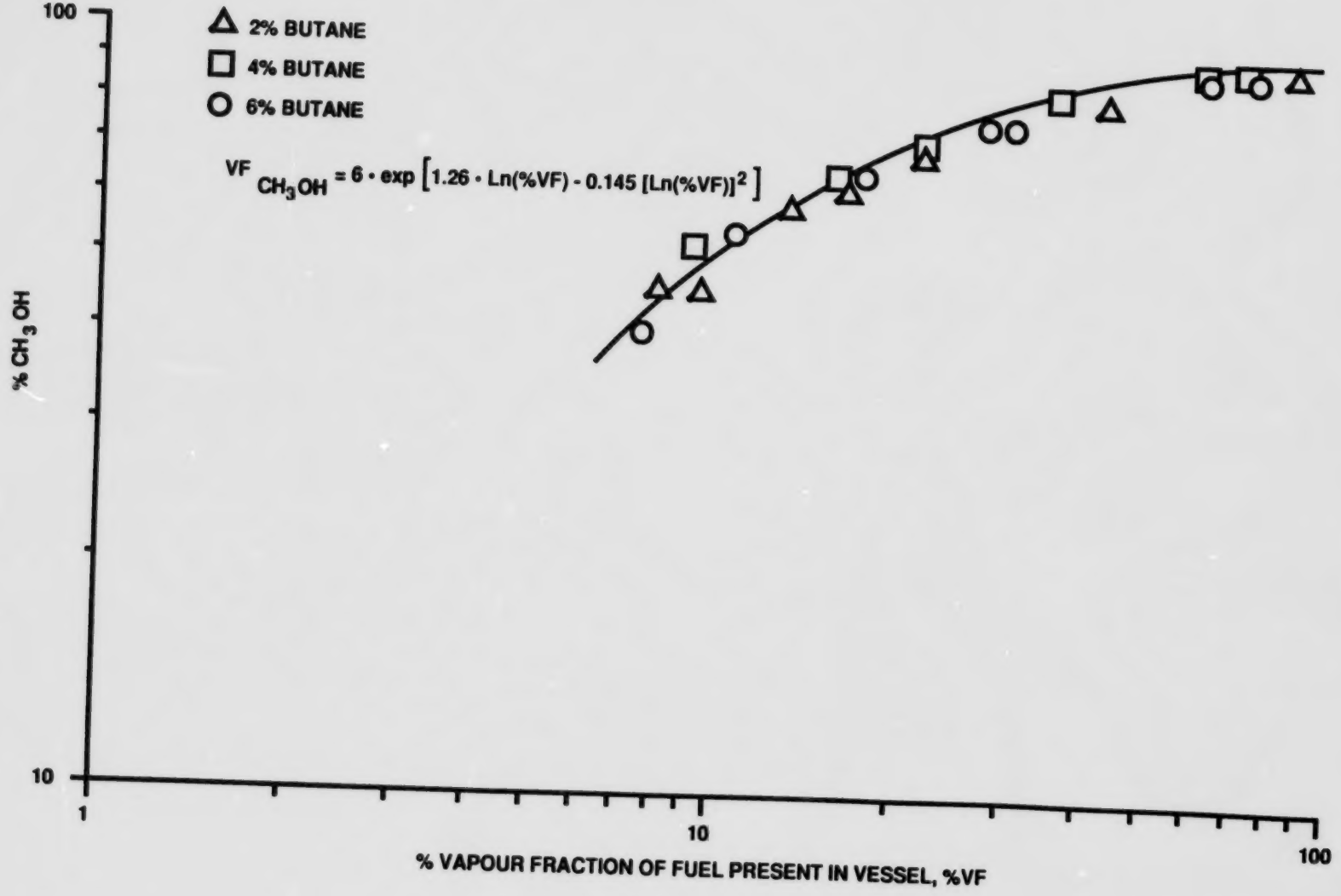

Figure 8/ Methanol Vapour Fraction for M85 Fuels with Butane – Curved Plot

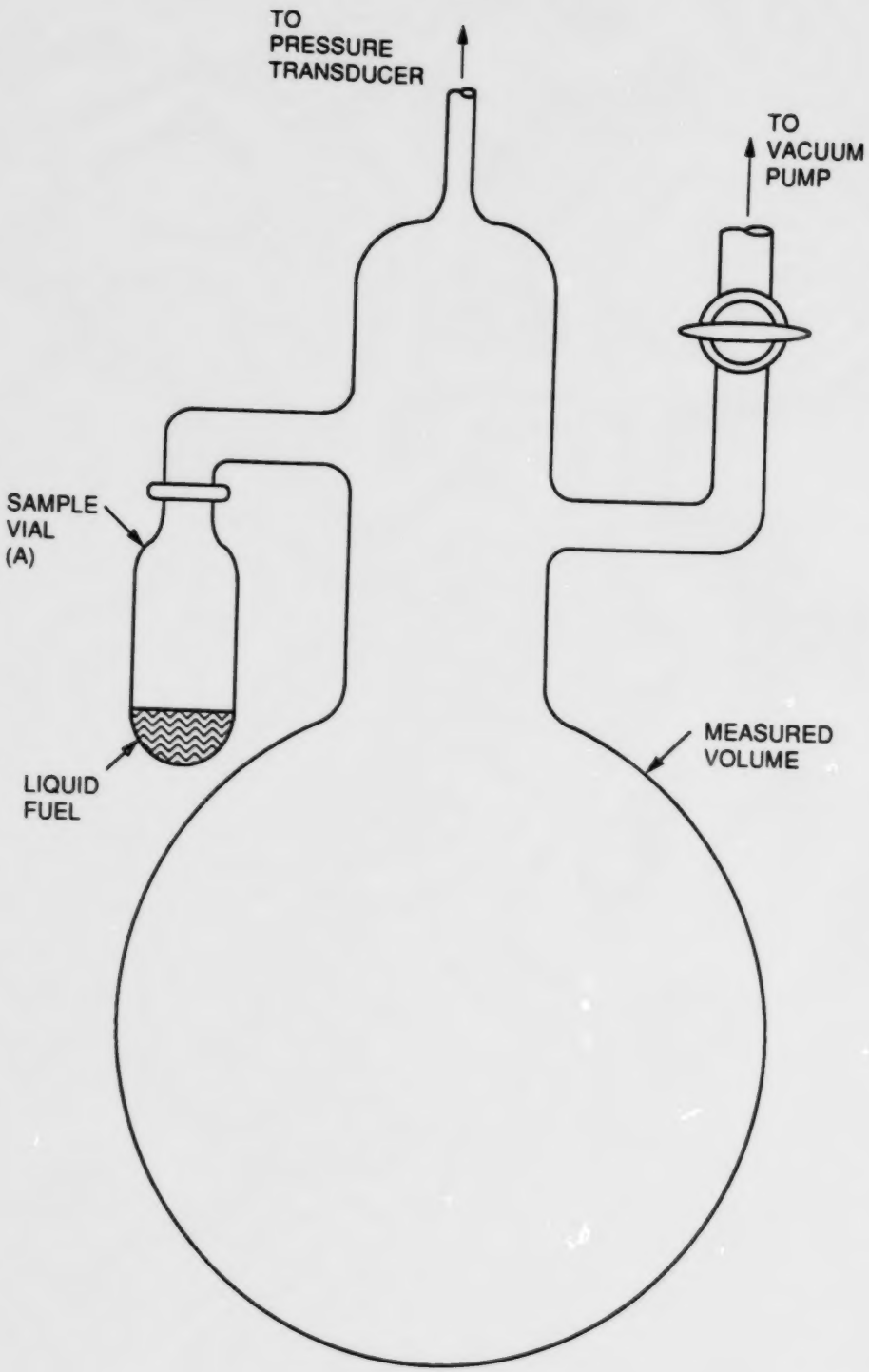

Figure 9/ Vapour Pressure Experimental Apparatus

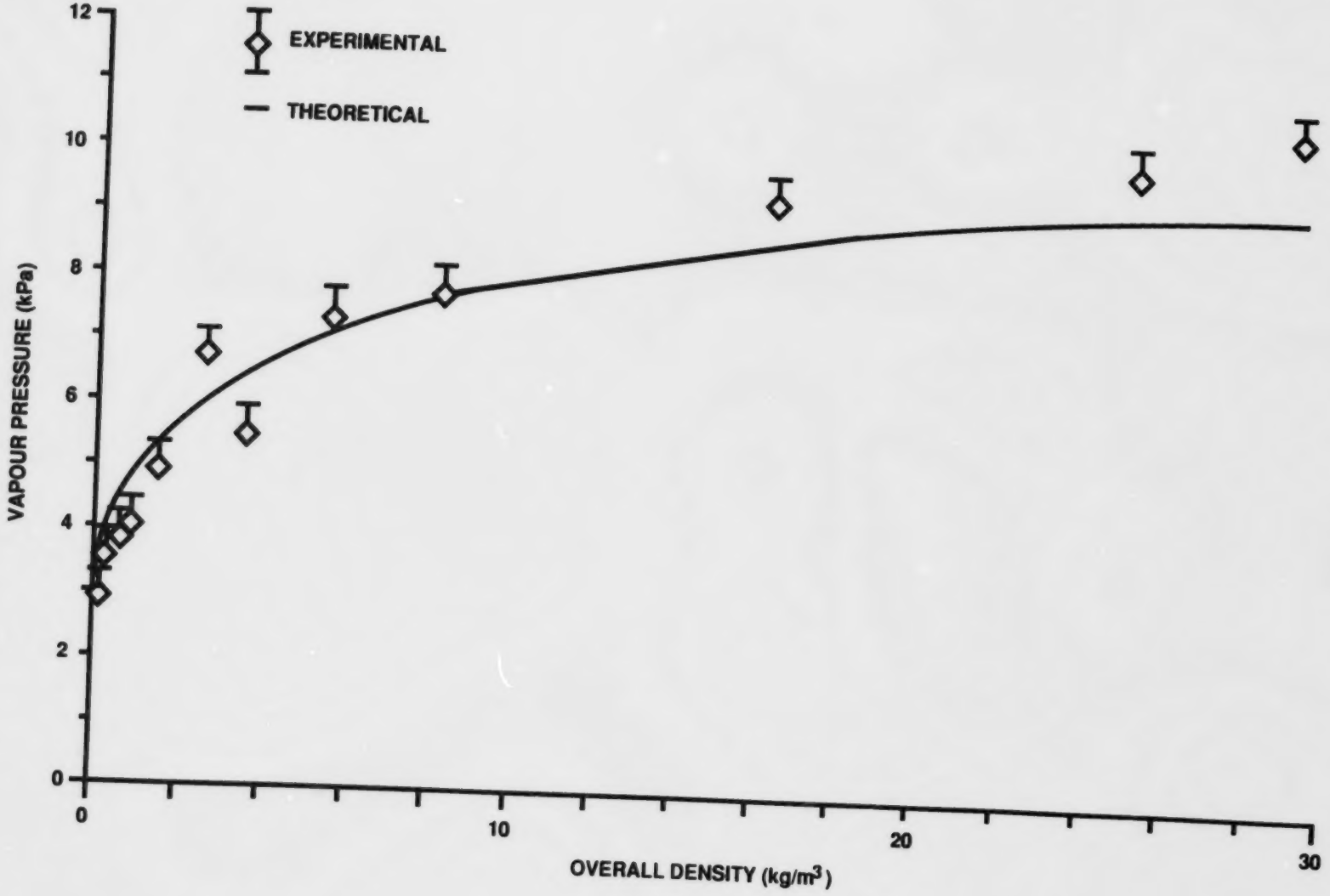

Figure 10/ Vapour Pressure vs Density: M85 at 0° C

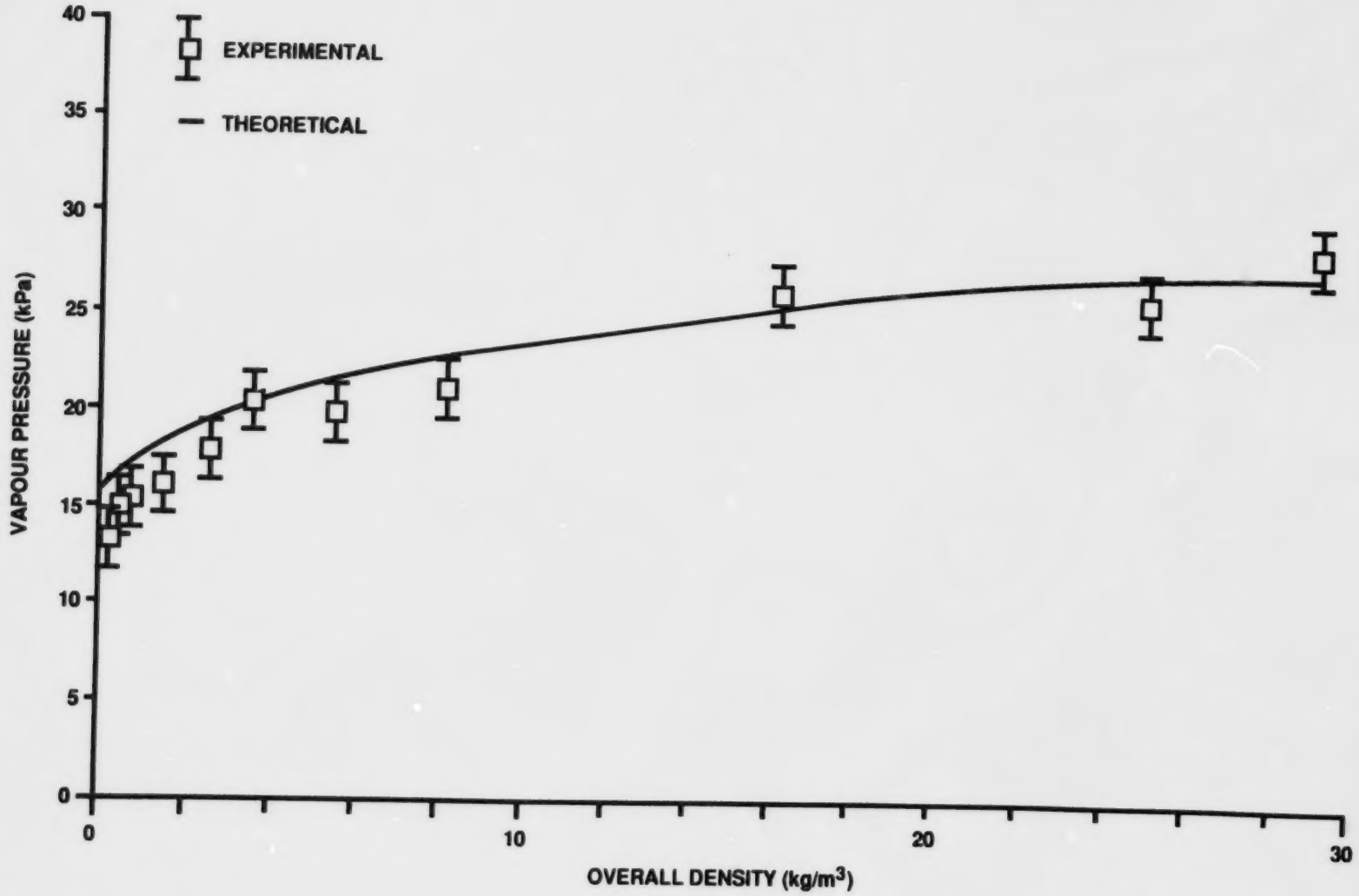

Figure 11/ Vapour Pressure vs Density: M85 at 25° C

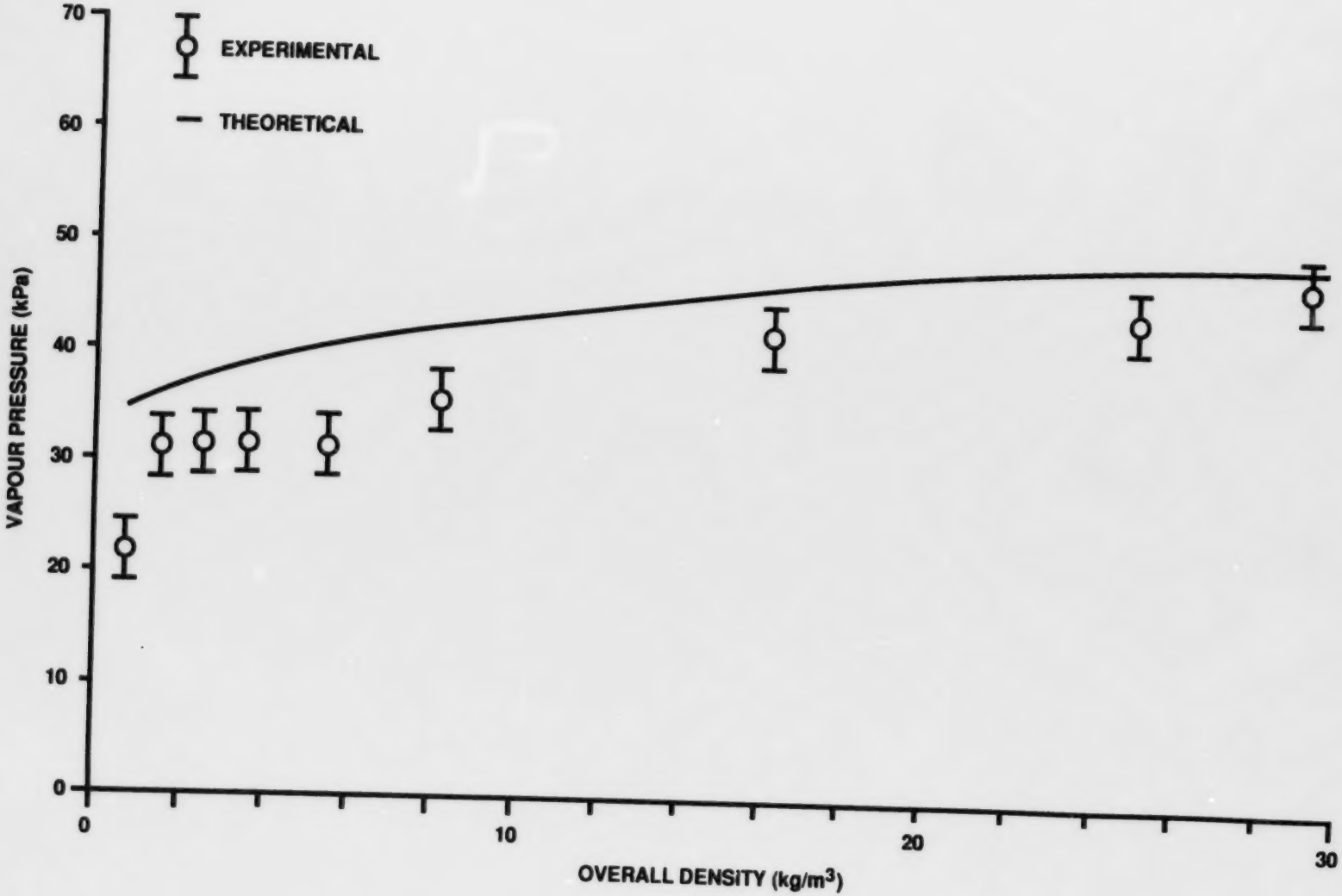

Figure 12/ Vapour Pressure vs Density: M85 at 40° C

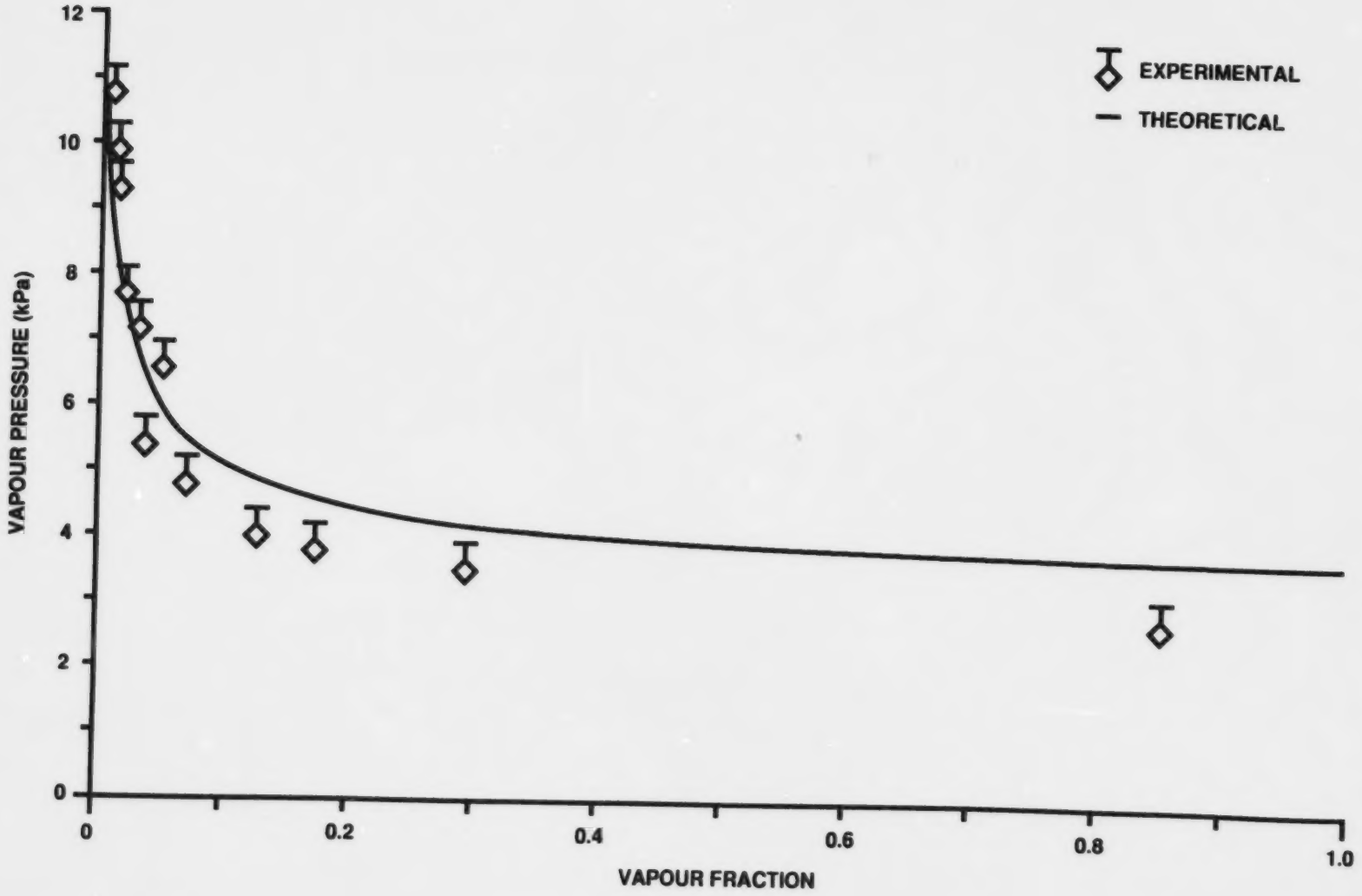

Figure 13/ Vapour Pressure vs Vapour Fraction: M85 at 0° C

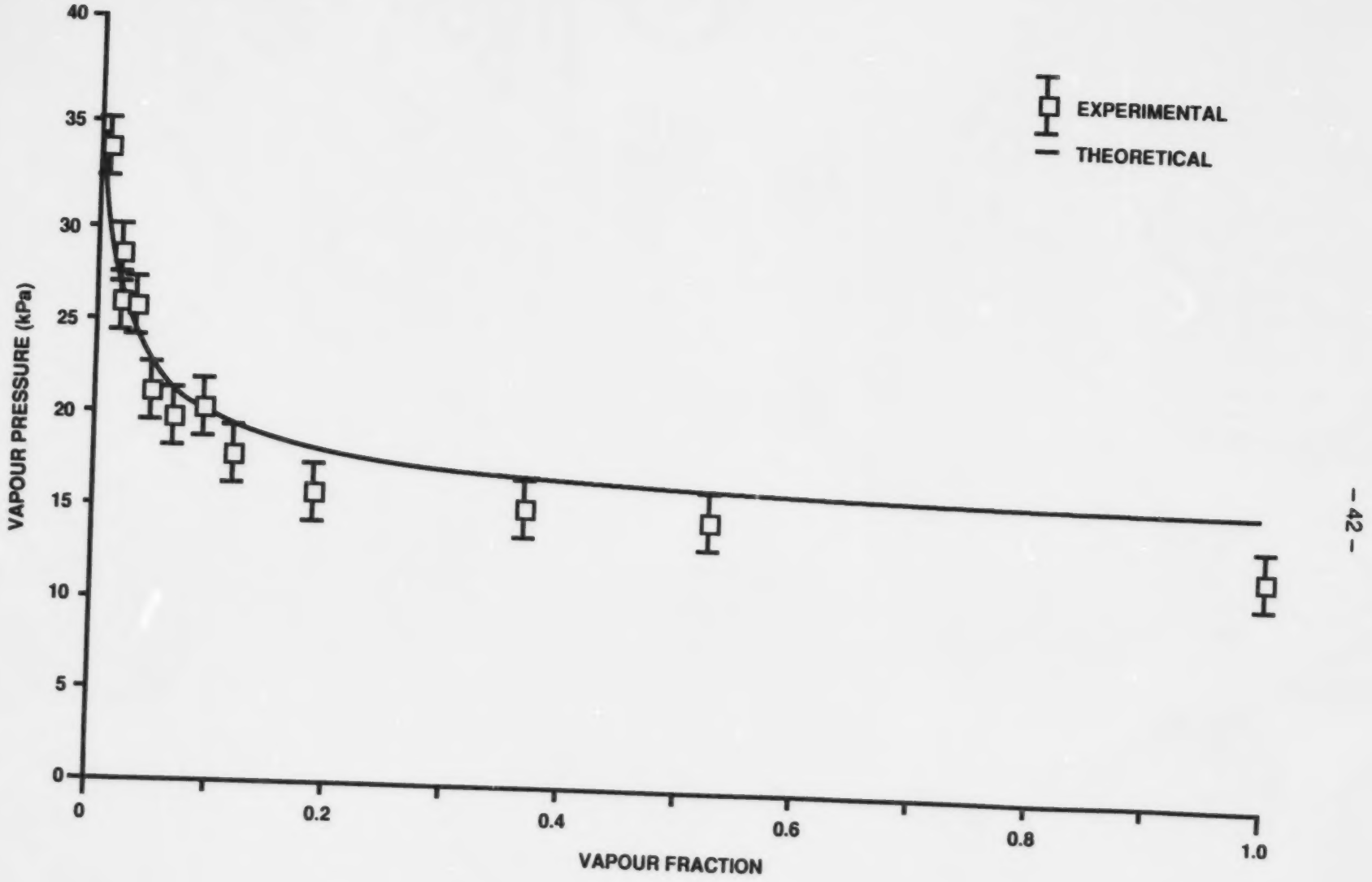

Figure 14/ Vapour Pressure vs Vapour Fraction: M85 at 25° C

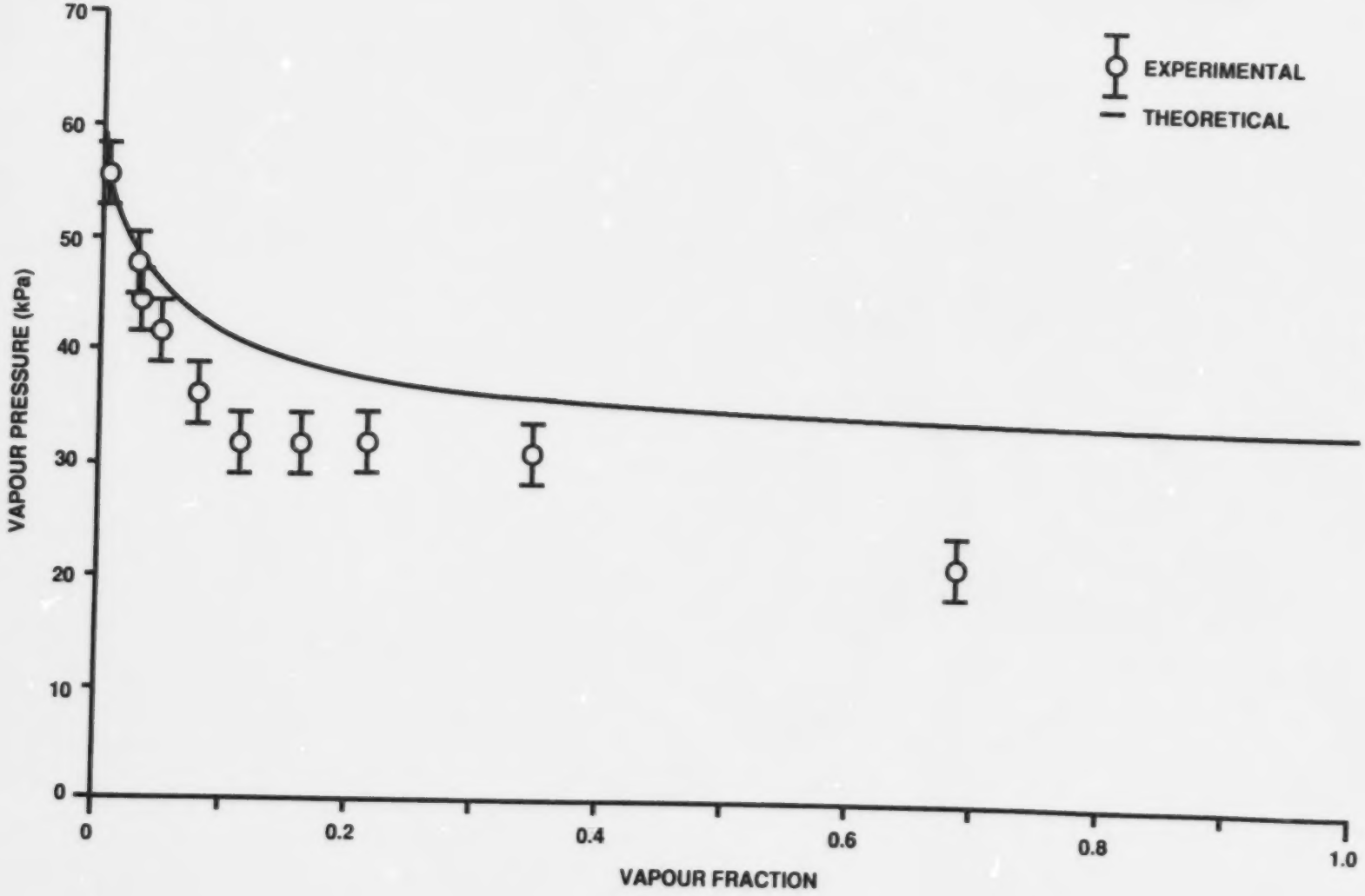

Figure 15/ Vapour Pressure vs Vapour Fraction: M85 at 40° C

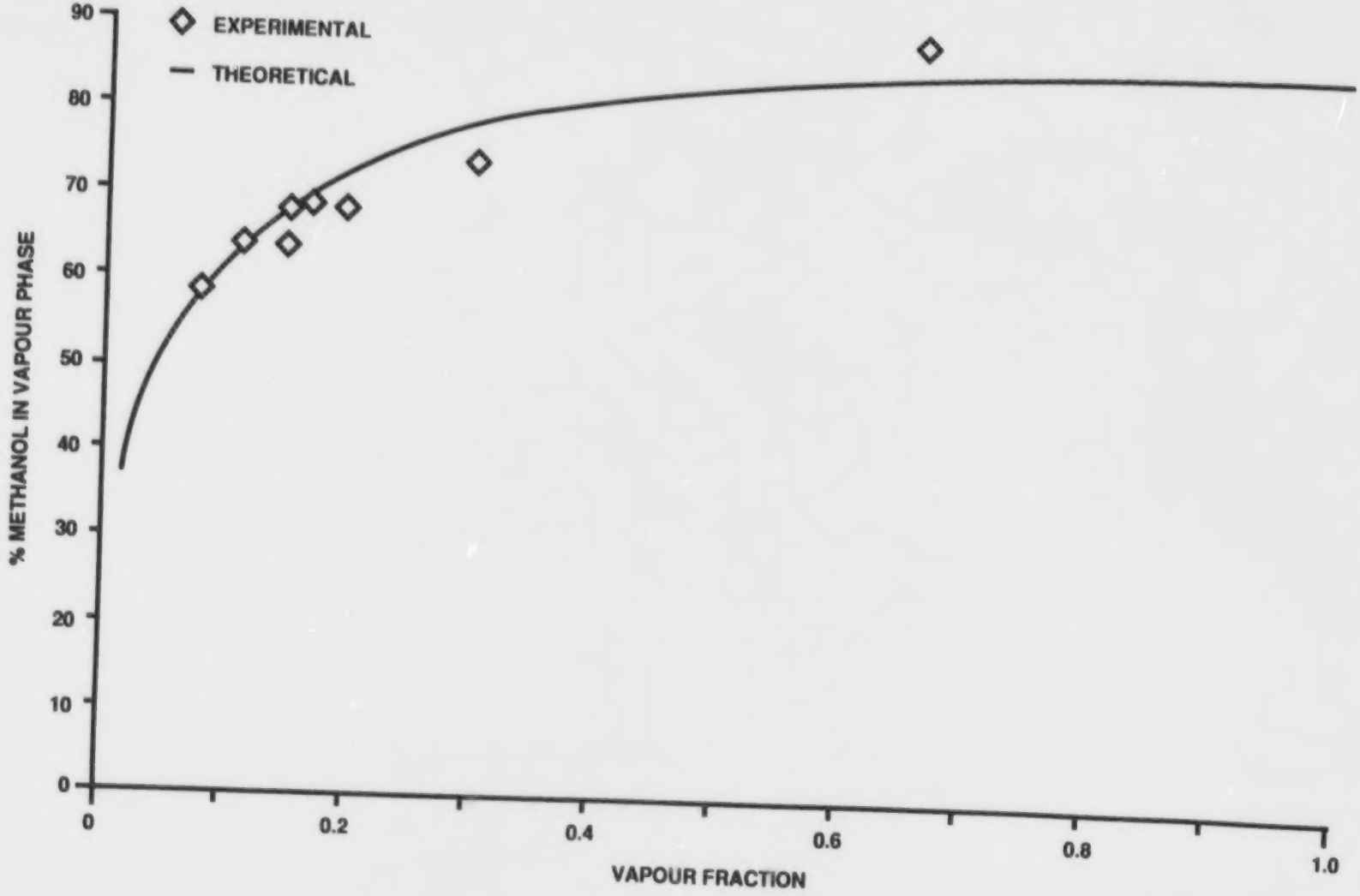

Figure 16/ Methanol Vapour Concentration: M85 at 25° C

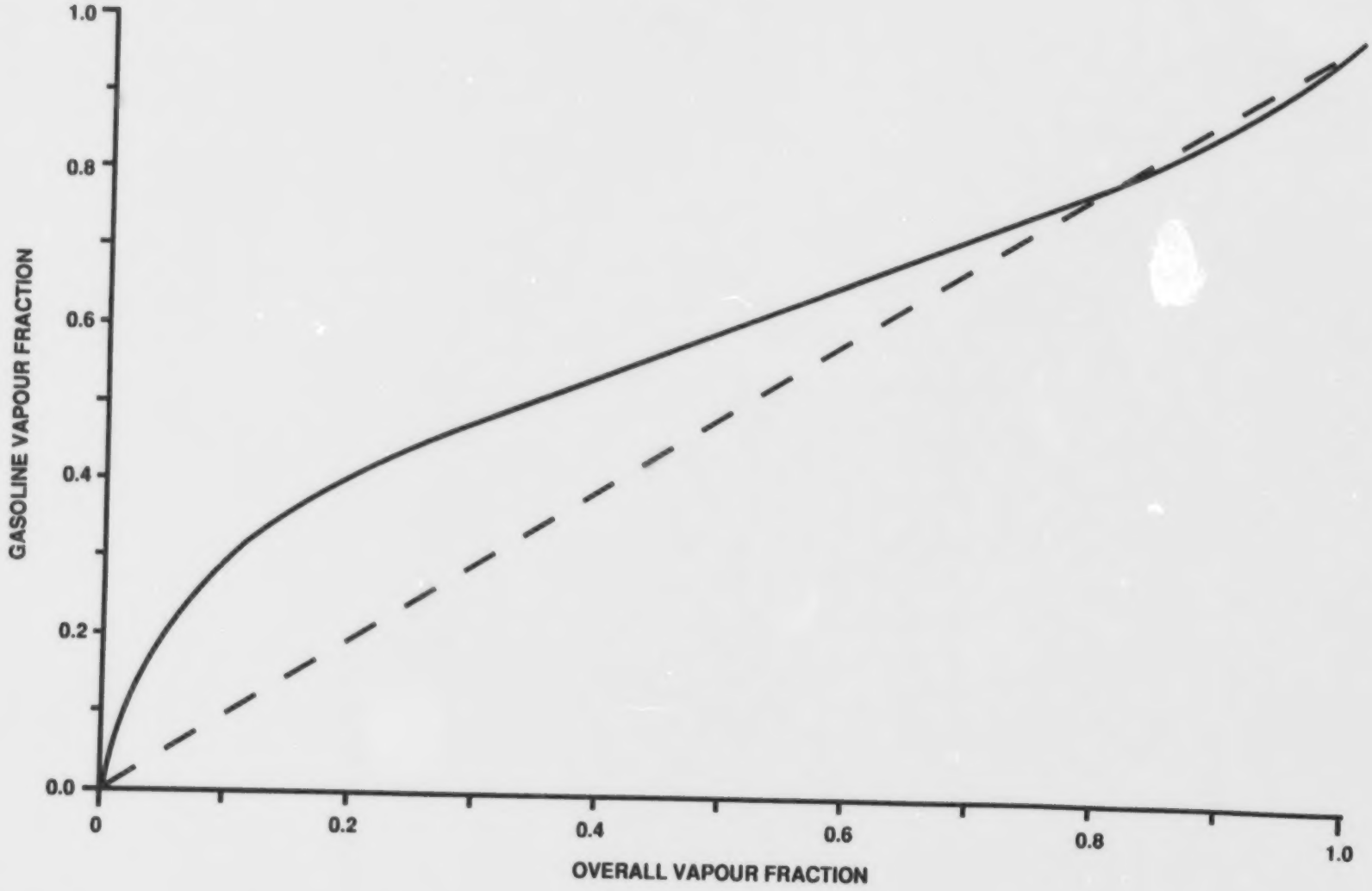

Figure 17/ Proportion of Gasoline Evaporated from M85 (15% Gasoline) at 0° C

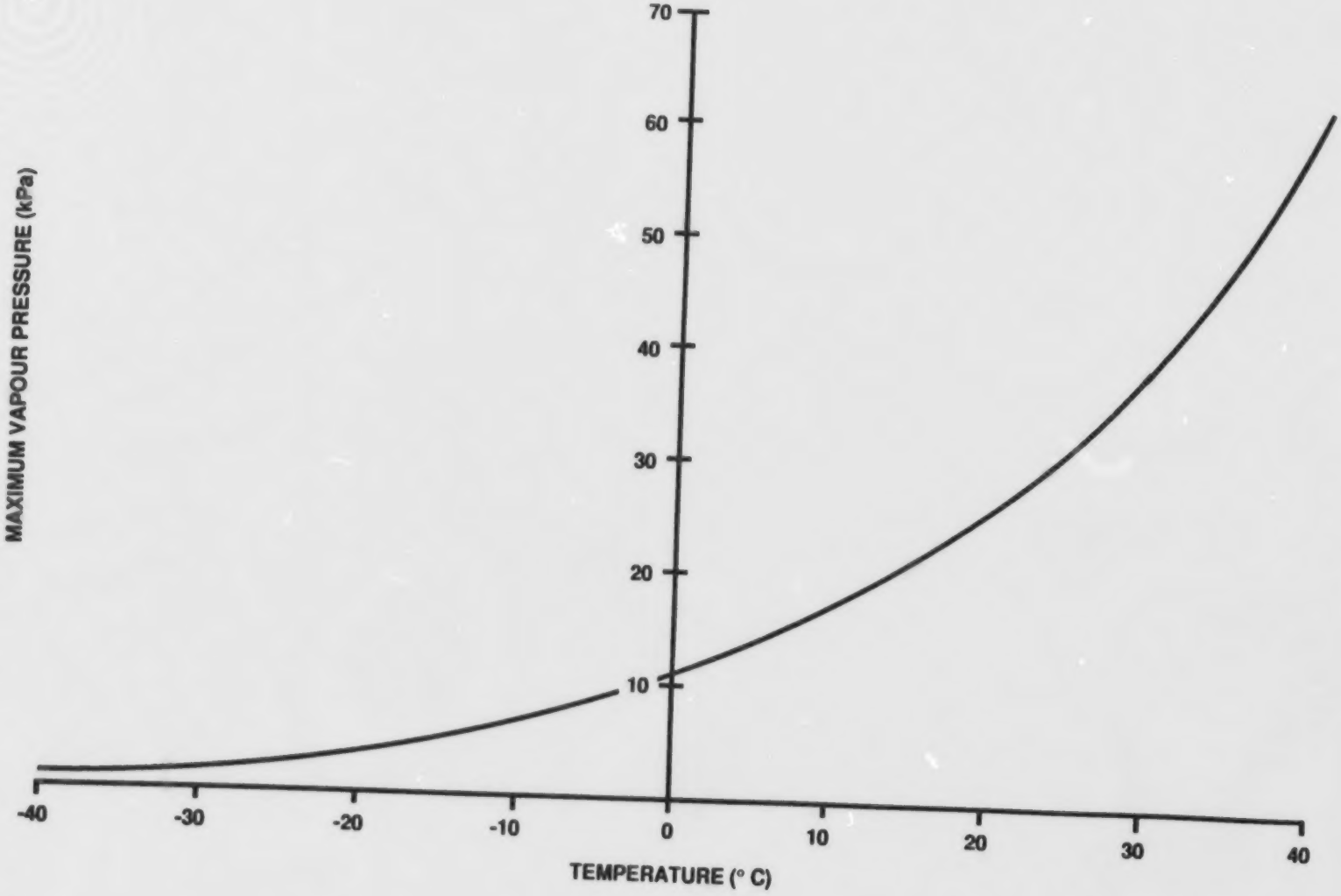

Figure 18/ Calculated Peak Vapour Pressure of M85 (15% Gasoline)

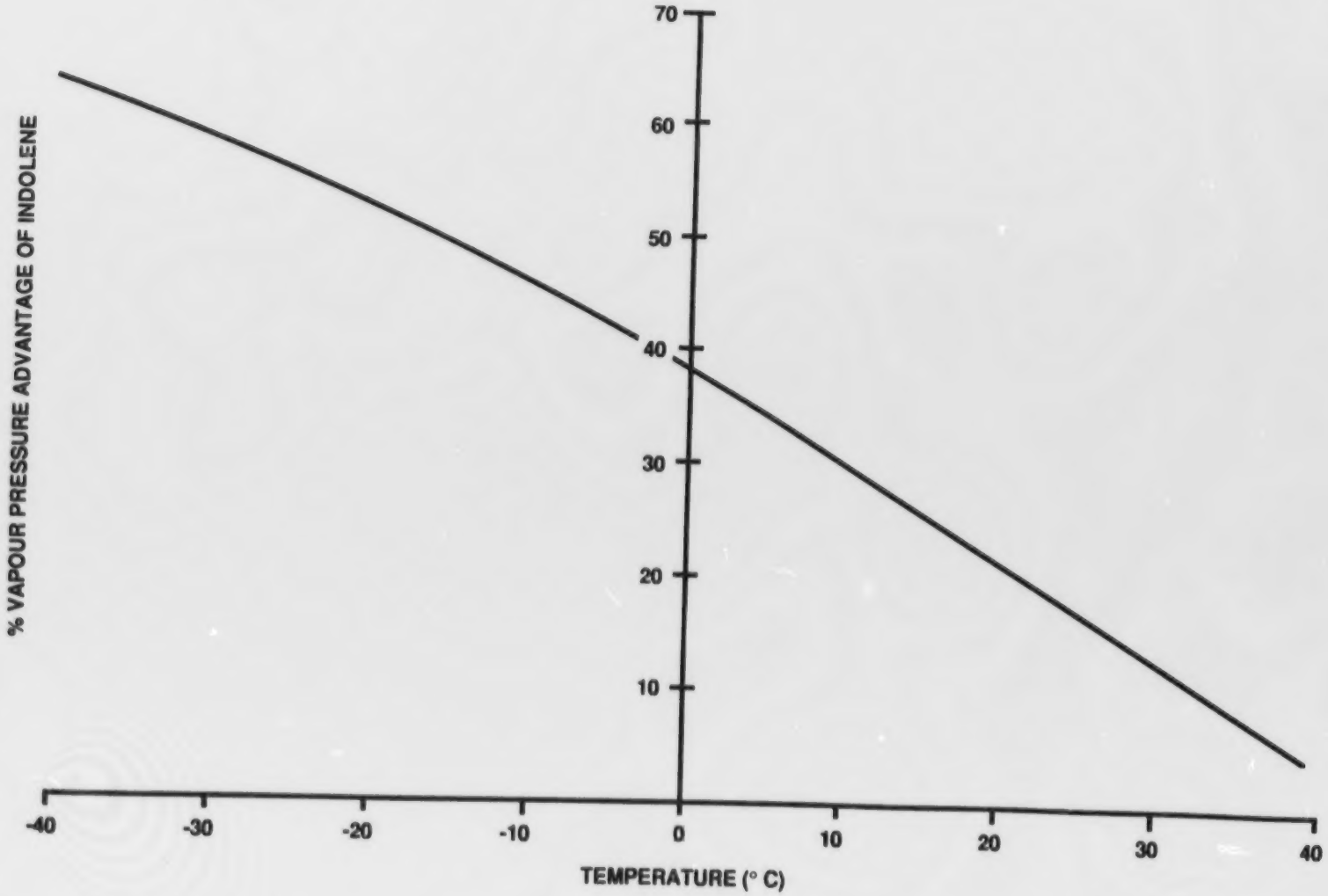

Figure 19/ Vapour Pressure Advantage of Indolene Compared to M85

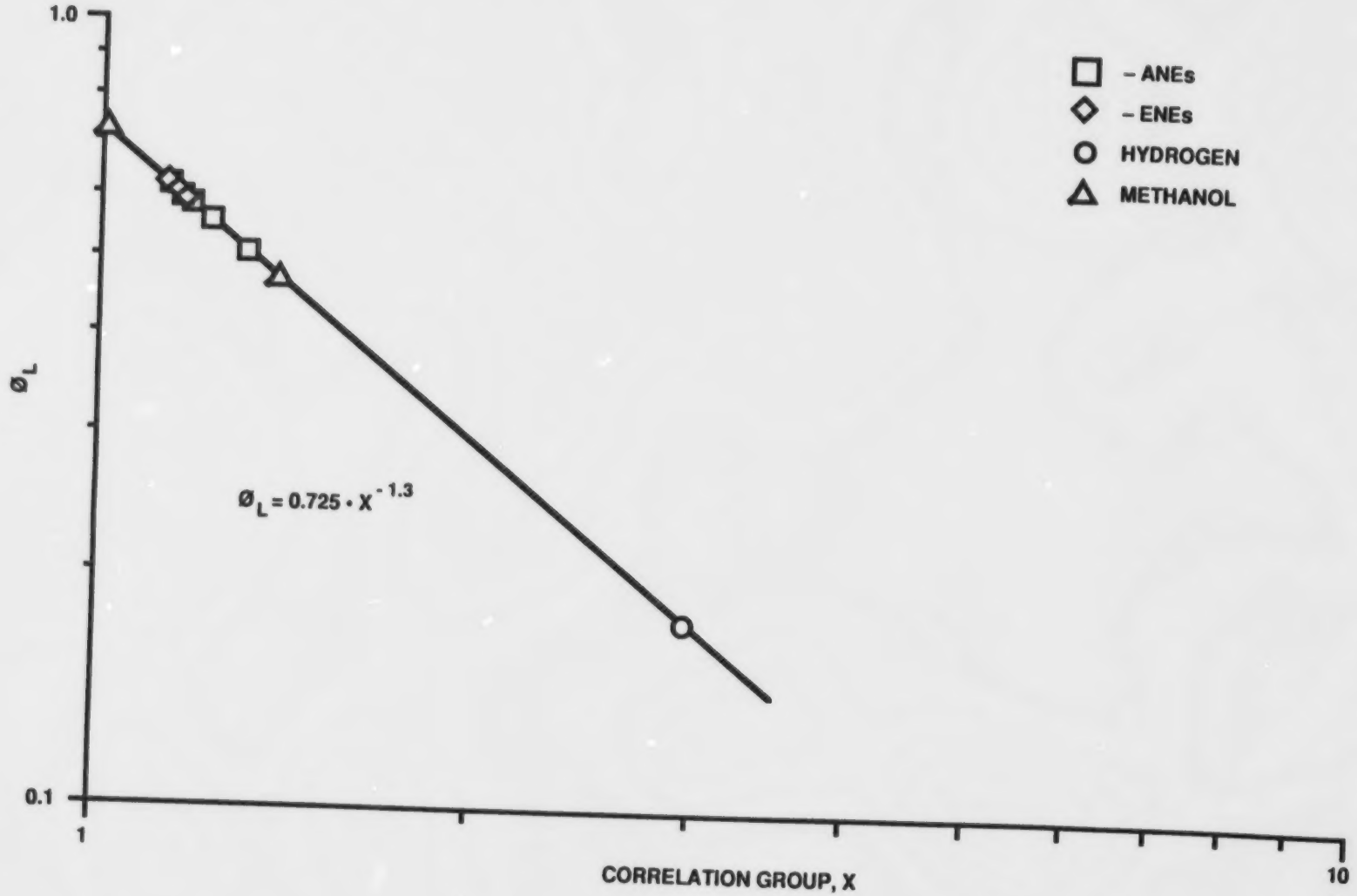

Figure 20/ Lean Burn Limits for Hydrocarbons

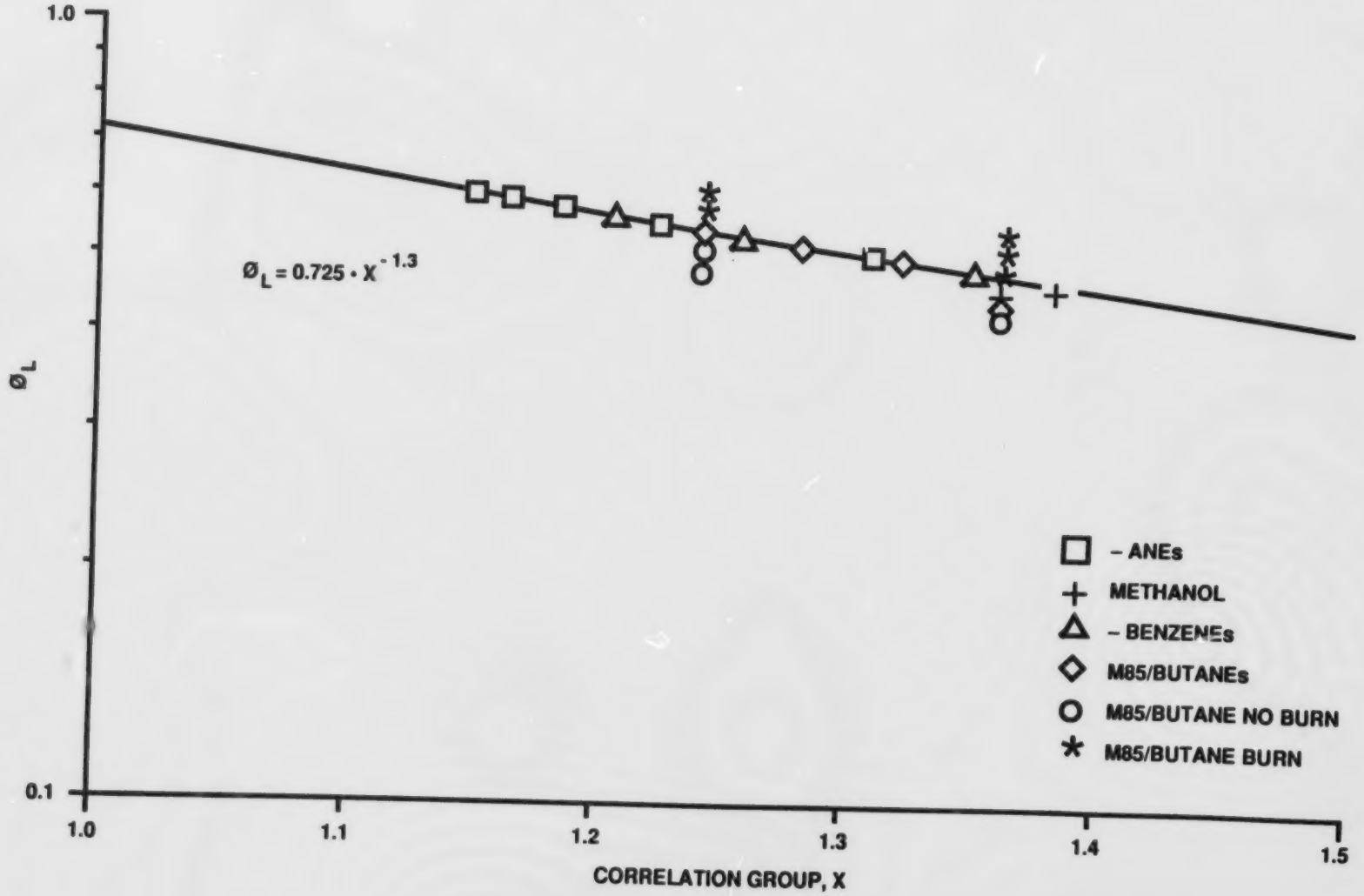

Figure 21/ Lean Burn Limits for M85/Butane

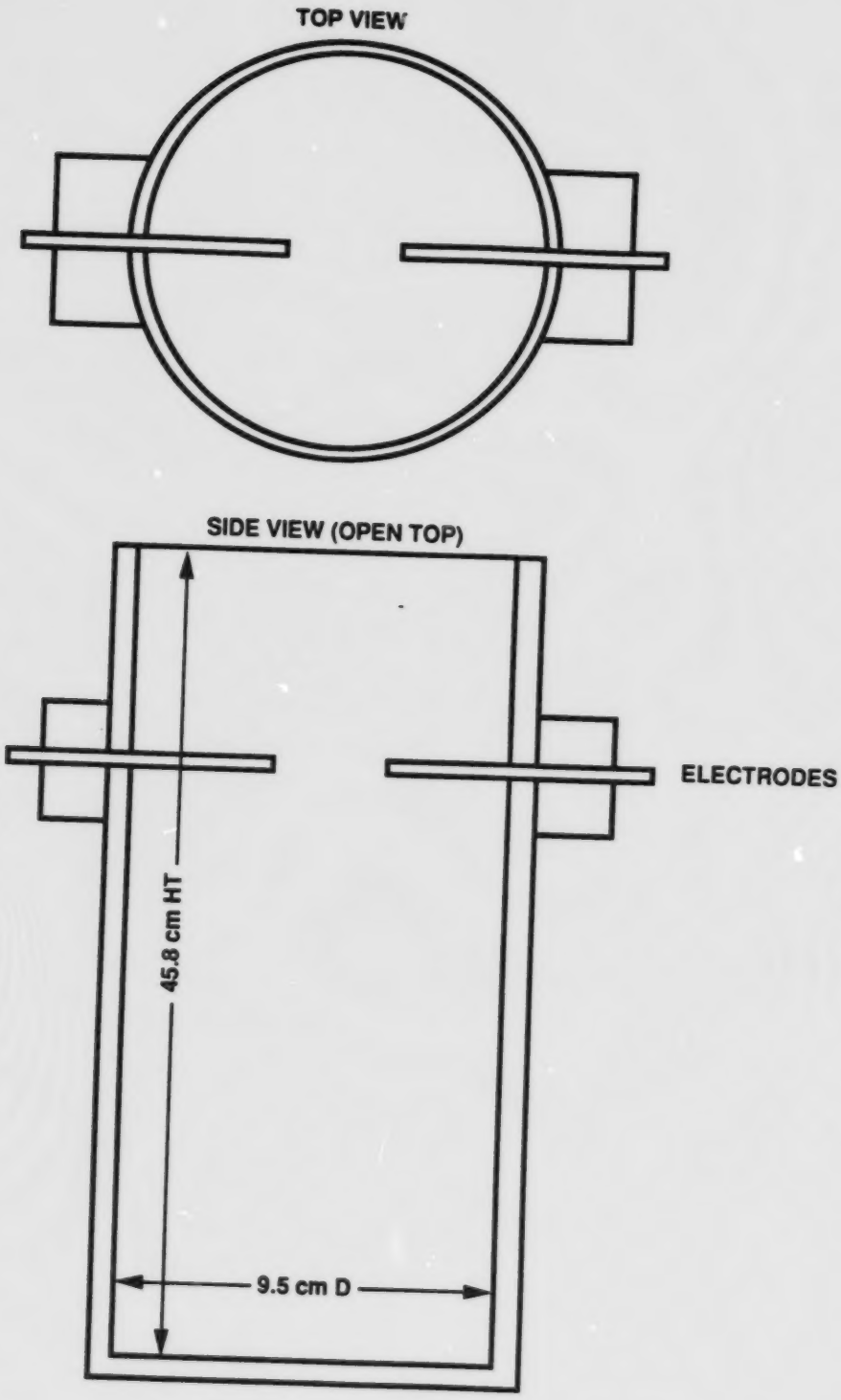

Figure 22/ Flame Tube Cylindrical Fuel Bomb

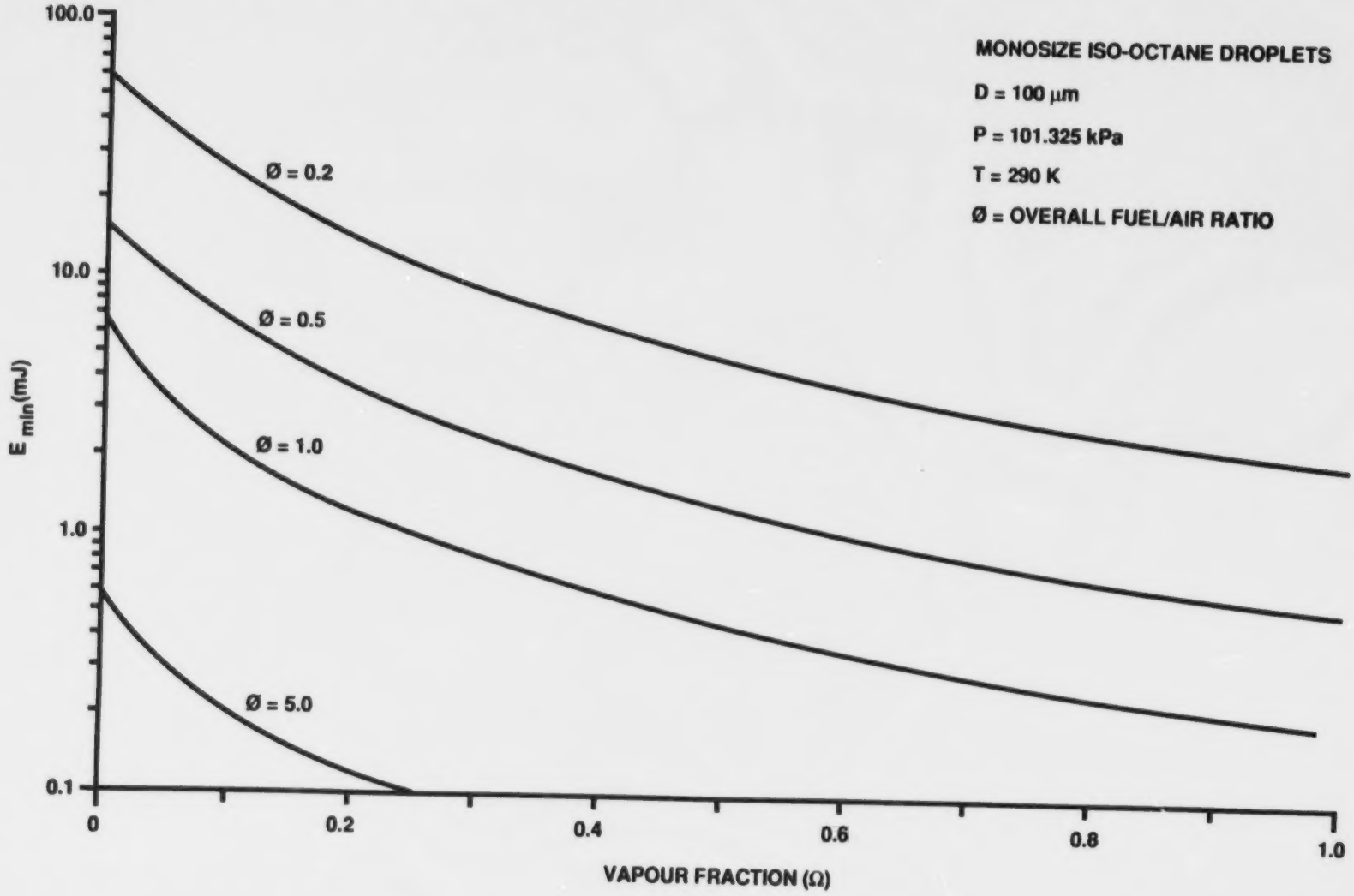

Figure 23/ Minimum Ignition Energy vs VF

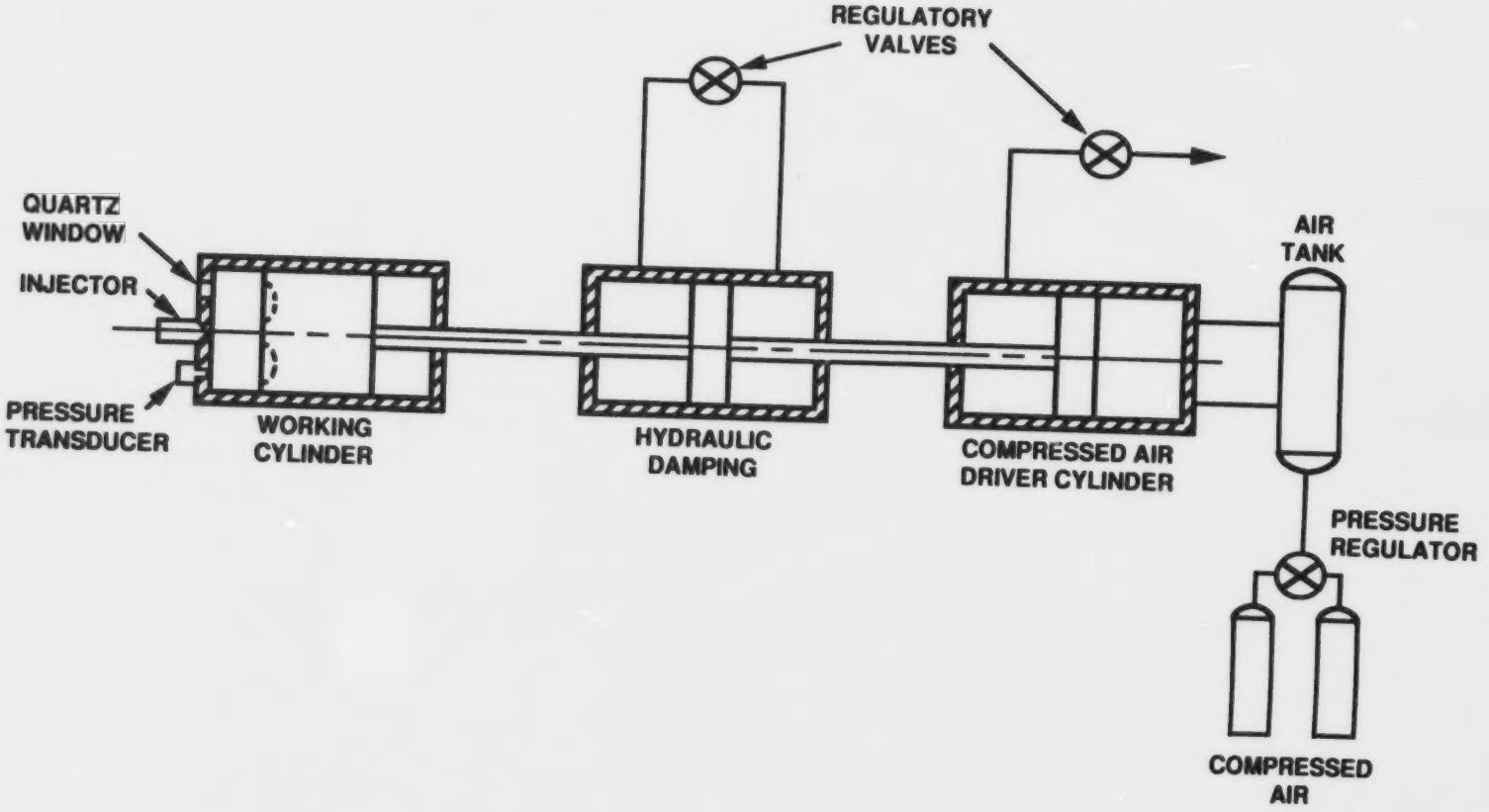

Figure 24/ Schematic of Rapid Compression Machine

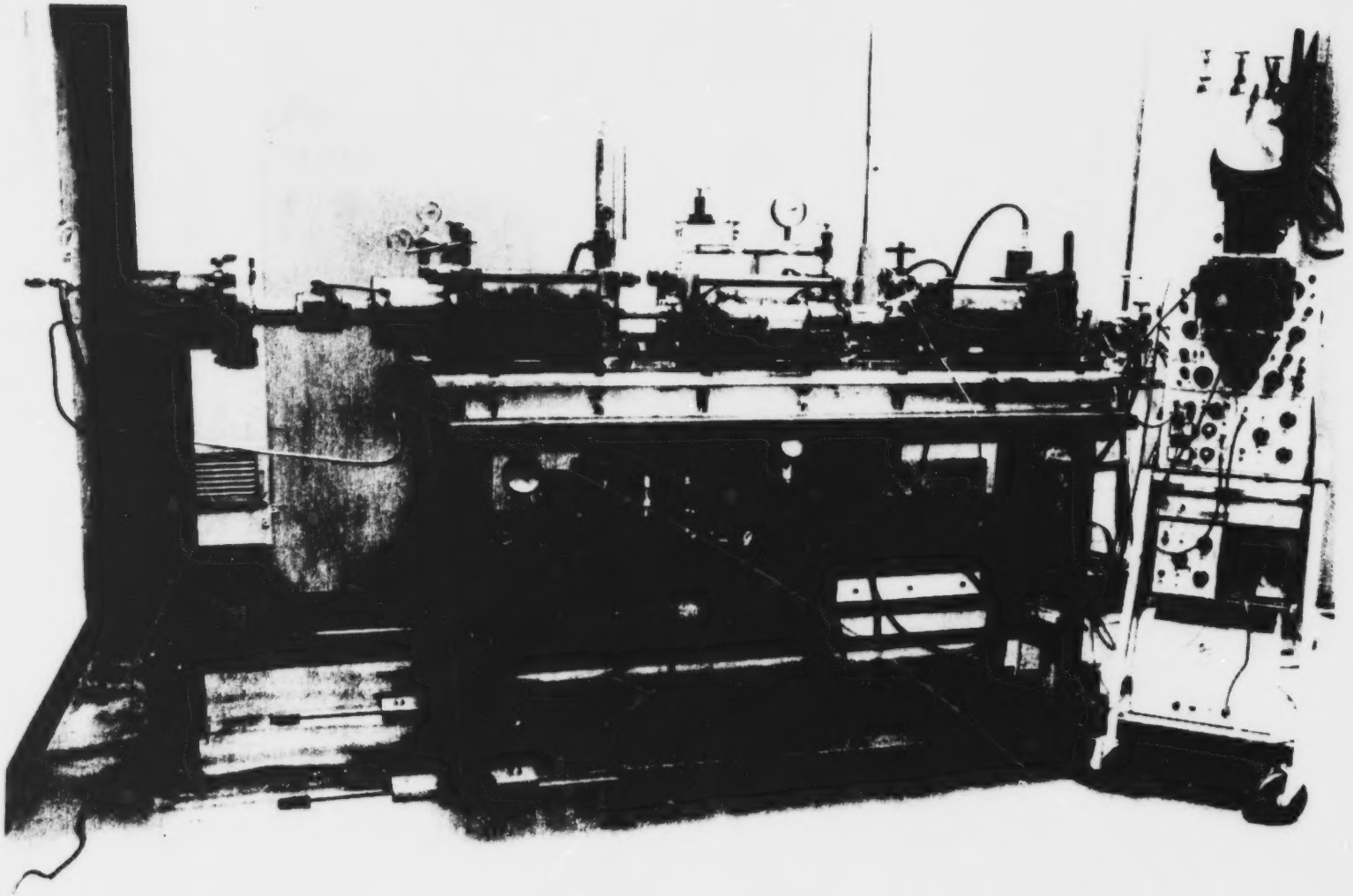

Figure 25/ Complete Installation

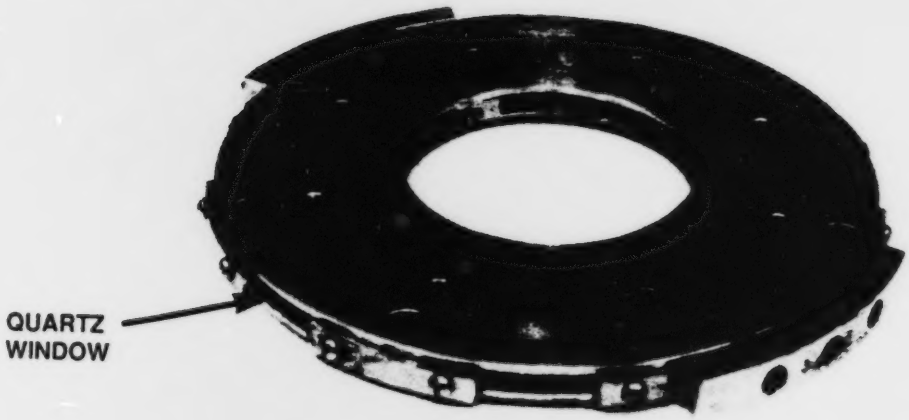

Figure 26/ Optical Disc

Figure 27/ Quartz Head

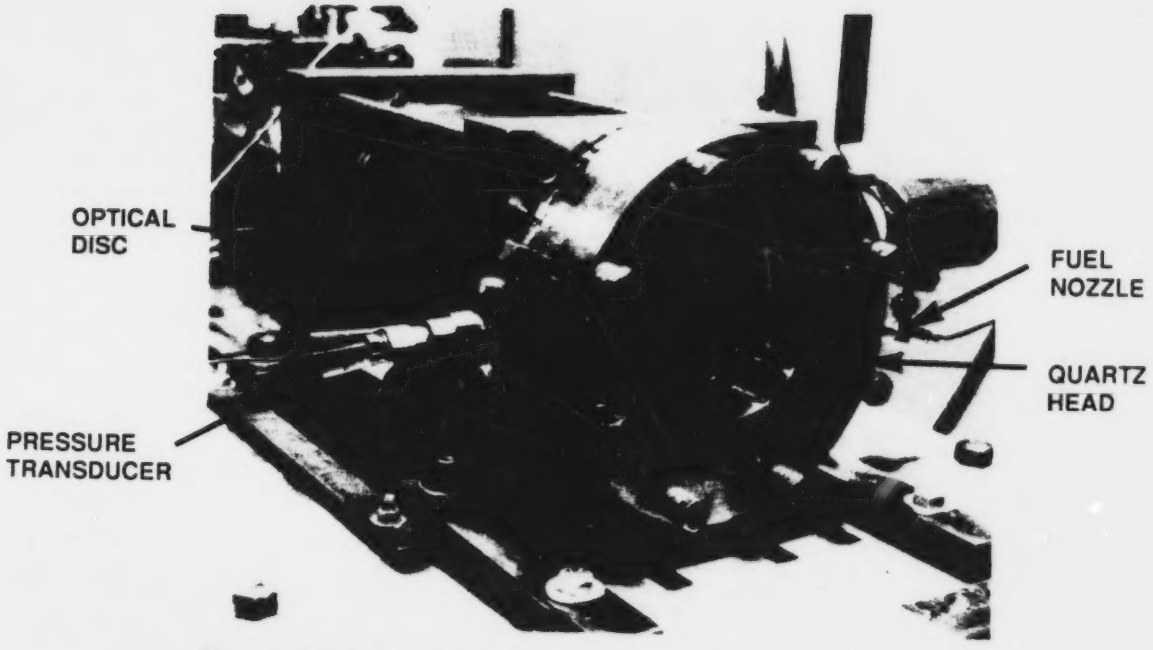

Figure 28/ Optical Disc and Quartz Head Assembly

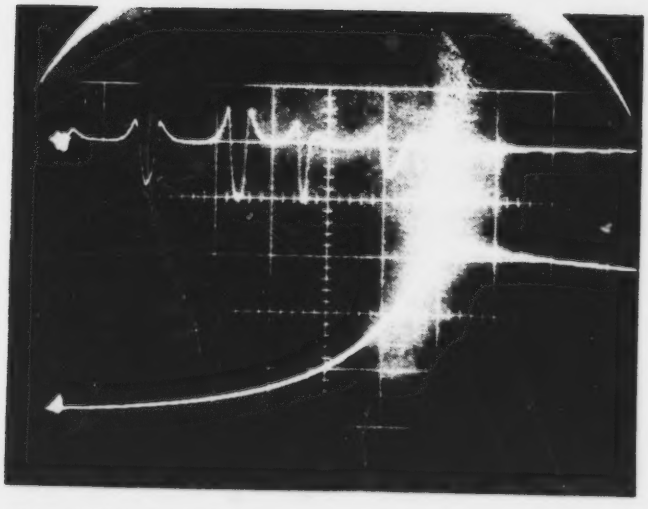

Figure 29/ Compression Pressure and Piston Position Record

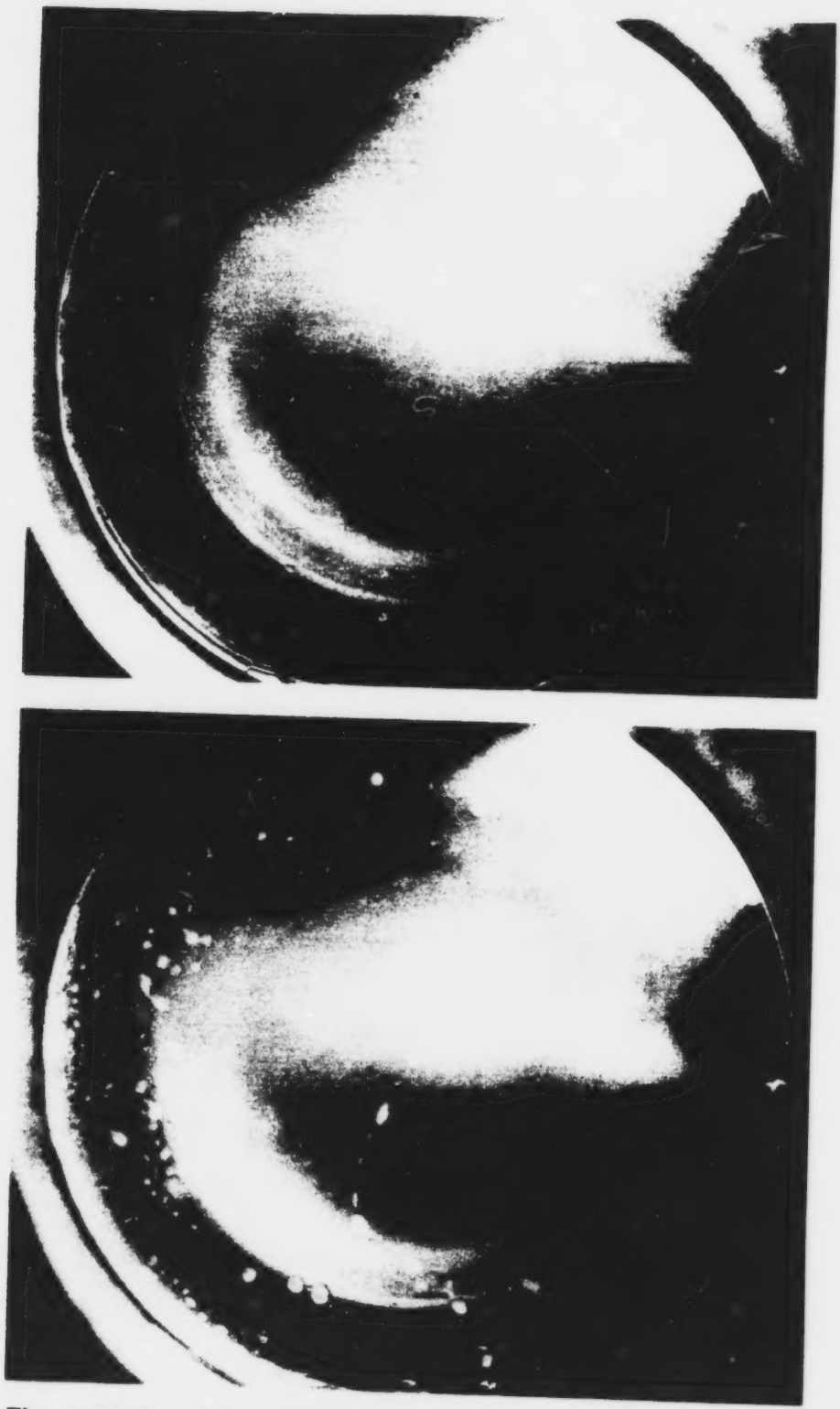

Figure 30/ Fuel Spray Pattern

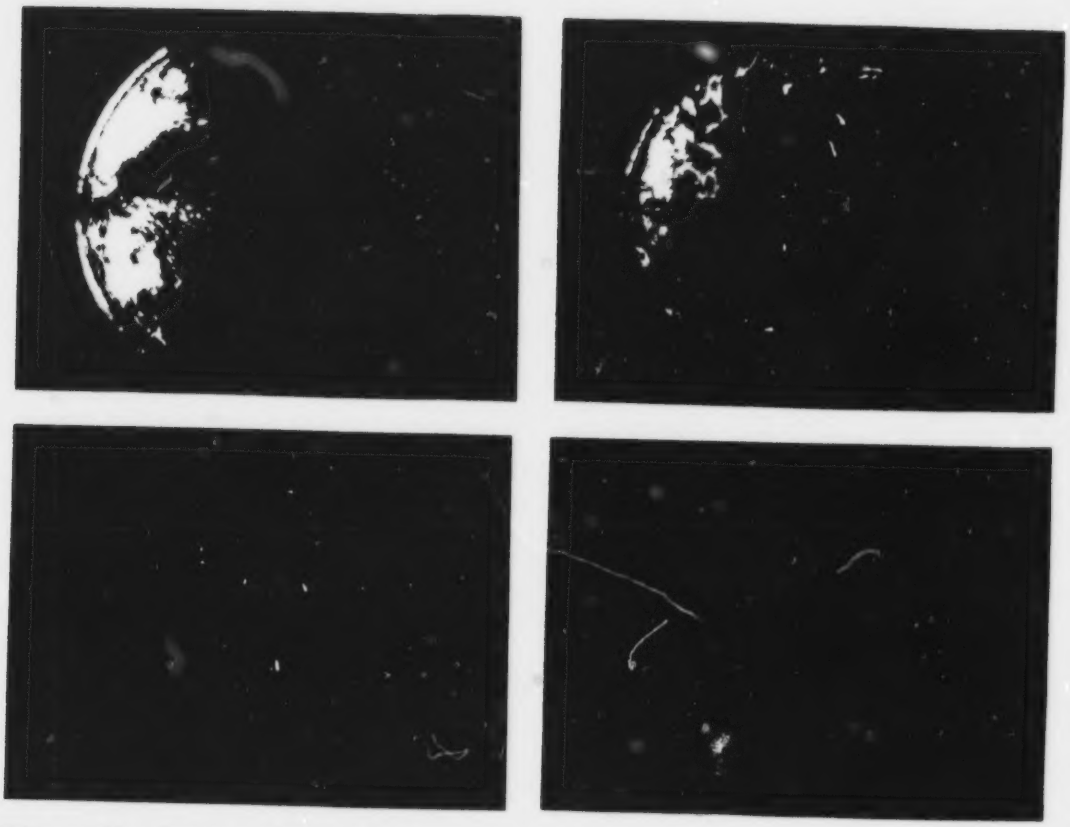

Figure 31a/ Combustion with Excess Fuel

Figure 31b/ Combustion with Less Fuel

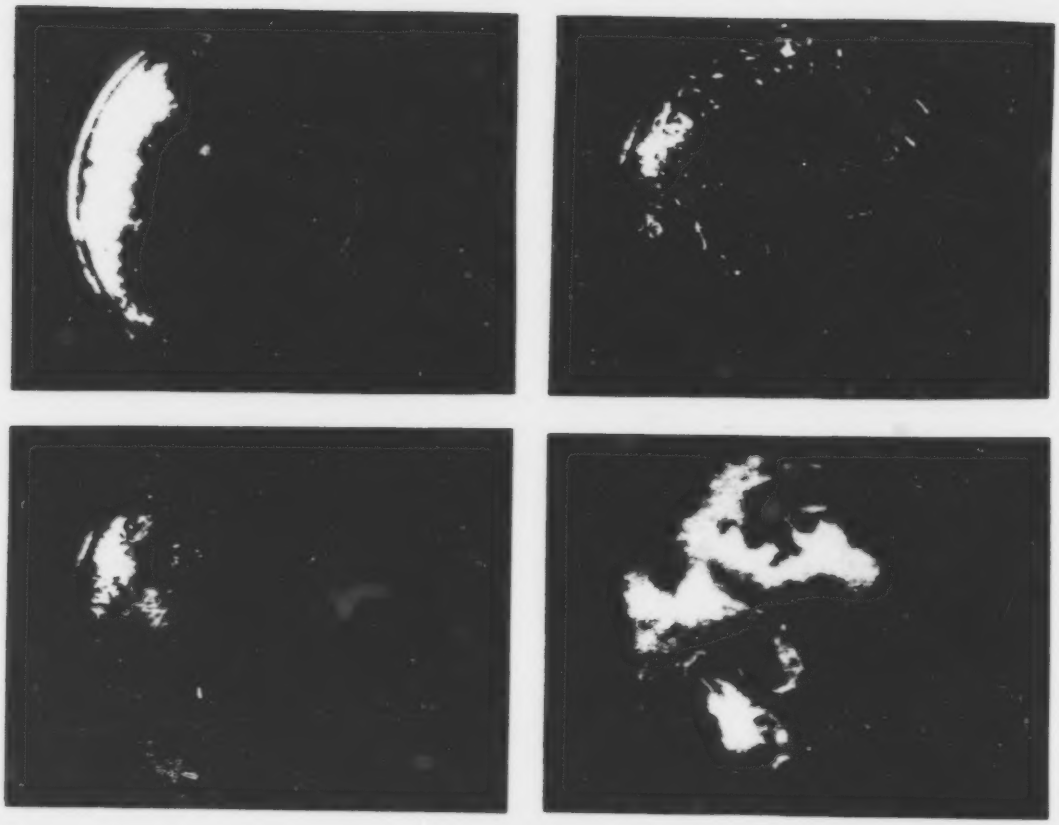

Figure 31c/ Combustion with Lean Air-Fuel Mixture

APPENDIX A/ DETAILS OF THE CHROMATOGRAPH APPARATUS AND TEST PROCEDURE

APPENDIX A/ DETAILS OF THE CHROMATOGRAPH APPARATUS AND TEST PROCEDURE

The instrument used for the mass spectroscopy of the methanol fuels was a GOW Mac Gas Chromatograph, Series 550P, thermal conductivity detector. The column used in this chromatograph was a Poropak Q tube that uses helium as its carrier gas. This apparatus was interfaced to a Hewlett-Packard 3390A integrator, which performed all of the mathematical computations and area integration under the curve so that the composition of each component of the fuel could be accurately determined.

The operating conditions for this apparatus consisted of the following:

- injection temperature, 165°C
- detector temperature, 250°C
- analog output, 100 mA
- stream flow rate, 30 mL/min
- sweep conditions:
  - initial start temperature, 40°C
  - initial start window, 2 min
  - sweep time, 60 min
  - ramp temperature rate, 10°C/min
  - final temperature, 250°C

Table A.1/ M10 LAB RESULTS

LAB MIX	Injected g	Gas g	VF %	Inject $\%CH_3OH$	Vapour $\%CH_3OH$	Injected CH_3OH, g	Gas CH_3OH, g	$\%CH_3OH$ in Gas
	11.75	3.27	27.8	9.5	22	1.12	0.72	64
	5.46	2.28	41.8	9.5	21.7	0.52	0.49	95
	3.08	1.66	54.1	9.5	16.6	0.29	0.276	95
	2.04	1.3	63.7	10.8	12.7	0.22	0.17	77*
	1.42	0.97	70	11.3	13	0.16	0.13	76
	32.77	5.57	17	9.9	16.8	4.23	0.82	23
	7.66	2.83	37	9.9	23.4	0.95	0.63	75
	15.76	4.41	28	9.5	22.6	1.50	0.94	62
OMTO M10	17.06	4.83	28.3	6.2	12.7	1.05	0.61	58
	6.77	3.1	45.0	6.8	12.1	0.45	0.38	84
	4.09	2.2	58.8	5.7	6.6	0.23	0.164	71
	2.2	1.42	64.5	6.8	9.3	0.16	0.13	81
*leakage								

Table A.2/ M85/15 Lab Results

Injected g	Gas g	VF %	Inject %CH_3OH	Vapour %CH_3OH	Injected CH_3OH, g	Gas CH_3OH, g	%CH_3OH in Gas
15.16	1.2	7.9	87.6	58.1	13.28	0.7	5.3
9.76	1.11	11.4	87.6	63.9	8.55	0.71	8.3
7.81	1.30	16.7	87.6	68.5	6.84	0.89	13
6.04	1.17	19.3	87.6	68.1	5.29	0.80	15
4.0	1.19	29.8	87.6	73.6	3.5	0.88	25
2.32	1.11	48	87.6	71	2.03	0.79	39
1.66	1.09	65.6	87.6	88.5	1.45	0.96	66

Table A.3/ M85/Butane's Lab Reports

	Injected g	Gas g	VF %	Inject % CH_3OH	Vapour % CH_3OH	Injected CH_3OH, g	Gas CH_3OH, g	% CH_3OH in Gas
BUTANE 2	15.06	1.2	8	90.4	46	13.6	0.55	4.0
	15.0	1.4	9.3	90.4	46.6	13.5	0.65	4.8
	10.02	1.31	13.1	90.4	58.6	9.1	0.77	8.5
	7.71	1.24	16.1	90.4	62.4	6.97	0.77	11.0
	6.02	1.29	21.5	90.4	69	5.44	0.89	16.4
	2.45	1.03	42	90.4	82.6	2.21	0.85	38.5
	1.52	1.28	84	90.4	91.5	1.37	0.71	85.4
BUTANE 4	15.04	1.37	9.1	89.9	51.9	13.5	0.71	5.3
	7.52	1.17	15.5	89.9	64.2	6.76	0.75	11.1
	6.04	1.28	21.1	89.9	70.5	5.43	0.90	16.6
	2.57	0.90	35	89.9	82.7	2.31	0.74	32.0
	1.54	0.92	59.5	89.9	90	1.38	0.83	60.1
	1.53	1.06	69	89.9	91	1.37	0.96	70.1
BUTANE 6	15.75	1.2	7.6	90.4	40	14.2	0.48	3.4
	10.08	1.07	10.6	90.4	53.8	9.11	0.58	6.4
	7.49	1.3	17.3	90.4	64.6	6.77	0.84	12.4
	4.08	1.11	27.3	90.4	75	3.69	0.83	22.5
	4.05	1.22	30	90.4	75.7	3.66	0.92	25.1
	1.57	0.96	60.9	90.4	89	1.42	0.85	59.9
	1.55	1.13	73.1	90.4	89.5	1.4	1.01	72.1

TABLE A.4/ M85/DME Mass Fractions

	Injected g	Gas g	VF %
DME 2	15.06	1.38	9.2
	10.0	1.3	13
	6.06	1.21	20
	1.53	1.08	70.6
DME 4	15.03	1.38	9.2
	10.03	1.25	12.5
	7.56	1.29	17
	6	1.2	20
	4.04	1.13	28
	1.54	1.22	79.2
DME 6	15.05	1.37	9.1
	10.05	1.21	12
	7.53	1.11	14.8
	6.05	1.17	19.3
	3.99	1.11	28

Table A.5/ Chromatograph Percentages and Odgers Lean Limits

	METH 85/13 BUT 2		METH 85/11 BUT 4		METH 85/9 BUT 6	
	RUN #1	RUN #2	RUN #1	RUN #2	RUN #1	RUN #2
Water	0.2	0.2	---	0.9	1.0	0.6
Methanol	90.5	90.3	90.8	88.9	88.9	88.9
Isobutane	---	0.2	0.2	0.2	0.2	0.2
Butane	2.1	2.0	3.1	3.1	4.1	4.4
Isopentane	0.7	0.7	0.6	0.5	0.4	0.5
Pentane	0.4	0.4	0.3	---	---	---
Hexame/ Methylpentane	---	1.0	0.8	0.9	0.7	0.8
Benzene	---	0.3	0.4	0.3	0.4	---
Heptane	---	0.8	0.8	0.9	0.8	0.6
Toluene/ Iso-octane	2.3	2.4	1.9	1.9	1.4	1.7
Octane/ Methylheptane	1.9	0.7	---	1.0	1.0	0.8
M+P Xylene	1.9	1.1	1.0	1.4	1.2	---
%	100.0	100.1	99.9	100.0	100.1	100.0
m	37.39	37.12	36.31	37.39	37.03	35.99
293 K ϕ_L	0.486	0.4866	0.486	0.488	0.489	0.489
X	1.36	1.359	1.359	1.356	1.355	1.355

Table A.6/ Methanol 85/13 But 2

Sample Temperature (K)		299.3	294.8	294.3	295.4	295.4	293.7	293.2
Sample Mass		1.5g	2.5g	4.0g	6.0g	7.5g	10.0g	15.0g
CO_2		---	1.1	---	---	---	---	---
Water		2.5	1.3	1.5	0.3	---	1.0	3.8
Methanol	32.042	89.2	80.6	82.9	68.8	62.4	58.0	44.2
Isobutane		---	0.7	1.0	1.1	1.6	2.1	2.6
Butane	58.124	3.7	4.6	7.2	9.9	12.2	16.6	21.2
Isopentane		1.0	0.8	2.0	2.6	3.3	4.6	6.4
Pentane	72.151	---	---	1.2	1.4	3.2	2.5	4.0
Hexame, Methylpentane	86.178	1.3	1.0	---	3.1	4.1	6.4	6.8
Benzene	78.114	---	---	---	---	0.6	---	---
Heptane	100.205	---	5.9	---	2.5	3.2	4.0	3.6
Toluene/ Iso-octane	92.141	2.3	3.8	4.2	6.7	5.2	4.7	5.1
Octane, Methylheptane	114.23	---	---	---	3.4	4.0	---	2.2
	%	100.0	99.8	100.0	99.8	99.8	99.9	99.9
	m	35.58	40.82	38.08	46.79	49.37	48.97	54.297
293 K	ϕ_L	0.486	0.497	0.493	0.511	0.521	0.527	0.543
	X	1.36	1.388	1.345	1.308	1.29	1.272	1.249

Table A.7/ Methanol 85/11 But 4

Sample Temperature (K)	294.8				294.3	294.3	293.7
Sample Mass	1.4g	2.5g	4.0g	6.0g	7.5g	10.0g	15.0g
CO_2	---	0.7	---	---	---	0.7	---
Water	3.1	2.0	0.8	---	6.0	---	---
Methanol	88.2	81.6	79.0	70.5	59.2	56.8	51.9
Isobutane	---	0.6	0.8	1.3	1.1	1.8	1.8
Butane	7.3	8.3	10.5	15.9	16.2	22.1	24.6
Isopentane	0.6	1.3	1.9	3.4	2.8	3.5	4.2
Pentane	0.8	---	---	1.8	---	1.8	2.3
Hexame, Methylpentane	---	0.2	0.5	4.8	4.0	5.7	5.5
Benzene	---	---	---	---	---	---	0.9
Dimethylpentane	---	---	---	---	---	---	0.7
Heptane	---	1.6	1.8	2.3	2.9	3.3	3.1
Toluene/Iso-octane	---	---	4.6	---	3.4	4.2	3.0
Octane, Methylheptane	---	3.7	---	---	2.6	---	2.0
%	100.0	100.0	99.9	100.0	99.9	99.9	100.0
m	34.59	39.32	40.09	42.78	47.18	48.39	50.96
293 K ϕ_L	0.4898	0.4998	0.4986	0.516	0.521	0.528	0.536
X	1.352	1.33	1.334	1.298	1.2897	1.2897	1.262

Table A.8/ Methanol 85/9 But 6

Sample Temperature (K)	293.8	294.9	294.3	295.9	295.9	294.8	294.3
Sample Mass	1.5g	2.5g	4.0g	6.0g	7.5g	10.0g	15.0g
CO_2	---	---	---	0.6	0.7	---	---
Water	2.0	1.7	---	---	6.0	0.3	4.8
Methanol	89.5	73.6	75.7	82.2	64.6	53.8	38.0
Isobutane	---	---	0.7	0.4	1.2	1.1	1.7
Butane	7.4	7.6	11.7	8.4	21.1	25.8	36.6
Isopentane	1.1	0.5	1.2	1.2	2.4	3.0	4.4
Pentane	---	---	---	---	1.8	1.7	---
Hexame, Methlpentane	---	2.3	2.7	1.8	3.8	3.9	7.5
Benzene	---	---	---	0.3	---	---	---
Heptane	---	2.5	1.9	1.3	1.9	1.6	3.5
Trimethyl Benzene	---	---	---	---	---	1.5	---
Toluene/Iso-octane	---	5.6	3.0	3.5	3.0	4.6	3.4
M+P Xylene	---	2.0	---	---	---	---	---
Octane, Methylheptane	---	4.0	2.9	0.4	---	2.5	---
%	100.0	99.8	99.8	100.1	100.0	99.8	99.9
m	34.46	45.57	42.72	39.29	44.57	50.29	53.33
293 K ϕ_L	0.4899	0.503	0.5067	0.495	0.5187	0.532	0.550
$\bar{X}$	1.352	1.324	1.317	1.34	1.294	1.269	1.237

Table A.9/ Moneyoctanes Supplied Values for RMC/MTO Blends

	Base Components				Blends						
					Base 1+ n-B				1+ DME		
Blend	MeOH	SNL	n-B	DME	1	2	3	4	5	6	7
MeOH, % by mass	100.0				14.1	12.3	10.4	8.7	12.3	10.5	8.6
SNL		100.0			85.9	85.7	85.7	85.6	85.7	85.6	85.7
n-Butane			100.0		--	2.0	3.9	5.7	--	--	--
DME				100.0	--	--	--	--	2.0	3.9	5.7
MeOH, % by volume	100.0				85.0	84.2	83.9	83.4	84.5	84.4	84.2
SNL		100.0			15.0	13.1	11.0	9.0	13.1	11.1	9.1
n-Butane			100.0		--	2.7	5.1	7.6	--	--	--
DME				100.0	--	--	--	--	2.4	4.5	6.7
DRY RVP, kPa	30	69	356	850	52	90	91	112	77	88	104
psi	44	10	52	123	7.5	13.1	13.2	16.2	12.2	12.8	15.1
D-86 IBP, °C	64	32	-0.5	-25	51	40	33	31	40*	37	32
10%, °C	64	52	--	--	63	64	49	47	60*	54	44
50%, °C	64	109	--	--	64	64	63	63	64*	64	64
90%, °C	64	153	--	--	64	64	65	65	64*	64	64
EP, °C	67	204	-0.5	-25	69	68	184	183	69*	153	169
Recovery, %	99.8	96.8	--	--	97.7	95.8	95.7	94.1	95.8*	94.3	91.8
DENSITY, kg/L	0.797	0.748	0.579	0.661	0.790	0.787	0.783	0.780	0.788	0.787	0.785
%C, by mass	37.5	86.6	82.8	52.1	44.4	44.4	44.3	44.4	43.8	43.2	42.6
%H, by mass	12.5	13.4	17.2	13.0	12.6	12.7	12.8	12.8	12.6	12.6	12.6
%O, by mass	50.0	--	--	34.9	43.0	42.9	42.9	42.8	43.6	44.2	44.8
					*Raoult Cost - estimated D-86						
		6451B			6456B	6454B	6453B	6455B	6452B	6457B	6458B

Table A.10/ Enthalpy of Combustion

		Formula	Hydrocarbons @25°C π 298.15 K Q-J/mol	X	ϕ L	X
Paraffins	Methane	CH_4	802 310.4	1.039	0.511	1.892929
	Ethane	C_2H_6	1 427 843.9	1.223	0.558	2.0882
	Propane	C_3H_8	2 044 028.2	1.185	0.582	1.17154
	Butane	C_4H_{10}	2 657 080.5	1.164	0.595	2.21733
	Pentane	C_5H_{12}	3 272 120	1.151	0.604	2.24615
	Hexane	C_6H_{14}	3 886 714	1.143	0.609	2.26592
	Heptane	C_7H_{16}	4 501 409	1.137	0.613	2.2803
	Octane	C_8H_{18}	5 116 133.2	1.133	0.616	2.29122
	Decone	$C_{10}H_{22}$	6 345 671	1.127	0.622	2.30669
	Dodecone	$C_{12}H_{26}$	7 574 508.8	1.122	0.624	2.31711
Olefins	Ethane	C_2H_4	1 322 970.5	1.186	0.581	2.37018
	Propane	C_3H_6	1 926 468.2	1.151	0.604	2.37018
	Bulane	C_4H_8	2 542 590.1	1.140	0.612	2.37018
	Pentane	C_5H_{10}	3 155 794.5	1.132	0.617	2.37018
	Hexane	C_6H_{12}	3 770 457.6	1.127	0.621	2.37018
	Heptane	C_7H_{14}	4 385 317.1	1.123	0.623	2.37018
	Octane	C_8H_{16}	5 000 034.5	1.121	0.625	2.37018
	Nonare	C_9H_{18}	5 614 657.4	1.119	0.627	2.37018
	Decare	$C_{10}H_{20}$	6 229 390.7	1.117	0.628	2.37018
Alkylbenzenes	Benzene	C_6H_6	3 169 553.7	1.349	0.491	2.05036
	Methylbenzene	C_7H_8	3 771 976.1	1.256	0.536	2.17371
	Ethylbenzene	C_8H_{10}	4 387 074.1	1.205	0.569	2.25102
	Propylbenzene	C_9H_{12}	5 000 472.6	1.172	0.5897	2.30327
	Butylbenzene	$C_{10}H_{14}$	5 614 237.8	1.149	0.605	2.34048
Alcohols	Methanol	CH_3OH	703 835	1.382	0.476	1.89292
	Ethanol	C_2H_5OH	1 298 175	1.233	0.552	2.0882
	Hydrogen	H_2	263 300	2.972	0.76	1.00019
Carbon	Monoxide	CO	260 633	1.383	0.475	2.05036
	Acetylene	C_2H_2	1.196325	1.527	0.418	2.05036

APPENDIX B/ IGNITION AND COMBUSTION OF MIXTURES OF AIR, FUEL DROPLETS, AND FUEL VAPOUR

Internal Report #860201

M.F. Bardon and D. Gauthier

February 1986

Department of Mechanical Engineering
Royal Military College of Canada
Kingston, Ontario

ACKNOWLEDGEMENTS

The investigation presented in this appendix was sponsored by the Department of National Defence and the Ontario Ministry of Transportation.

NOMENCLATURE

Latin Letters

a	constant
B	transfer number for droplet combustion
C_p	specific heat at constant pressure
C_1, C_2, C_3	droplet size distribution parameters [1]
C_{LL}	fuel concentration at the lean limit
d	spark kernel diameter
D	droplet diameter
D_{32}	Sauter mean diameter
E	activation energy
E_{min}	minimum ignition energy
k	thermal conductivity
ℓ	inter-droplet spacing
m	mass
$\dot{m}$	rate of mass transfer
n	number of moles
Nu	Nusselt number
Pr	Prandtl number
$\dot{q}$	rate of heat generation or loss
R	universal gas constant
Re	Reynolds number
S_L	laminar burning velocity
S_T	turbulent burning velocity
t	characteristic time
T	temperature
ΔT	temperature rise
Tu	percentage turbulence intensity (100u'/U)
U	mainstream air velocity
u'	RMS of fluctuating velocity components
V	air velocity in the ignition zone
w	constant
X	mole fraction
Z	droplet size distribution parameter [1]

Greek Letters

α	thermal diffusivity
β	constant
ν	kinematic viscosity
ϕ	fuel/air equivalence ratio = f/f_{st}
ρ	density
Ω	fraction of fuel in the form of vapour

Subscripts

a	air
ad	adiabatic
c	by conduction
ch	chemical term
D	based on sphere of diameter D
d	by diffusion
ev	evaporative term
f	fuel liquid
g	gas phase, or generation term
l	liquid phase
o	overall or initial condition
ph	physical term
q	quenching
st	stoichiometric
u'	based on turbulence intensity u' as characteristic velocity

B.1/ INTRODUCTION

The problem of ignition and combustion of the mixture of air, fuel droplets, and fuel vapour in the cylinder of a spark-ignition engine during cold starting is multifaceted:

1/ There is the distribution of the heterogeneous charge. This is composed of some fuel vapour and air plus a considerable amount of liquid fuel, which is at least partly in a thin film on the piston face and combustion chamber walls and, likely, also partly present in the form of droplets of various sizes. The droplet size distribution and their location are problematical but can have an overwhelming influence on the ignition and combustion processes. Because all the velocities are low with respect to sonic velocity, the pressure is essentially constant throughout the chamber, but there may be significant temperature and concentration gradients resulting from imperfect mixing, individual droplet evaporation, and heat losses to the cold chamber walls.

2/ The mixture must be ignited by the spark produced in the electrode gap. This depends upon the details of the vapour, air, and liquid present in the gap and the quantity and discharge time of the electrical energy of the spark.

3/ Once ignited, the flame must propagate at least partway through the mixture so as to produce a net energy gain available for self-sustained engine operation. This flame propagation, again, depends upon the details of the charge structure but may also be affected by the ongoing heat losses to the walls and the expansion resulting from the movement of the piston during the course of the combustion process. The presence of residual products from previous cycles may also affect propagation.

A full analytical treatment of the cold-starting combustion process must include a detailed specification of the physical conditions within the charge, the ignition process, and subsequent propagation. Mixture formation, transport through the induction system and into the cylinder, and processes within the cylinder, such as heat transfer compression, or expansion, are the subjects of a companion study aimed at modelling overall engine behaviour. This present study is restricted to the processes of ignition and flame propagation in arbitrary mixtures of fuel droplets, vapour, and air and is ultimately aimed at providing quantitative relationships for use in those specific aspects of the larger study.

In this report, ignition and propagation are reviewed separately. Although a mixture that fails to ignite will not undergo flame

propagation, it is not clear from the literature whether successful ignition is necessarily followed by successful propagation under cold-starting conditions. In fact, experience with fully vaporized mixtures in warmed-up engines suggests that ignition failure and propagation failure are distinct processes. Since the two are, therefore, at least potentially different, this review treats them separately. Chapter B.2 considers prior work on ignition, and Chapter B.3 reviews flame propagation once a flame front has somehow been established.

B.2/ IGNITION OF AIR-VAPOUR-DROPLET MIXTURES

2.1/ Introduction

Most of the literature on ignition of heterogeneous air-vapour-droplet mixtures has been conducted by workers primarily concerned with gas turbine combustors rather than spark-ignition engines. The basic physics and chemistry of the two devices are, however, virtually identical in spite of the obvious superficial differences. Most Otto-cycle engine spark studies have been concerned with fully vaporized mixtures, since that is usually the case for warmed-up engines by the time ignition occurs. On the other hand, since most gas turbines inject liquid fuel directly into the hot primary zone of the combustor under all conditions, the heterogeneous case has always been of interest there. There is, nonetheless, fairly limited literature on the topic, and reasonable models have, in fact, become available only recently.

The gas turbine case is inherently concerned with a relatively rapid flow of mixture past the ignitor, but preliminary studies naturally began by treating the more tractable case of quiescent mixtures before considering the flowing situation. On the other hand, the spark-ignition engine is, on the surface at least, a case of a relatively quiescent mixture. However, turbulence induced by piston motion and induction flow can result in fairly large velocity components in the region of the spark plug during ignition; therefore, ignition studies of flowing heterogeneous streams are not by any means irrelevant, in spite of their orientation towards gas turbine applications.

Thus, the differences between ignition under gas turbine conditions and in Otto cycle engines are those of degree only. The relative importance of various parameters and their typical values are different; the fundamental processes concerned are the same.

In this chapter, a review of ignition models is given. Conclusions are then drawn as to an appropriate model for use in cold-starting analyses. Both quiescent and flowing mixtures are considered. Ignition is defined here as the local initiation of a flame, termed the spark kernel, and its subsequent initial propagation out into the mixture.

Whereas a reasonable amount of information is available regarding ignition prediction both for quiescent [2-5] and flowing [4-7] homogeneous hydrocarbon fuel-air mixtures, less is known about the complex study of ignition for quiescent [5,8,9] and flowing heterogeneous fuel-air mixtures [1,5,10]. Most work on the heterogeneous cases have, in fact, been restricted to situations with no appreciable fuel vapour present.

That is partly because it is the simplest and is also, perhaps, of most interest in gas turbines where high flow velocities result in short time delays between creation of the droplets by the fuel injector and their entry into the spark zone.

B.2.2/ Basic Considerations

All the models discussed here treat ignition from a thermal viewpoint to develop some relatively simple relations for the prediction and correlation of ignition performance.

Two different approaches are used in the formulation of the models:

1/ The "rate" approach stipulates that, for a spark kernel, i.e., a critical volume of inflamed gas, to survive and propagate (after the spark is removed), its volume must be of sufficient size so that the rate of heat generated within its volume just exceeds its rate of heat loss to the surroundings.

2/ In the "time" approach, the ignition event is analysed by expressing the heat generation and loss rates in terms of characteristic times for the controlling physical and chemical processes.

Intrinsic to both approaches is the requirement for the buildup of an adequate concentration of fuel vapour in the ignition zone. This criterion has been verified experimentally by Ballal and Lefebvre [8] and by Naegeli et al. [11], who confirmed that over a wide range of test conditions, fuel evaporation is the rate controlling step in the ignition of fuel sprays. Ballal and Lefebvre [8] also added that "intrinsic to any model for the ignition of multi-droplet mists is the requirement that passage of the spark should release sufficient energy to heat the spark kernel to the stoichiometric flame temperature." The stoichiometric adiabatic flame temperature is used simply as a convenient reference temperature. It would not fundamentally change the analyses if some other reference temperature was used, such as that observed at the lean flammability limit.

The following are basic assumptions used in all models:

- The energy of the spark is considered purely thermal, i.e., the influence of active radicals produced at the very high plasma temperatures is neglected.
- All the energy released at the spark is available in the spark kernel.
- The spark kernel is spherical.
- Fuel droplets in the spray are spherical.
- Flame radiation is negligible.

B.2.3/ Review of Principal Ignition Models

Three specific cases will be considered in this review, namely, the cases of fuel spray ignition in
1/ quiescent air
2/ flowing air
3/ flowing air-fuel vapour mixtures

B.2.3.1/ Ignition in Quiescent Mixtures

Two different models addressing this specific case will be discussed. Although both of these models yield essentially the same results, they are both of interest because of the different approaches used to obtain the resulting equations.

B.2.3.1.1/ Model by Peters and Mellor

These investigators followed the "time" approach previously described. The limiting (or critical) condition for ignition is taken to be when the quenching time (heat loss) is of the same order as the heat generation time. This latter is evaluated as the sum of the chemical delay time and the evaporation time. The modelling relation [9] is given as

$$t_q \propto t_{ch} + a t_{ev} \tag{1}$$

where the proportionality and the constant weighting factor "a" were introduced by the authors because the times used are not absolute and are only calculated as relative values. Assuming that the chemical reaction rate is much larger than the evaporation rate, they rewrote Equation 1 as

$$t_q \propto t_{ev} \tag{2}$$

A characteristic quenching time was defined as the ratio of thermal energy within the spark to a representative rate of heat loss through conduction, yielding

$$\frac{t_q = \pi d_q^2 \rho_a C_{pa}}{k_a} \tag{3}$$

Here d_q is the distance between the electrodes. The initially slender spark strand is considered to rapidly diffuse into a spherical mass of flame kernel having this same diameter. The limiting value of the flame kernel for successful ignition is that below which the ignition would fail, i.e., the kernel would be quenched, hence, the term "quenching distance."

The evaporation time is evaluated using the well-known result of classical droplet theory [12].

$$t_{ev} = \frac{D_{32}^2 \rho_f C_{pa}}{8k_a \, Ln(1 + B_{st})} \tag{4}$$

Equation 4 is the evaporation time for one droplet having the representative diameter D_{32}, the Sauter mean diameter (SMD) of the entire set of droplets. Now, the number of droplets is directly proportional to the equivalence ratio ϕ. If it is assumed that all the droplets are sufficiently far apart that they don't affect each other's evaporation rates (i.e., if the spray is sufficiently dilute), then the characteristic time to achieve any particular average vapour concentration would be inversely proportional to ϕ, since the overall number of droplets, each evaporating at the same rate, is directly proportional to ϕ. This is consistent with the studies of Bellan and Cuffel [13], which showed that for lean mixtures and dilute sprays, the evaporation time is a decreasing function of the equivalence ratio.

Thus, the characteristic time for the entire set of droplets is

$$t_{ev} = \frac{D_{32}^2 \rho_f C_{pa}}{8k_a \phi \, Ln(1 + B_{st})} \tag{5}$$

Now substituting (3) and (5) into (2) and rearranging gives

$$d_q \propto D_{32} \left(\frac{\rho_f}{\rho_a \phi \, Ln(1 + B_{st})} \right)^{0.5} \tag{6}$$

or

$$d_q = \beta D_{32} \left(\frac{\rho_f}{\rho_a \phi \, Ln(1 + B_{st})} \right)^{0.5} \tag{7}$$

where β is proportionality constant and is determined empirically.

B.2.3.1.2/ Model by Ballal and Lefebvre

These authors [8] used the rate approach, i.e., ignition is assumed to occur when the rate of heat released within the spark kernel is just equal to the rate of heat loss by conduction from its surface. At this condition, the diameter of the spark volume is d_q. Then the modelling

equation is

$$\dot{q}_g = \dot{q}_c \tag{8}$$

Heat Generation, $\dot{q}_g$

Because the authors assumed that the reaction rate is infinitely fast, the rate of heat generated is given by the product of the evaporation rate for all droplets within the spark kernel and the heat of combustion of the fuel. Only the result is given here:

$$\dot{q}_g = \frac{2\pi k_a \rho_a d^3}{\rho_f D^2} \phi \Delta T_{st} \, \mathrm{Ln}(1 + B_{st}) \tag{9}$$

where ΔT_{st} is the difference between the stoichiometric adiabatic flame temperature and the temperature at the surface of the drops.

Heat Loss by Conduction, $\dot{q}_c$

The heat loss by conduction is given by

$$\dot{q}_c = 2\pi d k_a \Delta T_{st} \tag{10}$$

Equations 9 and 10 are consistent with currently accepted theories [12]. Substituting them into Equation 8 and rearranging gives

$$d_q = D \left(\frac{\rho_f}{\rho_a \phi \, \mathrm{Ln}(1 + B_{st})} \right)^{0.5} \tag{11}$$

B.2.3.1.3/ Comments on These Models

It should be noted that Equations 6 and 11 are derived directly from basic considerations of the mechanisms of heat transfer [8,9]. Moreover, they are equally valid for both monodisperse and polydisperse sprays on the reasonable assumption that the SMD can be used to characterize the evaporative behaviour of a polydisperse spray. The similarity between both relations is not surprising, considering that although the approaches used are different, the sets of conditions and assumptions are the same for either model.

However, a drawback of Equation 7 is the requirement for experimental data to evaluate the proportionality constant. Peters and Mellor [9] correlated their model with data available from Ballal and Lefebvre [8] using a least-squares fit to obtain the applicable proportionality constant.

Having deduced these relations for the minimum spark gap size d_q, both pairs of authors [8,9] defined the minimum ignition energy (E_{min}) as that energy required to heat a spherical volume of air with diameter d_q to the stoichiometric, adiabatic flame temperature, i.e.,

$$E_{min} = \rho_a c_{pa} \Delta T_{st} (\pi/6) d_q^3 \qquad (12)$$

B.2.3.1.4/ Validation of the Quiescent Models

Graphs of E_{min} versus D_{32} and ϕ are shown in Figures B.1 and B.2, respectively, to illustrate the results of both modelling expressions [8,12]. (These graphs are taken from Reference 8.) As expected, both models give similar results. Predicting/correlating models are in very good agreement with experimental data, except perhaps in the region of small diameter and low equivalence ratio. An explanation for this deviation will become clear in the review of subsequent models.

B.2.3.2/ Ignition of a Flowing Droplet-Air Mixture

The same two groups have extended their quiescent models to cover the case of a flowing mixture.

B.2.3.2.1/ Model by Peters and Mellor

Similar to their previous model [1], the characteristic time approach is followed; that is, ignition occurs when t_q is of the order of t_{ch} plus t_{ev}:

$$t_q \propto t_{ch} + a t_{ev} \qquad (1)$$

Quenching time, t_d

The quenching (mixing) time is defined here as

$$t_q = d_q/V \qquad (13)$$

The authors used V in Equation 13, assuming that the velocity at the spark gap is proportional to the mainstream velocity, i.e.,

$$t_q \propto d_q/U \qquad (14)$$

Equation 14 is "semi-consistent" with Ballal and Lefebvre [7], who stated that measurements showed that

$$\dot{q}_d \propto c_{pa} \rho_a u' d^2 \Delta T \qquad (15)$$

which results in

$$t_q \alpha d_q/u' \tag{14a}$$

Defining relative turbulence intensity as

$$Tu = \frac{u'}{U} 100 \tag{16}$$

Then, if Tu is kept constant,

$$t_q \alpha d_q/U$$

which is the same expression as (14). Thus, Equation 14 is consistent with Ballal's and Lefebvre's findings only if Tu is kept constant. When using data from Ballal and Lefebvre, Peters and Mellor selected cases of constant turbulence only.

An Arrhenius expression was used for the chemical time, t_{ch}:

$$t_{ch} = \frac{b \exp(E/RT_{st})}{\phi \rho g} \tag{17}$$

where the pre-exponential factor b was evaluated at 10^{-5} and E used was 26 100 cal/mol.

The evaporation time, t_{ev}, was as before:

$$t_{ev} = D_{32}^2 \rho_f C_{pa}/[8\phi k_a \text{ Ln}(1 + B_{st})] \tag{7}$$

In a subsequent publication [14], the authors indicated that they accounted for the effect of droplet Reynolds number, using

$$t_{ev} = \frac{D_{32}^2 \rho_f C_{pa}}{8\phi k_a \ln (1 + B_{st}) \frac{(0.37) Re_V^{0.6}}{2}} \tag{18}$$

which is consistent with Kanury [12], who gives the relation for a sphere with flowing air around it as

$$Nu_D = 0.37 Re_D^{0.6} \tag{19}$$

Nu for a sphere in quiescent air is equal to 2. Making the analogy between heat and mass transfer gives the evaporation in flowing air as a

function of the evaporation rate in quiescent air and the droplet Reynolds number:

$$\dot{m}_{Re_V} = \dot{m}_{Re_{V=0}} \frac{(0.37)Re_V^{0.6}}{2} \tag{20}$$

Now substituting (13), (17), and (18) into (1) and rearranging gives

$$d_q \alpha \frac{V10^{-5} \exp(E/RT_{st})}{\phi \rho_g} + \frac{aD_{32}^2 \rho_f C_{pa} V}{8\phi k_a \, Ln(1 + B_{st}) \frac{(0.37)Re_V^{0.6}}{2}} \tag{21}$$

The proportionality factor "a" was found to be equal to 0.021 using a least-squares fit [10]. Thus, Equation 21 becomes

$$d_q \alpha \frac{V10^{-5} \exp(E/RT_{st})}{\phi \rho_g} + \frac{0.014D_{32}^2 \rho_f C_{pa} V}{\phi k_a \, Ln(1 + B_{st}) Re_V^{0.6}} \tag{22}$$

which is the relationship used in Reference 14 to calculate E_{min}. Note that, assuming infinitely fast chemical reaction, Equation 22 becomes

$$d_q \alpha \frac{VD_{32}^2 \rho_f C_{pa}}{\phi k_a \, Ln(1 + B_{st}) Re_V^{0.6}} \tag{23}$$

B.2.3.2.2/ **Model by Ballal and Lefebvre**

Similar to their previous model [10], the "rate" approach is followed; that is, the critical size for the spark kernel is that at which the rate of heat release by fuel evaporation is just equal to the rate of heat loss by conduction and turbulent diffusion from its surface. The modelling relationship is

$$\dot{q}_g = \dot{q}_c + \dot{q}_d \tag{24}$$

Heat Generation, $\dot{q}_g$

The expression of $\dot{q}_g$ is identical to Equation 9 except that the effect of turbulence is taken into account, using the relationship

$$\dot{m}_{Re_{u'}} = \dot{m}_{Re_{u'}=0} (1 + wRe_{u'}^{0.5}) \tag{25}$$

where w is a constant which is assigned a value of 0.25 based on current empirical information [15]. The result is

$$\dot{q}_{g,Re_{u'}} = \dot{q}_{g,Re_{u'}=0} (1 + 0.25Re_{u'}^{0.5}) \tag{26}$$

The authors expressed the opinion that "as the fuel drops are usually quite small when injected into a flowing airstream, they tend to remain airborne and their velocity relative to that of the airstream is insufficient to appreciably enhance the rate of fuel evaporation. However, if the flow is turbulent, the fuel drops are fully subjected to the fluctuating components of velocity." For such conditions, these authors used the following definition for the droplet Reynolds number:

$$Re_{u'} = \frac{u'D}{\nu a} \tag{27}$$

Heat Loss by Conduction, $\dot{q}_c$

The heat loss by conduction is given by Equation 10:

$$\dot{q}_c = 2\pi dk_a \Delta T_{st} \tag{10}$$

Heat Loss by Diffusion, $\dot{q}_d$

The heat loss by diffusion is attributed to turbulent mixing and is given [7] as

$$\dot{q}_d = \pi\Delta T\ 0.16d^2\rho_a C_{pa} u' \qquad \text{for low turbulence} \tag{28}$$

$$\dot{q}_d = \pi\Delta T\ 0.63d^2\rho_a C_{pa} u' \qquad \text{for high turbulence} \tag{28a}$$

Equation 28 is more pertinent to this review since comparison between both models is done only for data of low turbulence experiments. Substituting (9), (26), (10), and (28) into (24), neglecting the heat by conduction (i.e., $Re_u >> 1$), the authors found

$$d_q = \frac{0.32\rho_f C_{pa} D^2 u'}{k_a \phi \, \mathrm{Ln}(1 + B_{st}) Re_{u'}^{0.5}} \tag{29}$$

For a polydisperse spray, they rewrote this as

$$d_q = \frac{0.32\rho_f C_{pa} D_{32}^2 u'}{Z k_a \phi \, \mathrm{Ln}(1 + B_{st}) \, Re_{u'}^{0.5}} \tag{30}$$

where the constant Z is a function of the injector only and is equal to one for a monodisperse spray. Note that intrinsic to Equation 26 (hence to Equation 20) is the assumption that the chemical rate is infinitely fast compared to the evaporation rate.

B.2.3.2.3/ Comments on Latter Two Models

Again, both models [1,10] are very similar, which is not surprising, considering the identical sets of assumptions used in the development of each. In subsequent work, Ballal and Lefebvre [5] extended the applicability of Equation 30 to account for the chemical time. They found

$$d_q = \frac{0.32\rho_f C_{pa} D_{32}^2 u'}{Z k_a \phi \, \mathrm{Ln}(1 + B_{st}) Re_{u'}^{0.5}} + \frac{10\alpha}{S_T - 0.63u'} \tag{29b}$$

which is based on their previous work [7].

Again, the model by Ballal and Lefebvre has the advantage that no proportionality constant need be found. This means that Equations 29 or 30 can be used to predict the value of d_q (hence, of E_{min}) given values of the variables in the equation.

This does not mean that the model by Peters and Mellor is not useful. On the contrary, one does not need to know the exact value of E_{min}, in general, but rather, it is used to predict how different parameter changes can affect the ignition performance and to what extent. This can be done as easily with Equation 22 as with Equation 30, except for the turbulence effect which is only accounted for in (30).

B.2.3.2.4/ Validation of the Models for Flowing Mixtures

Although, as previously mentioned, both Ballal and Lefebvre [8] and Naegeli et al [11] demonstrated that the heat generation is predominantly evaporation controlled, the inclusion of the effect of t_{ch} into the ignition models can significantly improve the ability of these models to

predict the value of E_{min} for some conditions. This is illustrated in Figure B.3, taken from Reference 7. This figure also shows that even when t_{ch} is neglected, the predictions are still quite reasonable. The modelling relations by Peters and Mellor (22) and (23) are not plotted here because of their equivalence with the equations by Ballal and Lefebvre.

B.2.3.3/ Fuel Spray Ignition into Flowing Air-Fuel Vapour Mixtures

Recently (1981), Ballal and Lefebvre [5] developed a general model of spark ignition for gaseous and liquid fuel-air mixtures, which has application to both quiescent and flowing mixtures of air with either gaseous, liquid, or evaporated fuel, or any combination of these fuels.

The assumptions for this model are identical to previous cases, except that now the presence of fuel vapour in the air is accounted for. It reduces to the previous results, such as Equation 30, for simpler cases.

Unlike these authors' previous work, this time they used the "characteristic time" approach because they found the rate approach cumbersome to apply for more than two rate processes. The modelling relationship used is

$$t_q = t_{ch} + t_{ev}$$

Quenching Time, t_q

The quenching time is given as the ratio of the initial heat capacity of the spark kernel divided by the average rate of heat loss from the kernel by thermal conduction and turbulent diffusion,

$$t_q = \frac{C_{pa}\rho_a \Delta T_{st} (\pi/6) d_q^3}{1.33\pi d_q \Delta T_{st} (k_a + 0.08 C_{pa}\rho_a u' d_q)} \qquad (31)$$

which reduces to

$$t_q = \frac{d_q^2}{8(\alpha_a + 0.08 u' d_q)} \qquad (31a)$$

In the case of low and high turbulence Equation 31a becomes, respectively,

$$t_q = \frac{d_q^2}{8\alpha_a}$$

and

$$t_q = \frac{d_q}{0.64u'}$$

where the denominator is based on Equation 5 of Reference 10.

Evaporation Time, t_{ev}

The evaporation time derived by these authors is based on the time it would take to evaporate the mass of all the fuel contained within the spark kernel ... the time it would have taken to produce the fuel vapour had it been present initially in the form of liquid drops of the same size as those that already exist in the system. Thus, the evaporation time is only what is required to vaporize the fuel still in the form of liquid. The resulting expression is given as

$$t_{ev} = \frac{(1 - \Omega)\, p_f C_{pa} D^2}{8k_a \phi\, \mathrm{Ln}(1 + B_{st})\, (1 + 0.25Re_{u'}^{0.5})} \quad \text{for monodisperse sprays} \qquad (32)$$

$$t_{ev} = \frac{C_3^3\, (1 - \Omega) p_f C_{pa} D_{32}^2}{C_1 8k_a \phi\, \mathrm{Ln}(1 + B_{st})\, (1 + 0.25C_2^{0.5} Re_{u'}^{0.5})} \quad \text{for polydisperse sprays} \qquad (32a)$$

where C_1, C_2, and C_3 are experimentally determined constants that define the distribution f the drop sizes in the spray and which are a function of the nozzle used only. Note that the use of both Sauter mean diameter, D_{32}, and the three additional constants, C_1, C_2, and C_3, is tacit admission that SMD alone is not adequate to quantify the behaviour of a polydisperse spray under these conditions.

Chemical Reaction Time, t_{ch}

The authors defined t_{ch} as a function of S_L and S_T, the laminar and the turbulent flame speeds, to give

- for low turbulence, $u' < 2S_L$

$$t_{ch} = 12.5\alpha\, (S_L - 0.16u')^2 \qquad (33)$$

• for high turbulence, $u' > 2S_L$

$$t_{ch} = 15.6\alpha\,[u'\,(S_T - 0.63u')] \tag{33a}$$

Quenching Distance, d_q

Expressions for quenching distance are readily derived by selecting the appropriate expression of t_q, t_{ev}, and t_{ch}, and inserting them into the limiting equation for ignition, namely:

$$t_q = t_{ch} + t_{ev} \tag{34}$$

For example, for the case of flowing heterogeneous mixture with high turbulence ($Re_{u'} >> 1$,), Equations 31, 32a, and 33a can be inserted into Equation 34 and rearranged to get

$$d_q = \frac{0.32\,(1 - \Omega)\rho_f C_{pa} D_{32}^2 u'}{Zk_a\phi\,\mathrm{Ln}(1 + B_{st})\,Re_{u'}^{0.5}} + \frac{10\alpha}{S_T - 0.63u'} \tag{35}$$

where $Z = (C_1 C_2^{0.5})/(C_3^3)$ (36)

and is the same Z as in Equation 29b.

Note that for $\Omega = 0$, i.e., fuel spray ignition into flowing air alone, Equation 35 reverts to the same expression as Equation 30. The case where $\Omega = 1$ is for gaseous and fully vaporized mixtures.

B.2.3.3.1/ Validation of the All-Inclusive Model

As shown in Figures B.4 and B.5 (reproduced from [5]) the model by Ballal and Lefebvre gives good correlation in the prediction of minimum ignition energy as a function of Ω. Note that the figures apply to low turbulence only, as the authors did not give correlation results for high-turbulence cases.

Ballal and Lefebvre's general model [5] seems to predict E_{min} for the complex-case flowing mixtures quite well. It has the additional virtue of being easily adapted to a variety of conditions relevant to practical combustion systems.

B.2.4/ Apparatus and Experimentation

The apparatus used to produce the data presented will now be briefly described to place the results into perspective.

B.2.4.1/ Apparatus of Ballal and Lefebvre

Ballal and Lefebvre described their two test facilities in detail in References 8 and 10 and in general in Reference 5.

> Two test facilities were used in the experimental program. For the study of ignition in quiescent mixtures air was induced to flow at low velocity and low turbulence through a vertical test section of 9 cm square cross section, and 31 cm in length. This section is fitted with glass side walls to permit visual observation of the spark and the onset of ignition. Heat resistant, stainless steel electrodes, 2 mm in diameter, project through opposing walls to form a spark gap at the center of the test section. One electrode is attached to a micrometer head in order to measure and control the spark gap width within fine limits. A similar test section, mounted horizontally, and supplied with air from a fan, was used to study the ignition of flowing mixtures.

Drop-size measurements were done in the vicinity of the spark gap, using a (laser) light-scattering technique. The influence of Ω was studied by injecting fuel vapour upstream of the fuel nozzle, and the quantity of vapour was measured in the ignition zone. Turbulence was measured in the plane of the electrodes using, a hot wire anemometer. The spark energy was measured at the electrodes from current and voltage traces recorded on a two-channel oscilloscope. The tests by Ballal and Lefebvre covered the following conditions:

- quiescent mixtures
  - air pressure = 0.2 to 1.0 x $10^5 N/m^2$
  - air temperature = 290 K
  - equivalence ratio = 0.65 and 1.0
  - transfer number = 1.5, 2.8, and 6.1
  - Sauter mean dia = 30, 60, 100, and 150 μ
  - fraction of fuel as vapour = 0.1 to 1.0
- flowing mixtures
  - air pressure = 0.2 to 1.0 x 10^5 N/m^2
  - air temperature = 290 K
  - equivalence ratio = 0.65 and 1.0
  - transfer number = 1.5, 2.8, and 6.1
  - Sauter mean dia = 60, 100, and 150 μ
  - fraction of fuel as vapour = 0.1 to 1.0

For all conditions tested, the general model by Ballal and Lefebvre [5] gave good agreement with experimental data.

B.2.4.2/ Apparatus of Mellor et al.

For the models by Peters and Mellor, the validation was done using two different sets of experimental data:
1/ data obtained from the apparatus of Ballal and Lefebvre
2/ data from existing engines

As previously mentioned, the model of Peters and Mellor [1,9] agreed well with the data of Ballal and Lefebvre. Naegeli et al. [11] (testing the model of Peters and Mellor [1]) and Peters and Mellor themselves [1] found satisfactory correlation for their models against data obtained from a total of six production gas turbine engines. Because of the equivalence between the models of Peters and Mellor and those of Ballal and Lefebvre [5] when applied to the same set of conditions, that of Ballal and Lefebvre would also be expected to give similar results for real engine data.

The scatter of the data about the correlation against actual gas turbine data was primarily attributed by the authors to the errors in the drop size estimates. Because in-situ drop size measurements are not available, the authors estimated the SMD using an empirical relation. From Figure B.1 it is evident that even small errors in SMD estimates can significantly affect the value of E_{min}. The scatter was also attributed, in part, to the assumptions of the model, but their affect was considered to be overshadowed by drop size errors.

B.2.5/ Conclusions and Discussion

The Ballal and Lefebvre model [5] seems to be the best presently available for the prediction of ignition performance over a wide range of conditions, including cases of fuel sprays in both quiescent and flowing mixtures.

This model agrees well with laboratory data for stoichiometric and lean mixtures and has been successfully applied to gas turbine engine data as well. It can also be used to predict the influence of flow and fuel characteristics on ignition performance. The principal difficulty in its application is the uncertainty in the required information needed for its evaluation in real devices, where droplet sizes may be difficult to predict.

In a later chapter, consideration will be given to the case of primary interest here, namely, very rich overall mixtures with significant vapour concentrations (though not necessarily high enough to sustain homogeneous combustion) and large excesses of liquid fuel.

B.3/ FLAME PROPAGATION IN AIR/VAPOUR/DROPLET MIXTURES

B.3.1/ Introduction

The mechanism of flame propogation into heterogeneous combustible mixtures (liquid droplets + vapour + air) is extremely complex and not yet well understood. The objective of this chapter is to review the experimental and theoretical published research relevant to flame propogation into heterogeneous droplet-vapor-air mixtures.

B.3.2/ Experimental Work

B.3.2.1/ Linear Streams

A brief review of experimental observations on flame propagation along mono-sized, equidistant linear fuel droplet streams in air is helpful to a better qualitative understanding of the propagation mechanisms involved in heterogeneous combustion. Over a wide range of conditions, the results reported by several authors were all in general agreement [15-21]. Their findings can be summarized as follows:

- Interaction effects between neighbouring droplets decrease sharply with increasing droplet distance, ℓ; they become negligible when the ratio of distance to drop diameter, ℓ/D, is larger than about 25 to 30.
- The ratio of flame diameter to droplet diameter increases significantly during combustion.
- The "d^2-law" is not rigorously valid; the burning constant becomes lower as ℓ decreases, and for strongly interactive streams (ℓ/D less than 5), a linear fit of D^2 versus time is not possible.
- At various stages, neighbouring droplet flames may be merged or droplets may burn independently. Merged flames tend to break up, that is, individual droplet burning may be resumed following a period during which neighbouring droplets burn in a single flame.
- The transfer of the flame from droplet to droplet does not require that the visible flame of one droplet touch the next droplet.
- Flame propagation velocity, S, is not uniform along the stream; the flame travels slowly in the spaces between droplets and much faster over the droplets.

In addition, work by Law [22] on the burning of single fuel droplets in a reactive atmosphere (fuel-vapour-air) suggests that the interaction between droplets is stronger in such mixtures than in air alone.

B.3.2.2/ Mono-Sized Arrays in Air

The study of flame propagation into controlled arrays has often been done using low volatility fuel mists falling freely into quiescent air inside a flammability tube. Some of the earliest research (1954) on such mixtures was done by Burgoyne and Cohen [23]. The mist was produced by fuel condensation on minute solid nuclei, and droplet diameter could be varied from 7 to 55 μm. The major drawback of their experimental work was that, in their study of flame speed, they could not investigate a range of mass concentration at any one drop size or vice versa. They reported the following:

- The burning velocity, S, increases for increased droplet diameter (see Table B.1).
- The flame can propagate at leaner fuel concentrations with increasing droplet size (see Figure B.6).
- For diameters below 10 μm, the heterogeneous combustion case is identical to premixed combustion with the same equivalence ratio, i.e, the burning velocity and the fuel concentration at the lean limit, C_{LL}, are essentially the same.
- For D above 40 μm, the drops burn individually in their own envelope, i.e., flame propagation is discontinuous (called relay transfer propagation).
- For diameters below 10 μm, addition of inert gas into the air increases the C_{LL} in similar fashion as for pre-vaporized mixtures, but larger sizes decrease the C_{LL} for a given concentration of inert gas. Furthermore, this concentration of inert gas, which can be added before extinction occurs, also increases with increasing diameter (Figure B.7).

In later research (1957), Burgoyne [24] observed similar results of C_{LL} versus D in the range of D between 70 and 135 μm. He also stated that flammability suppression by inert gas addition happens at higher concentrations of inert gas for increasing D (as previously reported [23]) but that there appeared to be a peak concentration allowable with increasing drop size. At 200 μm it was reported to be appreciably below the value for vapour and continuing to decrease.

Mizutani and Ogasawra [25] (1965) used mono-sized droplet mists with droplet diameters in the range of 100 to 200 μm. The mist was produced by a swirl atomizer and controlled with an elutriation wind tunnel. Under similar conditions, as for the previously mentioned work (combustion inside a 55 mm ID tube), the same trend of decreased C_{LL} with increasing diameter was observed (Figure B.8).

Also, these authors observed that over the entire range of diameters used, the flame propagation mechanism was by relay transfer, i.e., they observed droplets burning individually with no combustion in the inter-droplet spaces.

Hayashi et al. [26] (1981) used a rotating disk atomizer to produce a controlled mist with droplet sizes in the range of 40 to 150 μm. Their apparatus allowed independent control of diameter and droplet spacing, ℓ. These authors obtained similar results to previously reported ones for C_{LL} versus diameter. The distance between droplets at the lean limit of flammability versus D is shown in Figure B.9. These authors also identified three different modes of flame propagation, depending on droplet spacing, hence, depending on the number of droplets per unit volume (the number density). With increasing number density they observed the following sequence:

1/ If the number density is too low the flame cannot propagate in the mixture.
2/ At higher number density, isolated blue flames appear.
3/ At the highest number density used, interactive yellow flame propagation occurs.

Figure B.10 illustrates these mechanisms. Full circles represent propagation failures; triangles, individual flames; and empty circles, yellow-flame propagation.

B.3.2.3/ Mono-Sized Arrays in Vapour-Air Mixtures

Hayashi and Kumagai [27] (1975) studied the effect of fuel vapour on the burning velocity into mono-sized mists produced by an expansion apparatus based on the principle of the Wilson cloud chamber. The maximum droplet diameter was 7 μm; they reported that flame speed S drops with increased diameter up to a certain value of overall fuel concentration and then rises with further increases (Figure B.11). Note that with increasing vapour fraction, the droplet diameter of the mist decreased; D for λ_1 = 1.0 and 0.25 are estimated to be about 7 and 4 μm, respectively. λ_1 is defined by the ratio η_1/η_{air} and λ_0 by η_f/η_{air}.

These same authors, in a subsequent publication [28] (1977), with D up to 40 μm produced in the same type of apparatus, found similar results, that is, they observed that the presence of a liquid phase in lean mixtures resulted in flame speeds smaller than the premixed flame speed at the same overall fuel concentration. The rich mixtures, on the other hand, showed an increase in flame speed compared to the premixed flame speed. These authors also observed that droplets as small as 5 μm can affect flame propagation in droplet-vapour-air mixtures.

To generate well-controlled droplet mists, Aggarwal et al. [29] (1984) used a multi-orifice impulse spray generator. This apparatus allowed selection of droplet spacing for any diameter used. The droplets varied from 104 to 330 μm. The experiment was carried out in flowing mixtures. These authors stated that, depending on fuel vapour/air mixture ratio at the flame front, the flame propagation mechanism can be either kinetically controlled or diffusion controlled:

> If there is enough prevaporization, or there is enough fuel vapour in the fresh mixture so that the fuel vapour/air mixture ratio ahead of the ignition zone is flammable then flame propagation is by the premixed, laminar or turbulent gas flame propagation. But if there is not enough vaporization, then overall fuel vapour/air mixture would not be flammable, although it is observed that flame propagates in such mixtures also. This type of flame propagation is different than that of premixed gas combustion. In such conditions the mixture is eigher very dilute that relay-type flame propagation is observed, whereof an ignited droplet increases in size due to oxygen retardation, and eventually ignites the adjacent droplets. And if spray is very rich, the group combustion phenomena is observed... Both of these phenomena are diffusion controlled. [4,5]

These authors also associated an increase in flame speed with an increase in the fuel vapour fraction.

B.3.2.4/ Poly-Sized Droplet-Vapour-Air Mixtures

Cekalin [30] (1962) studied the flame propagation velocity of turbulent flames using a burner fed with a flowing poly-sized droplet-vapour-air mixture. He found that

- S decreases with an increase in average spacing between droplets (or a decrease in number density),
- S increases with turbulence intensity,
- S varies as a function of the fuel liquid fraction (Figure B.12),
- S is higher for larger drops (30 μm) than for smaller drops (20 μm) for same value of average spacing between drops.

Mizutani and Nishimoto [31] (1972) studied turbulent flame velocities in heterogeneous mixtures using diameters between 10 and 40 μm. They used a burner fed with overall lean mixtures to measure S, and found that

- S increases linearly with overall fuel/air ratio;
- S increases with turbulence intensity;
- S decreases when Sauter mean diameter increases;
- S increases with fuel volatility;

- intensity of turbulence has a great effect on flame speed, whereas flow velocity, per se, does not exert much influence;
- as observed by Schlieren image, a continuous high temperature gradient zone exists in the flame region in spite of its discontinuous appearance with a cine-camera photograph.

The authors suggested that this thin zone is what primarily governs the process of flame propagation.

Ballal and Lefebvre [32] (1981) studied the effect of several parameters on flame propagation into quiescent droplet-vapour-air mixtures. Effects of buoyancy and settling of fuel drops were minimized by conducting the flame speed measurements in a tube while it fell freely under the influence of gravity. Those authors varied Sauter mean diameter between 30 and 150 μm, using a pressure atomizer to produce the mist.

They found the following:
- S decreases with increased Sauter mean diameter.
- S increases with increased vapour fraction (Figures B.13 and B.14).
- S increases with increased fuel volatility.
- Individual droplet combustion occurs just ahead of, as well as behind, the advancing flame front.

B.3.2.5/ Conclusions Based on Experimental Work

The work outlined provides a number of conclusions with general application to the phenomenon of flame propagation into droplet-vapour-air mixtures.

1/ Overall Fuel Concentration at the Lean Limit:
Lean limit concentration decreases with increasing diameter.

2/ Dilution by Inert Gas Addition:
The allowable addition of inert gas before suppression of flammability appears to increase with increased diameter up to a certain value, then decreases with further diameter increase.

3/ Burning Velocity:
Burning velocity can be affected differently by some parameters, depending on whether the mixture is fuel lean or fuel rich overall.

For lean conditions,
- S increases with decreasing diameter or SMD,
- S increases with increasing overall fuel concentration
- S increases with increasing turbulence intensity,
- S increases with increasing fuel vapour fraction,
- S increases with increasing fuel volatility.

For rich conditions, the limited amount of research done suggests that

- S increases with increasing diameter or SMD;
- S increases with increasing turbulence intensity;
- S decreases with increasing fuel vapour fraction up to a certain value, then increases with further increases;
- S increases with decreased average droplet spacing.

4/ Flame Characteristics

The concentration of droplets and vapour appears to have important effects on the flame characteristics. Flame merging between neighbouring droplets is encouraged by close droplet spacing and the presence of fuel vapour, which are conditions conducive to group combustion in sprays. Individual droplet burning is encouraged by the absence of vapour, increased droplet separation, and large initial droplet diameter.

B.3.3/ Theoretical Work and Modelling

B.3.3.1/ Mono-Sized Arrays in Air

Mizutani and Ogasawara [25] (1965) modelled the process of flame propagation through a mono-sized, monodispersed spray of droplets falling freely in quiescent air. The model application is limited to relay transfer propagation, i.e., to dilute sprays. The range of droplet diameters for which they suggest that their model is valid lies between about 40 and 100 μm. The lower limit is based on their observation that below about 40 μm, pure relay transfer no longer occurred. The upper limit was chosen because, above 100 μm, the settling velocity exerted a large effect. Their analysis is based on the one-dimensional flame shown in Figure B.15. All the droplets on plane A are assumed to ignite at the same instant, and the flames surrounding individual droplets are replaced by a hypothetical planar flame front. Ignition of the adjacent B plane of droplets then occurs after a time lag corresponding to the time required for these droplets to heat up and ignite, that is, after the elapse of the ignition delay time. Their criterion for ignition was that the temperature of the air reach a specified minimum value. The major assumptions for their model were the following:

- The flame acts only as a heat source of constant temperature.
- The existence of fuel vapour in the unburned mixture is ignored.
- The droplets maintain their settling velocity until ignited, and then during the burning lifetime the velocity decreases linearly (due to diameter reduction).
- The chemical reaction is infinitely fast.

- Any decrease in droplet diameter due to evaporation up to the instant of ignition is ignored.
- Radiation effects are negligible.

Their results give the correct general trend when compared to the experimental findings previously discussed. In particular, their model predicts that
- S increases linearly with increased mixture concentration,
- S increases with decreasing droplet diameter,
- lean limit concentration decreases with increased diameter.

Polymeropoulos [33] (1974) modelled the process of flame propagation through a dilute mist of mono-sized droplets in air. The major assumptions were as follows:
- The gas flow is one-dimensional, steady, laminar, and obeys the ideal gas equation.
- The gaseous mixture is homogeneous, i.e., there is instantaneous mixing, and the presence of the liquid phase affects the gas only through providing sources and sinks for species produced or consumed around the droplets.
- Preignition evaporation is considered.
- Droplet ignition occurs at a pre[illegible]bed gas temperature.
- Physical properties are computed [illegible] function of gas phase temperature and concentration.

The mathematical procedure followed to solve the set of equations required that coupling between the solutions for gas and liquid phases converge through successive iterations. The author concluded that the results were physically reasonable because the model predicts that
- S increases with decreasing diameter,
- S increases linearly with increasing fuel concentration,
- lean limit concentration decreases with increasing diameter.

B.3.3.2./ Poly-Sized Droplet-Vapour-Air Mixtures

Mizutani and Nishimoto [31] obtained an empirical relation for the burning velocity of mist of droplets in turbulent flow based on measurements made at the exit of a burner. The experimental results were collected over the following conditions:
- S less than 2.5 m/s
- Sauter mean diameter between 30 and 100 μm
- fuel/air ratio between 0.015 and 0.05
- u' less than 1 m/s
- flow velocity between 4 and 10 m/s

Their equation is

$$S = \frac{K}{SMD} (\text{FA ratio} - 0.012) (u')^{1.15} \text{ m/s} \quad (37)$$

where K is a constant whose value was found to be 6800 for kerosene sprays and 4300 for light diesel oil.

Equation 37 correlates their experimental results well, especially for the highest value of flow velocity (10 m/s) used.

Mizutani [34] (1972) modelled flame propagation using a numerical, iterative approach. In this case, the thermodynamic differential equations governing the process of flame propagation were numerically integrated and solved iteratively until the temperature distribution converged, which then gave the flame velocity. His major assumptions were the following:

- The mixture is fuel droplets and air.
- Droplets do not change direction before or after passing through the flame front.
- Droplets are accelerated by thermal expansion.
- Vaporization, condensation, and chemical reaction are replaced by heat sources and sinks. Only the effect of the decrease in oxygen concentration on the burning rate of droplets is taken into account.
- Radiation effects are neglected.
- As soon as the droplet reaches the ignition temperature, it ignites.

The author summarized his results as follows:

- The predicted dependence of S on the fuel concentration is much weaker than observed in the experimental results.
- u' (turbulence intensity) affects S considerably, whereas the flow velocity effect is rather weak.
- S increases with decreasing Sauter mean diameter.
- S is higher for more volatile fuels.
- The effect of the shape of the droplet size distribution is surprisingly weak.

Ballal and Lefebvre [32] proposed a model applicable to quiescent mixtures in which the fuel is present in the form of a mist, or vapour, or both. The basis of their model is that "...under normal steady-state condition, the rate of flame propagation through a fuel mist is always such that the quench time of the reaction zone is just equal to the sum of the evaporation and chemical reaction times." Using only thermal considerations, they found the following equation:

$$S = \alpha_g \left[\frac{C_3^2 (1 - \Omega)\rho_l SMD^2}{8 C_1 \rho_g \, Ln(1 + B)} + \frac{\alpha_g^2}{S_L^2} \right]^{-0.5} \qquad (38)$$

where

C_1, C_3 are constants that describe the droplet size distribution and whose value is 1 for mono-sized mists

B is the Spalding transfer number

S_L is the burning velocity in a gas mixture with the same ratio

For the conditions tested (fuel lean, quiescent mixture, SMD between 30 and 100 μm), the results are in good agreement with experimental findings (Figures B.13 and B.14). Note that the only influence of equivalence ratio is in the value of S_L.

B.3.3.3/ Other Modelling

Numerical solution of the governing partial differential equations for three-dimensional, steady or unsteady, incompressible, turbulent, and chemically reacting flows have recently been modelled by a number of researchers [35-42]. These models have been used to calculate various parameters as functions of time and position, e.g., species concentration, temperature, droplet velocity, flame front velocity, and droplet diameter.

In particular, Seth et al. [37] modelled flame propagation through a droplet-vapour-air mixture in a cylindrical one-dimensional closed combuster. Their model predicts that S increases with the following:

- increased pre-exponential factor;
- decreased activation energy, which is consistent with the model of Ballal and Lefebvre (38), since it is known [43] that

$$S_L \propto A \exp(-E/RT) \qquad (39)$$

  where A is the pre-exponential factor and E the activation energy;
- increased ambient temperature;
- decreased initial droplet diameter;
- increased diffusivities.

However, in the words of the authors, "These results are more useful for studying the process involved in a qualitative way than making quantitative predictions."

Perhaps the biggest difficulty with these elaborate numerical models is that the predicted values cannot all be measured accurately; consequently, reliable validation of the model is not easy. Qualitatively, however, the results obtained are at least plausible.

B.4/ AN IMPROVED IGNITION MODEL FOR DROPLET-VAPOUR-AIR MIXTURES

B.4.1/ Introduction

Based on the review in Chapter B.2, it is concluded that the various versions of the Ballal and Lefebvre model [5] are the best currently available. However, their model suffers from several failings. Chapter B.4 will discuss its inadequacies and derive a new model.

To be useful over the entire range of conditions of interest in all engine types, a comprehensive ignition model must provide for the case of overall rich mixtures ($\phi > 1$) and also for the case in which a flammable or near flammable vapour phase exists in conjunction with a significant quantity of liquid fuel. Since it was derived primarily for the most common cases of interest for gas turbines, the Ballal and Lefebvre model was validated experimentally only for stoichiometric and leaner mixtures. For such conditions, the vapour phase approaches flammability only as the liquid disappears; consequently, their model is simply a composite which degenerates to the purely gaseous case when the vapour fraction $\Omega = 1$.

In fact, their model tacitly assumes that evaporation and chemical reaction are literally sequential. In the following discussion, the case of the mono-sized spray with some vapour will be used to illustrate the points. For that situation their equation is

$$d_q = \left[\frac{(1 - \Omega)\rho_f D^2}{\rho_a \phi \ln (1 + B)} + \left(\frac{10\alpha}{S_L} \right)^2 \right]^{1/2} \qquad (40)$$

The second term on the right is the chemical one, and the first is the evaporatively controlled droplet burning term. The factor $(1 - \Omega)$ causes the physical term to decrease linearly to 0 as the fraction vaporized approaches 100%. This then leaves only the chemical term which Ballal and Lefebvre had previously shown to be valid for ignition of premixed reactants.

One major difficulty with this relation is that it becomes physically unrealistic when both the reactions in the vapour phase as well as droplet combustion are important, i.e., when the vapour phase concentration approaches or becomes a flammable mixture while still in the presence of significant quantities of liquid fuel. This occurs when the product $\Omega\phi$ is greater than about 0.5 or thereabouts. Under such conditions, the vapour phase is flammable in its own right, and a flame can propagate between droplets without necessarily being rate controlled by the evaporation term. Under very rich conditions, the evaporation term can cease

to be a heat source and instead become a heat sink. This case would be particularly likely to occur in a spark-ignition engine under cold-starting conditions but could also arise in other situations of practical interest.

To properly model the gas phase reaction-rate-controlled as well as the droplet evaporation-rate-controlled parts of the heat generation during ignition, it must be taken into account that these two mechanisms are cumulative rather than sequential. In effect, the Ballal and Lefebvre equation merely uses their two separate models, one for droplet-controlled ignition and one for chemically controlled ignition and adds them such that the droplet term decreases linearly with the fraction vaporized.

B.4.2/ Derivation of the Improved Ignition Model

Ballal and Lefebvre used the concept of characteristic times because of the difficulty of defining the chemical reaction rate parameters needed for a conventional Arrhenius equation. They were, however, able to define characteristic physical (i.e., evaporative) and chemical times. They then assumed as an ignition criterion that the sum of these times must equal the characteristic quenching time in the limiting case. As mentioned, this implies that the two processes are sequential, whereas, in fact, they are simultaneous. In the following discussion, the characteristic times used by Ballal and Lefebvre, and also by others such as Peters and Mellor, can be used to derive rate expressions that allow a better physical representation to be obtained.

Now, the basis of all ignition models is that the hot kernel produced by the spark passage appears instantaneously as a sphere in which the gas portion is at a high temperature. (Usually the stoichiometric flame temperature is used, but this is mainly for convenience and does not seriously restrict the model. The use of any other representative kernel temperature would not greatly change the results). After the step change in gas temperature resulting from the spark, any liquid fuel droplets will be essentially unchanged because of their vast thermal inertia compared to the air and vapour. That the thin cylindrical spark thread rapidly degenerates into such a hot sphere is well established.

The start point for ignition is therefore the case in which: the air and any previously existing fuel vapour find themselves instantly transported to the stoichiometric flame temperature, reaction begins in the gas phase, and evaporation begins about each droplet. If the vapour phase is not too fuel rich, then evaporatively controlled combustion occurs about each droplet. The criterion for ignition is that the instantaneous heat

production rate (from both droplet and gas phase terms) must be equal to or greater than the heat loss rate due to conduction from the kernel and convective losses, if any.

The usual and apparently satisfactory assumption regarding the droplet term is that the classical quasi-steady droplet model can be used. The difficulty is in defining unambiguously the relative size of the chemical term. The following physical interpretation provides a means to solve this dilemma.

The characteristic time can be interpreted as the ratio of the total energy contained in the kernel to the apparent instantaneous rate of heat gain or loss. Thus, the characteristic quench time is the time which would be required to lose all the thermal energy in the kernel at a cooling rate constant and equal to its initial value. Similarly, the evaporation time is calculated by all workers as the total energy divided by the initial evaporation rate of the droplets, rather than what their average rate would be if evaporation went to completion.

This is physically justified because from the point of view of the kernel of gas, ignition is successful (and, hence, combustion proceeds outwards into the mainstream) provided that there is as much or more heat being instantaneously generated within the kernel as is being instantaneously lost. Because all these processes would not actually continue at this initial rate is irrelevant, since by the time they change, the flame has spread outwards into the remainder of the unignited mixture.

By adding the evaporative and chemical generation terms, Ballal and Lefebvre force them to be sequential. This may, in fact, be partly justified when the gas phase produces a negligible amount of heat. Under those circumstances, the chemical term might better be explained as an induction period needed before the quasi-steady, evaporation-controlled combustion about the droplets begins to produce energy. However, when the gas phase produces heat simultaneously with droplet evaporation (with or without combustion), then this sequential model breaks down.

In the improved model presented here, the ignition criterion is expressed in terms of the instantaneous heat loss and gain rates. In all the expressions used in the following, the simplest case of a mono-sized spray of droplets with heat loss by conduction only is used for illustrative purposes. The modifications to account for polydisperse sprays and convective heat losses can be easily be incorporated following the methods used by Ballal and Lefebvre [5].

Quenching rate: This is taken to be the heat loss rate from a spherical kernel of air at T_{st}:

$$\dot{q}_q = 2\pi d k_a \Delta T_{st} \tag{41}$$

Heat generation via droplet combustion: This term will turn out to be slightly different from that of Ballal and Lefebvre, so a fuller outline will be given:

$$\dot{q}_{ev} = n\dot{m}Q_{st} \tag{42}$$

where

n = number of droplets of diameter D
$\dot{m}$ = mass rate of evaporation of a single droplet of diameter D
Q_{st} = heat released by the combustion of unit mass of fuel

Now n, the number of droplets present, is given by

$$n = \frac{(1 - \Omega)\, f\pi d^3 \rho_a\, \pi D^3 \rho_f}{36} \tag{43}$$

where

f = the overall fuel/air ratio by mass
Ω = the mass fraction of fuel present in the form of vapour
d = diameter of the spark kernel
D = droplet diameter
ρ_f = fuel density
ρ_a = air density

The heat release per unit mass of fuel is

$$Q_{st} = \frac{\Delta T_{st} C_{pa}}{f_{st}} \tag{44}$$

where

f_{st} = stoichiometric fuel/air ratio
C_{pa} = specific heat of air
ΔT = temperature rise after stoichiometric combustion

The rate of evaporation of one fuel drop when surrounded by the individual flame shell implied by the quasi-steady theory is given by

$$\dot{m} = \frac{2\pi k_a D \, Ln(1 + B)}{C_{pa}} \tag{45}$$

Substituting these results into Equation 42 and simplifying yields

$$\dot{q}_{ev} = \frac{\pi d^3 \rho_a}{6} C_{pa} \Delta T_{st} \frac{(1 - \Omega)\phi 12 K_a \, Ln(1 + B)}{\rho_f C_{pa} D^2} \tag{46}$$

where

ϕ = the overall fuel/air equivalence ratio
k_a = thermal conductivity of air
B = transfer number for combustion of droplets of the fuel concerned

The difficulty which prompted Ballal and Lefebvre and other workers to adopt the summed characteristic time approach was that of defining the necessary constants in the Arrhenius equation for reaction rate. However, the Ballal and Lefebvre expression for characteristic chemical time plus some simple assumptions can avoid this uncertainty.

Using the concept that a characteristic time can be viewed as the quotient of energy in the spark kernel and instantaneous heat generation rate, then

$$\dot{q}_{ch} = \left[\frac{\pi d^3}{6}\right] \rho_a C_{pa} \Delta T_{st} / t_{ch} \tag{47}$$

where t_{ch} = characteristic chemical time for gas phase reactions:

$$t_{ch} = \frac{8.33\alpha}{S_L^2} \tag{48}$$

Ballal and Lefebvre used slightly different constants in their various publications [5,7]. The value of 8.33 is consistent with the remainder of this analysis and those of Ballal and Lefebvre. This can be seen by considering the case of the completely vaporized mixture in which heat generation via chemical production equals heat losses at the limiting condition. Equations 47 and 41 give

$$\left[\frac{\pi d^3}{6}\right]\rho_a C_{pa}\Delta T_{st}\left[\frac{1}{\frac{8.33\alpha}{S^2_L}}\right] = 2\pi d K_a \Delta T_{st} \qquad (49)$$

which simplifies to

$$d = \frac{10\alpha}{S_L} \qquad (50)$$

which is the same expression found by Ballal and Lefebvre [5,7,8].

This chemical term can be evaluated provided S_L is known. However, determining S_L is convenient only for well-defined cases, such as stoichiometric, and breaks down entirely for the case in which the vapour phase would not normally support a flame, i.e., when $\Omega\phi < 0.5$ or so. A means out of this impasse is obtained by recalling that the kernel is, in all cases, assumed to start at T_{st}. The Arrhenius equation is

$$\dot{q}_{ch} \propto AC_f C_{O_2} \exp(-E/RT) \qquad (51)$$

where

A = pre-exponential constant
E = activation energy
R = universal gas constant
C_f = concentration of fuel vapour
C_{O_2} = concentration of oxygen

This follows the common assumption of one step global kinetics, which are first order in both fuel and oxygen. The relative rates for conditions other than stoichiometric may be found by taking the ratio and using the known stoichiometric flame speed as follows:

$$\dot{q}_{ch} = \frac{\pi d^3}{6}\rho_a C_{pa}\Delta T_{st}/t_{chst}\,\frac{\dot{q}_{ch}}{\dot{q}_{ch_{stoich}}} \qquad (52)$$

where t_{chst} = time constant evaluated for the standard conditions (stoichiometric mixture at 1 atm)

$$= \frac{8.33\ \alpha_o}{S^2_{Lo}} \tag{53}$$

Since, in all cases, the temperature at which the reaction rate is to be evaluated after the spark passes is T_{st}, the usual problem of assigning appropriate values to activation energy and pre-exponential constants is avoided. Whatever their values, they are identical for all cases, as is the temperature in the exponential term. The result is then

$$\dot{q}_{ch} = \left[\frac{\pi d^3}{6}\right] \rho_a C_{pa} \Delta T_{st} / t_{chst} \frac{C_f C_{O_2}}{(C_f C_{O_2})_{st}} \tag{54}$$

The concentrations are evaluated as follows. For unit mass of air there are f units of fuel in the mixture. The number of moles of fuel is, therefore,

$$n_f = f/M_f \tag{55}$$

and similarly the number of moles of air is

$$n_a = 1/M_a \tag{56}$$

where M_f = molecular weight of the fuel
M_a = molecular weight of air

The mole fractions in such a mixture are, therefore,

$$X_f = \frac{fM_a}{(M_f + fM_a)} \tag{57}$$

and

$$X_{O_2} = \frac{0.21M_f}{(M_f + fM_a)} \tag{58}$$

The concentration of fuel is then given by

$$C_f = X_f \frac{\eta_t}{VoT} = \frac{fM_a}{(M_f + fM_a)} \frac{P_t}{RT} \tag{59}$$

where P_t = total mixture pressure

The product of concentrations required for Equation 54 is thus

$$C_f C_{O_2} = \frac{0.21\ fM_a M_f}{(M_f + fM_a)^2}\left(\frac{P_t}{RT}\right)^2 \tag{60}$$

With some algebraic rearrangement the ratio of reaction rates becomes

$$\frac{(C_f C_{O_2})}{(C_f C_{O_2})_{st}} = \Omega\phi\left(\frac{P_t}{P_o}\right)^2\left(\frac{1 + K}{1 + K\Omega\phi}\right) \tag{61}$$

where $K = f_{st}M_a/M_f$

The heat generation rate due to gas phase reactions is, therefore, given by

$$\dot{q}_{ch} = \left[\frac{\pi d^3}{6}\right]\rho_a C_{pa}\Delta T_{st}\left[\frac{1}{t_{chst}}\right]\Omega\phi\left(\frac{P_t}{P_o}\right)^2\left(\frac{1 + K}{1 + K\Omega\phi}\right) \tag{62}$$

Recalling the ignition criterion, i.e.,

$$\dot{q}_q = \dot{q}_{ev} + \dot{q}_{ch}$$

the result when the chemical evaporative and quenching terms are inserted is

$$2\pi d k_a \Delta T_{st} = \left[\frac{\pi d^3}{6}\right]\rho_a C_{pa}\Delta T_{st}\left[\frac{(1 - \Omega)\phi 12\ \mathrm{Ln}(1 + B)k_a}{\rho_f C_{pa} D^2}\right]$$

$$+ \left[\frac{\pi d^3}{6}\right]\rho_a C_{pa}\Delta T_{st}\left[\frac{S_{L_o}^2}{8.33\alpha}\right]\Omega\phi\left(\frac{P_t}{P_o}\right)^2\left(\frac{1 + K}{1 + K\Omega\phi}\right) \tag{63}$$

For those cases in which the vapour phase is very rich, flames cannot form about each droplet as assumed in the evaporative term. In that case, the droplets will, in fact, act as heat sinks, absorbing part of the energy produced by the gas phase reactions. An additional heat loss is therefore added to incorporate this effect. Following similar reasoning as in the case of droplet combustion leads to the following similar equation:

$$\dot{q}_{sink} = \frac{\pi d^3}{6} \rho_a C_{pa} \Delta T_{st} (1 - \Omega)\phi \frac{L}{HV} \frac{12 k_a \, Ln(1 + B_{ev})}{\rho_f C_{pa} D^2} \qquad (64)$$

where

$L = h_{fg} + Cpl\ (T_B - T_0) + C_{pfv}\ (T_{st} - T_B)$
h_{fg} = enthalpy of evaporation of the fuel
C_{pl} = specific heat of the fuel liquid
C_{pfv} = specific heat of the fuel vapour
T_0 = initial fuel temperature
T_B = boiling temperature
HV = heating value of the fuel
B_{ev} = transfer number of evaporation

This heat sink term is only present when the droplet combustion term is no longer significant. Similarly, when the vapour phase reactions become dominant ($\Omega\phi \rightarrow 1$), the droplet heat generation must drop out since there is no longer combustion around each droplet. Exactly when this transition from droplets acting as sources to sinks occurs is not clear and requires experimental study. For the present, a plausible description is that up to about $\Omega\phi = 0.5$, droplets are entirely sources, beyond $\Omega\phi = 1$ they are entirely sinks, and the transition between the two is linear. Using this hypothesis and including the sink term given by Equation 64 in the heat balance equation gives the following resulting overall equation (instead of Equation 63) after some algebraic rearrangement:

$$d_q = \frac{(1 - \Omega)\phi \rho_a}{\rho_f D^2} A \, Ln(1 + B) - (1 - A) \frac{L}{HV} Ln(1 - B_{ev}) + \frac{S_{L_o}^2}{100\alpha} \Omega\phi \left(\frac{P_t}{P_o}\right)^2 \frac{(1 + K)}{(1 + K\Omega\phi)}^{-1/2} \qquad (65)$$

where

A = 1.0 for $\Omega\phi < 0.5$
= $2\ (1 - \Omega\phi)$ for $0.5 < \Omega\phi < 1.0$
= 0 for $\Omega\phi > 1.0$
B = combustion transfer number
B_{ev} = evaporative transfer number

Using the usual concept that ignition energy is the energy required to heat up a spherical kernel of air to T_{st}, then the corresponding equation for minimum ignition energy is

$$E_{min} = \frac{\pi d_q^3}{6} \rho_a C_{pa} \Delta T_{st} \qquad (66)$$

B.5/ IMPROVED FLAME PROPAGATION MODEL

The limitations of the Ballal and Lefebvre propagation model are similar to those of their ignition model. An improved version is presently under study.

B.6/ REFERENCES

[1] Peters, J.E. and A.M. Mellor, "A Spark Ignition Model for Liquid Fuel Sprays Applied to Gas Turbine Engines," J. Energy: 6(4), pp. 272-274, 1982.

[2] Chen, N.K., Y.H. Zhao, S.S. Wu, Q.S.Zhao, and J.S. Chi, "Effect of Oxygen Addition on Ignition of Aero-Gas Turbine at Simulated Altitude Facility," J. Energy: 6(6), pp. 425-429, 1982.

[3] Fenn, J.B., "Lean Flammability Limit and Minimum Spark Ignition Energy," J. Ind. Eng. Chemistry: 43, pp. 2865-2869, 1951.

[4] De Soete, G.C., "Propagation Behaviour of Spark Ignited Flame in Early Stage," Comb. in Engineering: 1, 1983.

[5] Ballal, D.R. and A.H. Lefebvre, "A General Model of Spark Ignition for Gaseous and Liquid Fuel-Air Mixtures," 18th Symp. (Int.) on Combustion, Combustion Institute, Pittsburgh, 1981.

[6] Chin, J.S., "The Effect of Oxygen Addition on the Minimum Ignition Energy of a Homogeneous Combustible Mixture," Research Report BH-B429, Beying Inst. of Aero., Astro: 3, 1979.

[7] Ballal, D.R. and A.H. Lefebvre, "Ignition and Flame Quenching in Flowing Gaseous Mixtures," Proc. Roy. Soc. Lond., A.357, pp. 163-181, 1977.

[8] Ballal, D.R. and A.H. Lefebvre, "Ignition and Flame Quenching of Quiescent Fuel Mists," Proc. Roy. Soc. Lond., A.364, pp. 277-294, 1978.

[9] Peters, J.E. and A.M. Mellor, "An Ignition Model for Quiescent Fuel Sprays," Comb. and Flame: 38, pp. 65-74, 1980.

[10] Ballal, D.R. and A.H. Lefebvre, "Ignition and Flame Quenching of Flowing Heterogeneous Fuel-Air Mixtures," Comb. and Flame: 35, pp. 155-168, 1979.

[11] Naegeli, D.W., C.A. Moses, and A.M. Mellor, "Preliminary Correlation of Fuel Effects on Ignitability for Gas Turbine Engines," ASME 83-JPGC-GT-8, 1983.

[12] Kanury, A.M., Introduction to Combustion Phenomena, Gordon and Breach, New York, 1977.

[13] Bellan, J. and R. Duffel, "A Theory of Nondilute Spray Evaporation Based upon Multiple Drop Interactions," Comb. and Flame: 51, pp. 55-67, 1983.

[14] Peters, J.E. and A.M. Mellor, "Liquid Fuel Spray Ignition Predictions for JP-10," J. Energy: 7(1), pp. 95-96, 1983.

[15] Williams, A., "Combustion of Droplets of Liquid Fuels: A Review," Combustion and Flame: 21, pp. 1-31, 1973.

[16] Reichenbach, R., D. Squires, and S.S. Penner, "Flame Propagation in Liquid-Fuel Droplet Arrays," Eighth Symp. (Int.) on Combustion, p. 1068, Combustion Institute, Pittsburg, 1962.

[17] Nuruzzaman, A.S., A.B. Hedley, and J.M. Beer, "Combustion of Monosized Droplet Streams in Stationary Self-Supporting Flames," Thirteenth Symp. (Int.) on Combustion, p. 787, Combustion Institute, Pittsburg, 1971.

[18] Brzustowski, T.A., A. Sobiesiak, and S. Wojcicki, "Flame Propagation Along an Array of Liquid Fuel Droplets at Zero," Combustion Institute, Pittsburgh, 1981.

[19] Miyasaka, K. and C.K. Law, "Combustion of Strongly-Interacting Linear Droplet Arrays," Eighteenth Symp. (Int.) on Combustion, p. 283, Combustion Institute, Pittsburgh, 1981.

[20] Sangiovanni, J.J. and M. Labowsky, "Burning Times of Linear Fuel Droplet Arrays: A Comparison of Experiment and Theory," Combustion and Flame: 47, p. 15, 1982.

[21] Sobiesiak, A. and S. Wojcicki, "Spread of a Flame Through a System of Fuel Droplets under Conditions of Weightlessness," Heat Transfer-Soviet Research: 14(5), p. 71, 1982.

[22] Law, C.K., "Deflagration and Extinction of Fuel Droplet in a Weakly Reactive Atmosphere," J. Chem. Phys: 68(9), 1978.

[23] Burgoyne, J.H. and L. Cohen, "The Effect of Drop Size on Flame Propagation in Liquid Aerosols," Proc. Roy. Soc., A225, p. 375, 1954.

[24] Burgoyne, J.H., "Mist and Spray Explosions," Engng Progr: 53, p. 121, 1957.

[25] Mizutani, Y. and M. Ogasawara, "Laminar Flame Propagation in Droplet Suspension of Liquid Fuel," Int. J. Heat Mass Transfer: 8, p. 921, 1965.

[26] Hayashi, S., T. Ohtani, K. Iinuma, and S. Kumagai, "Limiting Factor of Flame Propagation in Low-Volatility Fuel Clouds," Eighteenth Symp. (Int.) on Combustion, p. 361, Combustion Institute, Pittsburg, 1981.

[27] Hayashi, S. and S. Kumagai, "Flame Propagation in Fuel Droplet-Vapor-Air Mixtures," Fifteenth Symp. (Int.) on Combustion, p. 445, Combustion Institute, Pittsburg, 1975.

[28] Hayashi, S., S. Kumagai, and T. Sakai, "Propagation Velocity and Structure of Flame in Droplet-Vapour-Air Mixtures," Combustion Sci. and Tech.: 15, p. 169, 1976.

[29] Aggarwal, S.K., N. Ashgrizzadeh, W.A. Sirignano, and S.C. Yao, "Ignition and Flame Propagation In Sprays," U.S. A.R.O.; Contract #DAA629-80-C-0002, Carnegie-Mellon University, 1984.

[30] Cekalin, E.K., "Propagation of Flame in Turbulent Flow of Two-Phase Fuel-Air Mixture", Eighth Symp. (Int.) on Combustion, p. 1125, Combustion Institute, Pittsburg, 1962.

[31] Mizutani, Y. and T. Nishimoto, "Turbulent Flame Velocities Premixed Sprays Part I. Experimental Study," Combustion Sci. and Tech.: 6, p. 1, 1972.

[32] Ballal, D.R. and A.H. Lefebvre, "Flame Propagation in Heterogeneous Mixtures of Fuel Droplets, Fuel Vapour and Air," Eighteenth Symp. (Int.) on Combustion, p. 21, Combustion Institute, Pittsburgh, 1981.

[33] Polymeropoulos, C.E., "Flame Propagation in a One-Dimensional Liquid Fuel Spray," Comb. Sci. and Tech.: 9, p. 197, 1974.

[34] Mizutani, Y., "Turbulent Flame Velocities in Premixed Sprays Part II. Theoretical Analysis," Comb. Sci. and Tech.: 6, p. 11, 1972.

[35] Ganesan, V. and D.B. Spalding, "Numerical Modelling of the Combustion of Fuel Sprays in Three Dimensional Can Combustors," Proc. of Fourth ISABE, Florida, p. 177, 1979.

[36] Aggarwal, S.K. and W.A. Sirignano, "One-Dimensional Turbulent Flame Propagation in an Air-Fuel Droplet Mixture," ASME 80-WA/HT-37, 1980.

[37] Seth, B., S.K. Aggarwal, and W.A. Sirignano, "Flame Propagation Through an Air-Fuel Spray Mixture with Transient Droplet Vaporization," Comb. and Flame: 39, p. 149, 1980.

[38] Boysan, F., W.H. Ayers, J. Swithenbank, and Z. Pan, "Three Dimensional Model of Spray Combustion in Gas Turbine Combustors," J. Energy, AIAA 81-0324R, 1981.

[39] Sampath, S., V.Ganesan, and D.B. Spalding, "Numerical Prediction of Droplet Combustion in a Gas Turbine Combustor Using a Two Step Reaction Model," Colloque Int. First Specialist Meeting (International) of the Combustion Institute, TOME I, p. 217, 1981.

[40] Aggarwal, S.K. and W.A. Sirignano, "Effect of Numerical Modeling on One-Dimensional Enclosed Homogeneous and Heterogeneous Deflagrations," ASME Heat Transfer Division, Winter Annual Meeting, 1981.

[41] Ward, P., N. Collings, and N. Hay, "A Comparison of Two Alternative Models for a Burning Fuel Spray and an Assessment of the Effect of Inter-Phase Slip," Nineteenth Symp. (Int.) on Combustion, Combustion Institute, p. 953, 1982.

[42] Aggarwal, S.K. and W.A. Sirignano, "Numerical Modelling of One-Dimensional Enclosed Homogeneous and Heterogeneous Deflagrations," Computers and Fluids: 12(2), p. 145, 1984.

[43] Lefebvre, A.H., Gas Turbine Combustion, McGraw-Hill, New York, 1983.

Table B.1/ Burning Velocity of Sprays

Drop Diameter (μm)	Mass Concentration (mg/L)	Number Density (drops/cm^3)	Burning Velocity (cm/s)
8	67	2.5×10^5	28
9	62	1.6×10^5	31
10	87	1.7×10^5	39
11	84	1.2×10^5	42
15	69	3.9×10^4	59
17	61	2.4×10^4	62
22	64	1.1×10^4	55
29	60	4.7×10^3	68
30	60	4.3×10^3	67
34	45	2.2×10^3	58
34	52	2.5×10^3	57
38	48	1.7×10^3	58

Data from Reference 23, for tetralin ($C_{10}H_{12}$)

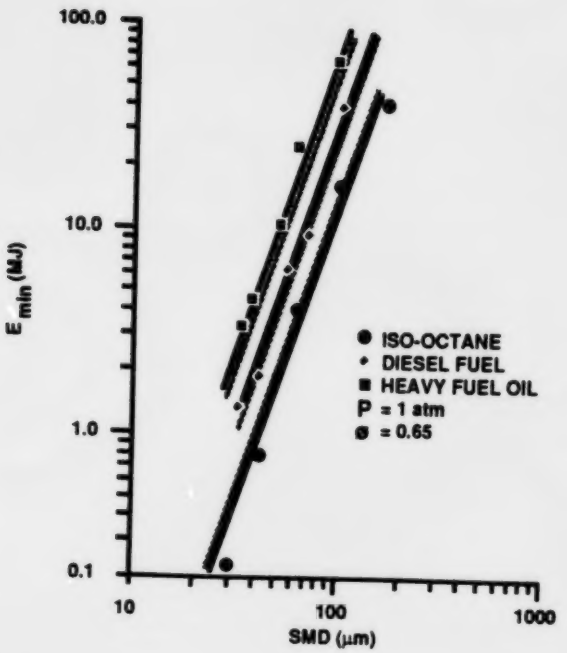

Figure B1/ E_{min} vs SMD for Quiescent Mixtures

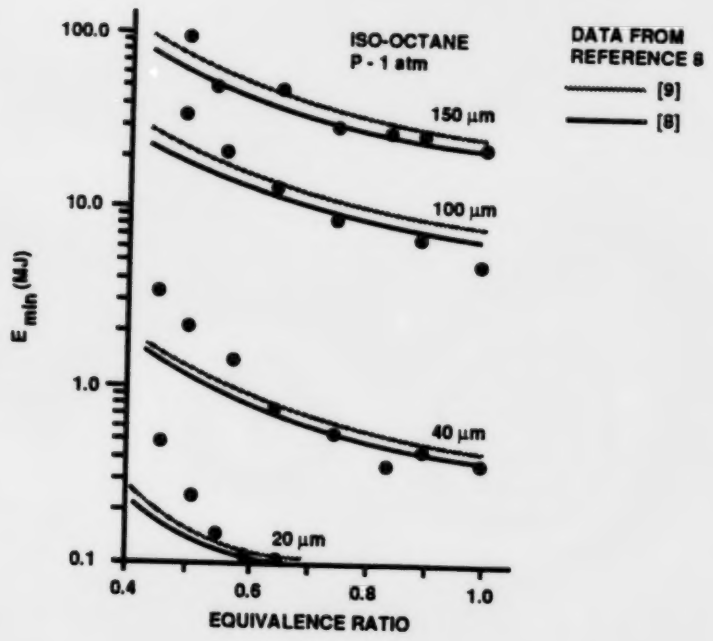

Figure B2/ E_{min} vs ø for Various Drop Sizes in Quiescent Air

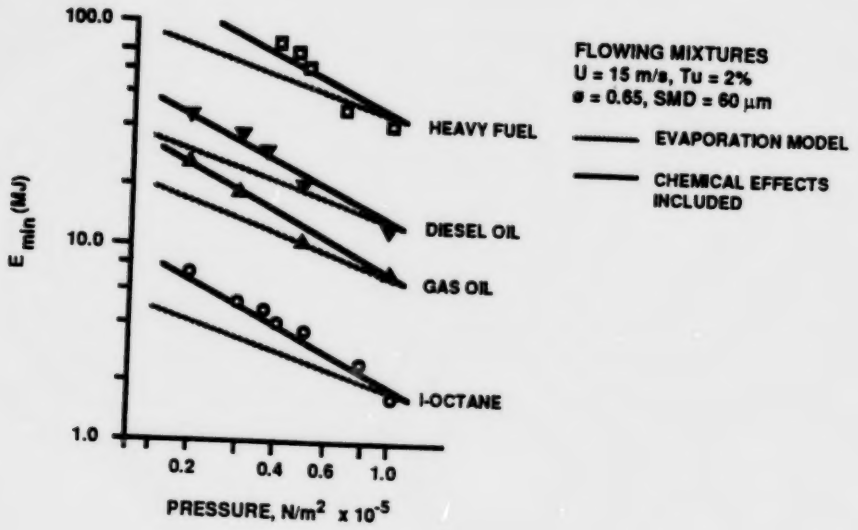

Figure B3/ E_{min} vs Pressure for Flowing Mixtures

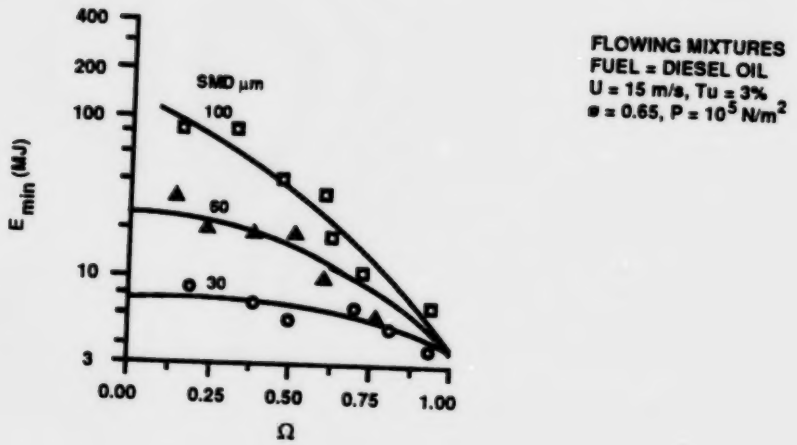

Figure B4/ E_{min} vs Vapour Fraction for Flowing Mixtures: Diesel Fuel

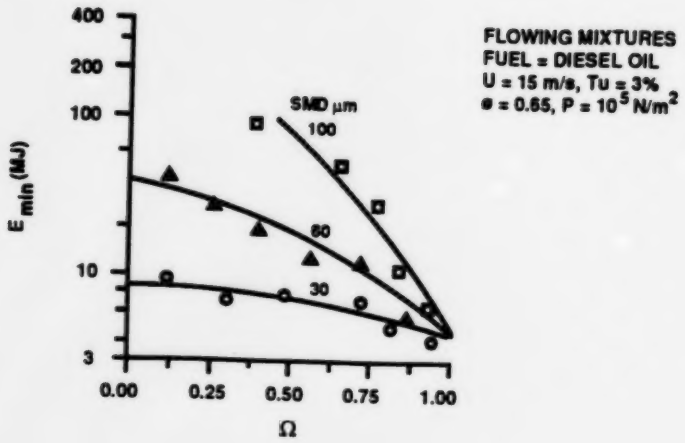

Figure B5/ E_{min} vs Vapour Fraction for Flowing Mixtures: Heavy Oil

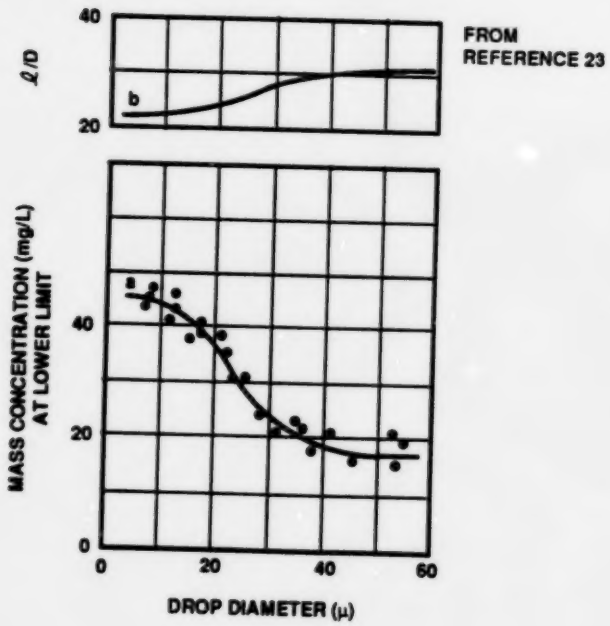

Figure B6/ Variation of Drop Separation/Size Ratio and C_{LL} with Drop Size

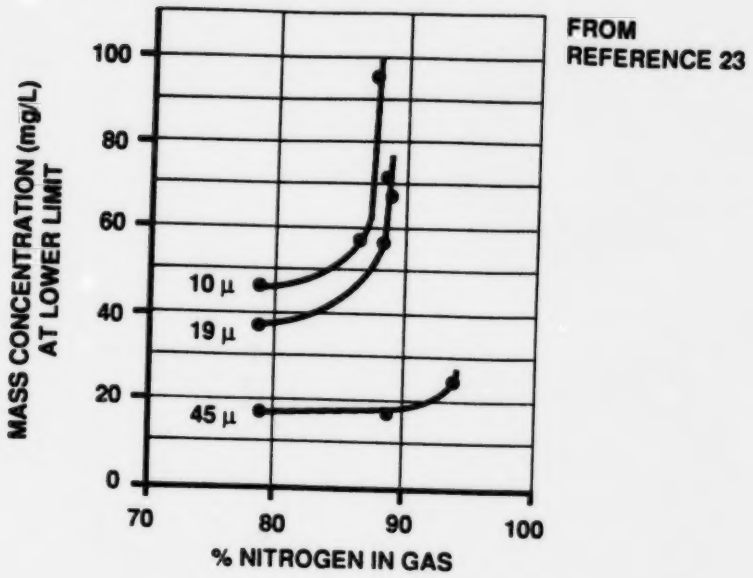

Figure B7/ Lower Limit of Flammability in Presence of Nitrogen

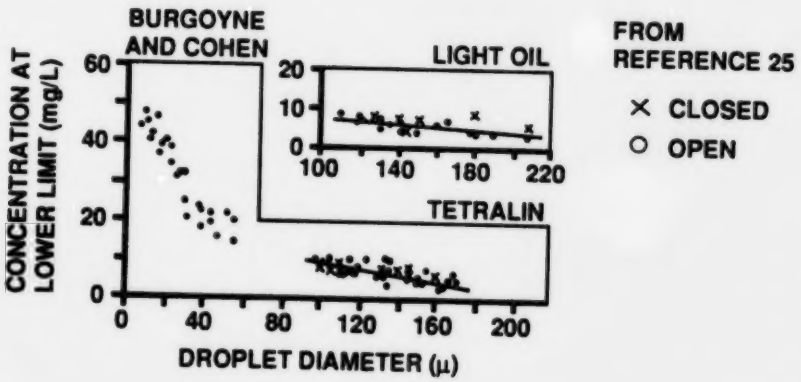

Figure B8/ Lower Limit of Flammability with Open and Closed Tubes

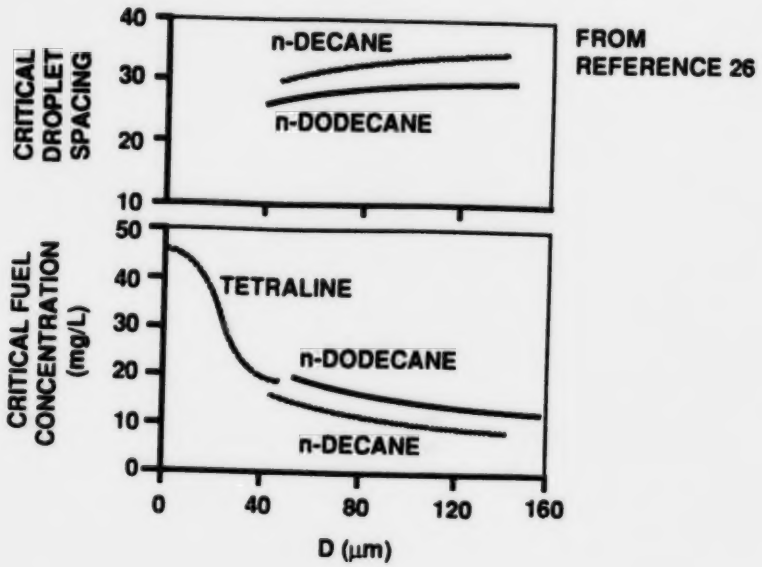

Figure B9/ Propagation Limits: Critical Droplet Spacing and Critical Fuel Concentration vs Droplet Size D

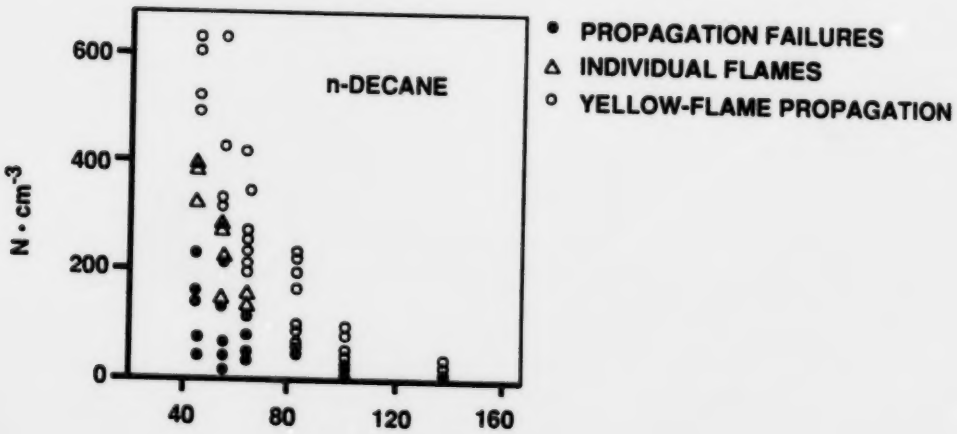

Figure B10/ Effects of Number Density, N, and Size D of Droplet on Modes of Flame Propagation

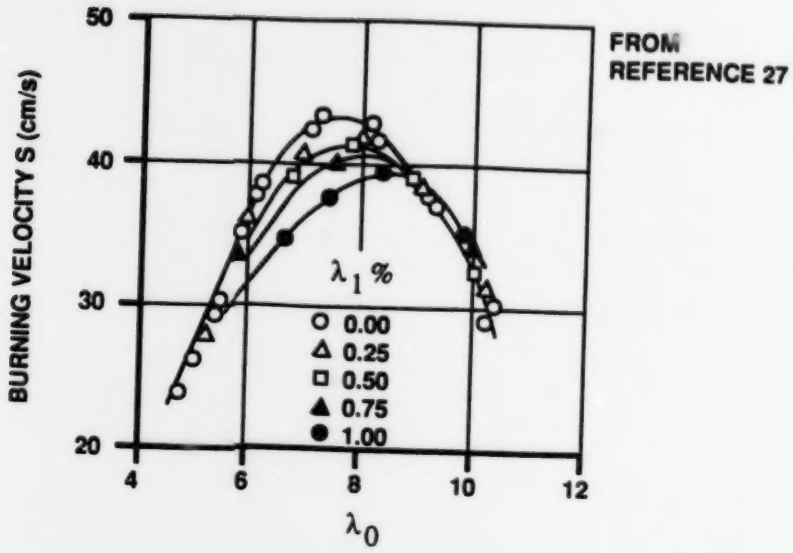

Figure B11/ Effect of Liquid Phase and Overall Fuel Concentration on Burning Velocity

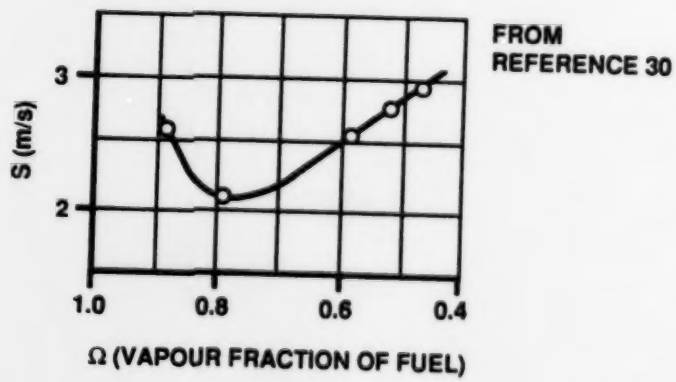

Figure B12/ Effect of Vapour on Flame Speed

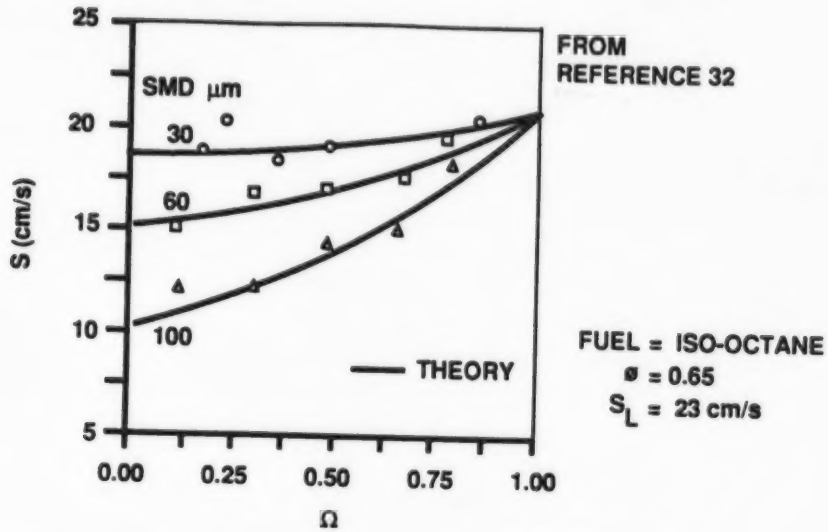

Figure B13/ Influence of Vapour Fraction and SMD on Flame Speed for Iso-octane Fuel: Equivalence Ratio 0.65

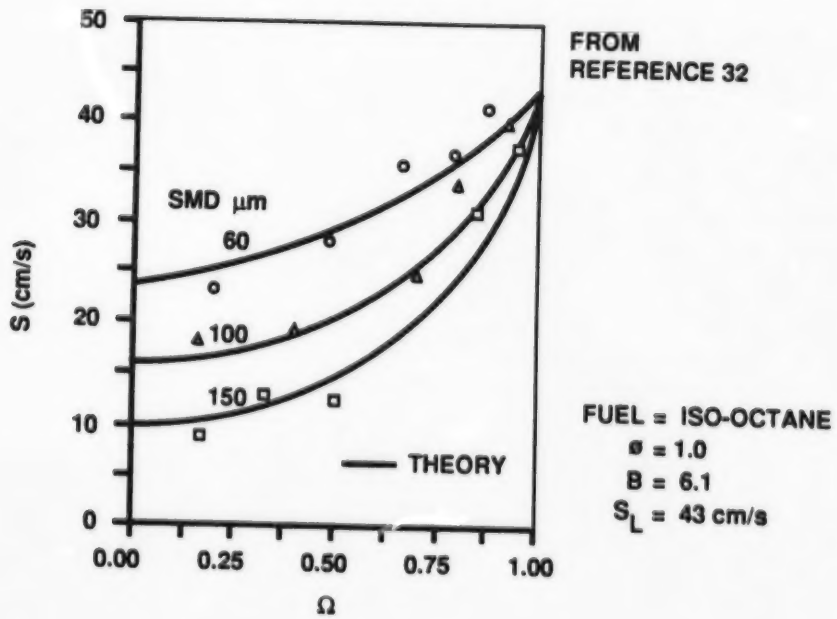

Figure B14/ Influence of Vapour Fraction and SMD on Flame Speed for Iso-octane Fuel: Equivalence Ratio 1.0

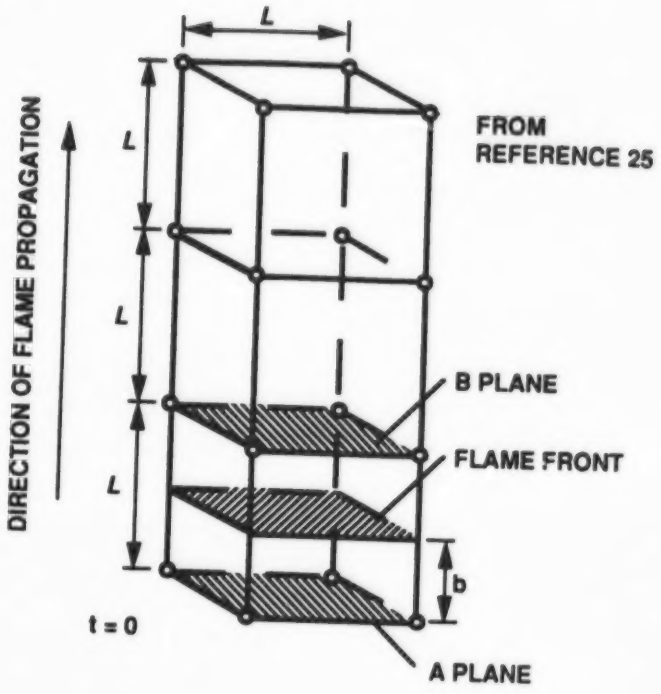

Figure B15/ Relay Transfer Propagation Model